VILNIUS GEDIMINAS TECHNICAL UNIVERSITY

Paulius BUTKUS

RESEARCH AND DEVELOPMENT OF THE HIGH-FREQUENCY SQUARE-WAVE PULSE ELECTROPORATION SYSTEM

DOCTORAL DISSERTATION

TECHNOLOGICAL SCIENCES,
ELECTRICAL AND ELECTRONIC ENGINEERING (T 001)

Vilnius, 2020

Doctoral dissertation was prepared at Vilnius Gediminas Technical University in 2016–2020.

Supervisor

Assoc. Prof. Dr Sonata TOLVAIŠIENĖ (Vilnius Gediminas Technical University, Electrical and Electronic Engineering – T 001).

The Dissertation Defense Council of Scientific Field of Electrical and Electronic Engineering of Vilnius Gediminas Technical University:

Chairman

Prof. Dr Vytautas URBANAVIČIUS (Vilnius Gediminas Technical University, Electrical and Electronic Engineering – T 001).

Members:

Prof. Dr Kęstutis ARLAUSKAS (Vilnius University, Materials Engineering – T 008),

Dr Francesco CARDELLINI (National Agency for New Technologies, Energy and Sustainable Economic Development, Italy, Physics – N 002),

Prof. Dr Dalius NAVAKAUSKAS (Vilnius Gediminas Technical University, Electrical and Electronic Engineering – T 001),

Assoc. Prof. Dr Dainius UDRIS (Vilnius Gediminas Technical University, Electrical and Electronic Engineering – T 001).

The dissertation will be defended at the public meeting of the Dissertation Defense Council of Electrical and Electronic Engineering in the Senate Hall of Vilnius Gediminas Technical University at **9 a. m. on 18 December 2020**.

Address: Saulėtekio al. 11, LT-10223 Vilnius, Lithuania.
Tel.: +370 5 274 4956; fax +370 5 270 0112; e-mail: doktor@vgtu.lt

A notification on the intend defending of the dissertation was send on 17 November 2020.

A copy of the doctoral dissertation is available for review at Vilnius Gediminas Technical University repository http://dspace.vgtu.lt and at the Library of Vilnius Gediminas Technical University (Saulėtekio al. 14, LT-10223 Vilnius, Lithuania) and the Wroblewski Library of the Lithuanian Academy of Sciences (Žygimantų st. 1, LT-01102, Vilnius, Lithuania).

Vilnius Gediminas Technical University book No 2020-040-M

doi:10.20334/2020-040-M

paulius.butkus@vgtu.lt

VILNIAUS GEDIMINO TECHNIKOS UNIVERSITETAS

Paulius BUTKUS

AUKŠTO DAŽNIO STAČIAKAMPIŲ IMPULSŲ ELEKTROPORACIJOS SISTEMOS KŪRIMAS IR TYRIMAS

DAKTARO DISERTACIJA

TECHNOLOGIJOS MOKSLAI,
ELEKTROS IR ELEKTRONIKOS INŽINERIJA (T 001)

Vilnius, 2020

Disertacija rengta 2016–2020 metais Vilniaus Gedimino technikos universitete.

Vadovas

doc. dr. Sonata TOLVAIŠIENĖ (Vilniaus Gedimino technikos universitetas, elektros ir elektronikos inžinerija – T 001).

Vilniaus Gedimino technikos universiteto Elektros ir elektronikos inžinerijos mokslo krypties disertacijos gynimo taryba:

Pirmininkas

prof. dr. Vytautas URBANAVIČIUS (Vilniaus Gedimino technikos universitetas, elektros ir elektronikos inžinerija – T 001).

Nariai:

prof. dr. Kęstutis ARLAUSKAS (Vilniaus universitetas, medžiagų inžinerija – T 008),

dr. Francesco CARDELLINI (Nacionalinė naujųjų technologijų, energetikos ir tvarios ekonominės plėtros agentūra, Italija, fizika – N 002),

prof. dr. Dalius NAVAKAUSKAS (Vilniaus Gedimino technikos universitetas, elektros ir elektronikos inžinerija – T 001),

doc. dr. Dainius UDRIS (Vilniaus Gedimino technikos universitetas, elektros ir elektronikos inžinerija – T 001).

Disertacija bus ginama viešame Elektros ir elektronikos inžinerijos mokslo krypties disertacijos gynimo tarybos posėdyje **2020 m. gruodžio 18 d. 9 val.** Vilniaus Gedimino technikos universiteto senato posėdžių salėje.

Adresas: Saulėtekio al. 11, LT-10223 Vilnius, Lietuva.
Tel.: (8 5) 274 4956; faksas (8 5) 270 0112; el. paštas doktor@vgtu.lt

Pranešimai apie numatomą ginti disertaciją išsiųsti 2020 m. lapkričio 17 d.

Disertaciją galima peržiūrėti Vilniaus Gedimino technikos universiteto talpykloje http://dspace.vgtu.lt ir Vilniaus Gedimino technikos universiteto bibliotekoje (Saulėtekio al. 14, LT-10223 Vilnius, Lietuva) bei Lietuvos mokslų akademijos Vrublevskių bibliotekoje (Žygimantų g. 1, LT-01102 Vilnius, Lietuva).

Abstract

The dissertation provides the research and development of the high-frequency square wave pulse electroporation system and proposes a topolgy of planar electroporation electrodes for real-time electroporation applications. An analysis and applied research of the electrical pulse forming circuits, the electric field generation technologies and the compensation circuits for high-frequency transient as well as the electric field distribution of planar electroporation electrodes are carried out.

The introductory chapter deals with the problem of the thesis, research goals and newness, describes the research methodology and defended statements.

The first chapter presents the most relevant scientific literature related to the main subjects of this dissertation. The electroporation phenomena and the dependence of the cell response on electrical pulses duration and frequency are presented. The review of submicrosecond and nanosecond electric pulse generators and high-frequency transient process compensation circuits are also presented. This Chapter concludes in formulating tasks the dissertation.

The second chapter presents simulation models of the high-voltage, high-frequency submicrosecond pulsed electric field (nsPEF) generator and planar electrodes for real-time electroporation. The SPICE model of pulse forming circuit is developed and the effects of the parasitic circuit elements and transient processes to the generated electric pulse are investigated. The chapter includes the potential applications and needs of the planar electrodes for electroporation. The topology of planar electrodes and its influence on electric field homogeneity are analysed using finite element method (FEM) in COMSOL Multiphysics environment.

The third chapter presents the research and development of novel high-frequency square-wave electroporation system. The developed system can produce single and bursts deliver adjustable square-wave electric pulses with load independent pulse fall time. The pulse amplitude, repetition frequency and pulse duration can be adjusted accordingly up to 3 kV, from 1 Hz to 3.5 MHz and from 100 ns to 1 ms. In this chapter, the system simulation and the experimental results are compared. The prototype system is successfully tested for the inactivation of the human pathogen *Candida albicans*.

The main results of the thesis were published in 6 scientific articles: three – in scientific journals included in Clarivate Analytics Web of Science database with impact factor, two – in international conference publications which are referred by Clarivate Analytics Web of Science database Proceedings, one article is printed in peer-reviewed scientific journal listed in Index Copernicus database. The research results were presented in 10 scientific conferences.

Reziumė

Disertacijoje patekiamas aukšto dažnio stačiakampių impulsų elektroporacijos sistemos kūrimas ir tyrimas. Pasiūlyta planarių elektroporacijos elektrodų topologija realaus laiko elektroporacijos tyrimams. Atlikti elektrinio lauko generavimo technologijų taikymo, aukšto dažnio pereinamųjų vyksmų kompensavimo grandinių ir elektrinio lauko pasiskirstymo planariuose elektroporacijos elektroduose analizė ir taikomieji tyrimai.

Įvadiniame skyriuje nagrinėjama disertacijos problema, tyrimo tikslai bei naujumas, aprašoma tyrimų metodologija ir ginamieji teiginiai.

Pirmame skyriuje pateikiama aktualiausios mokslinės literatūros analizė disertacijos tema. Pristatomas elektroporacijos reiškinys, ląstelių reakcijos priklausomybė nuo skirtingos trukmės ir dažnio elektros impulsų. Skyriuje taip pat pateikiama submikrosekundžių ir nanosekundžių elektros impulsų generatorių ir aukšto dažnio pereinamųjų vyksmų kompensavimo grandinių apžvalga. Skyriaus pabaigoje suformuluojami pagrindiniai darbo uždaviniai.

Antrame skyriuje pateiktas aukšto dažnio ir aukštos galios submikrosekundžių impulsų elektroporacijos sistemos ir planarių elektroporacijos elektrodų imitacinių modelių sudarymas. Sudaromas impulsų formavimo grandinės SPICE modelis ir atliekami parazitinių grandinės elementų bei pereinamųjų vyksmų įtakos impulsų formai analizė. Skyriuje taip pat diskutuojamos planarių elektroporacijos elektrodų panaudojimo perspektyvos ir poreikis. Panaudojant COMSOL Multiphysics programinį paketą atliekamas planarių elektroporacijos elektrodų topologijos ir elektrinio lauko pasiskirstymo tyrimai taikant baigtinių elementų metodą.

Trečiajame skyriuje pateikiamas aukšto dažnio stačiakampių impulsų elektroporacijos sistemos sukūrimas ir atliekamas įrangos bandymas. Sukurta sistema gali generuoti pavienius stačiakampius impulsus arba jų serijas, visų impulsų galinio fronto kritimo trukmės nepriklauso nuo apkrovos varžos. Impulsų amplitudė, dažnis ir impulso trukmė gali būti parenkama atitinkamai nuo 0 kV iki 3 kV, nuo 1 Hz iki 3,5 MHz ir nuo 100 ns iki 1 ms diapazonuose. Skyriuje įvertinama sistemos imitacinio modelio atitiktis eksperimentiniams rezultatams bei atliekami sukurtos sistemos *in vitro* elektroporacijos taikomieji tyrimai su *Candida albicans* grybų ląstelėmis.

Disertacijos tema paskelbti 6 moksliniai straipsniai: trys – recenzuojamuose mokslo žurnaluose, įtrauktuose į Clarivate Analytics Web of Science duomenų bazę, du tarptautinių konferencijų medžiagose, įtrauktose į Clarivate Analytics Web of Science „Conference Proceedings“ duomenų bazę, vienas – mokslo žurnale, referuojame kitose tarptautinėse duomenų bazėse. Disertacijoje atliktų tyrimų rezultatai buvo paskelbti dešimtyje mokslinių konferencijų.

Notations

Symbols

C	–	capacitance, F;
C_P	–	parasitic load capacitance, F;
C_s	–	snubber circuit capacitance, F;
f	–	pulse repetition frequency, Hz;
I_D	–	continuous drain current, A
I_{DM}	–	pulsed drain current, A
l	–	transmission line length, m;
L	–	inductance, H;
L_P	–	parasitic line inductance, H;
R	–	resistance, Ω;
R_{DRn}	–	driver circuit current limiting resistance, Ω;
R_{LIM}	–	maximum current limiting resistance, Ω;
R_{LOAD}	–	load resistance, Ω;
R_s	–	snubber circuit resistance, Ω;
t_D	–	pulse duration, s;
t_F	–	pulse fall time, s;
t_R	–	pulse rise time, s;
U	–	pulse voltage, V;

U_{max} – pulse maximum voltage, V;
U_{series} – pulse voltage in series delivery, V;
U_{min} – pulse minimum voltage, V;
Z – impedance, Ω;
τ – exponential decay time constant.

Abbreviations

AC – alternating current;
BJT – bipolar junction transistor;
C – capacitor;
D – diode;
DC – direct current;
DNA – deoxyribonucleic acid;
DR – switch driver;
FEM – finite element method;
IGBT – insulated-gate bipolar transistor;
L – inductor;
MOSFET – metal-oxide-semiconductor field-effect transistor;
nsPEF – submicrosecond and nanosecond pulsed electric field;
PCB – printed circuit board;
PEF – pulsed electric field;
R – resistor;
RNA – ribonucleic acid;
SiC – silicon carbide;
SPICE – simulation program with integrated circuit emphasis;
SW – switch;
V – power supply;
ZD – Zener diode.

Contents

[1] The annexes are supplied in the attached compact disc.

Introduction

Problem Formulation

Pulsed electric field (PEF) treatment, also called electroporation, has a growing interest in various applications. Due to the transdisciplinary nature of the scientific field, the selection of the PEF parameters is influenced by intended electroporation applications. For optimal effectiveness, the parameters like pulse amplitude, duration, electric field strength, pulse repetition frequency, pulse waveform and number of pulses must be carefully selected.

Most of electroporation protocols are designed for microsecond range devices, but there is a newly growing scientific interest in research of the high-power and high-frequency nsPEF due to the primarily non-thermal effects and ability to target cell internal organelles. In addition, capability to variate the pulse frequency in wide range offers the possibility to investigate electroporation effectiveness frequency dependence and develop new type of electroporation protocols. Lack of the available high-voltage and high-frequency electroporators is one of the main reasons, why the research and application area of submicrosecond range electroporation is still poorly addressed.

However, the recent progress of silicon carbide (SiC) MOSFETs has opened a new opportunity to apply SiC MOSFETs switches in the submicrosecond electroporation range, where the management of high-voltage pulses of several

kV range in high frequencies is required. This shortly resulted the new wave of the advanced MOSFET based nsPEF electroporators with adjustable pulse parameters. Nevertheless, the generation of higher amplitude pulses in nsPEF range is still complicated by the occurring oscillations. Thus, nearly 1/3 of newly developed devices still struggle with the quality of the pulse shape, while the pulse fall-time in most cases is dependent on the load.

Relevance of the Thesis

In different electroporation applications, the applied electric pulses can have different waveform and the individual pulse duration can range from several hundred picoseconds to seconds. Pulse amplitude can vary from several mV to several kV. The pulse repetition frequency – from Hz to a few GHz. Generation of such wide spectra of parameters with single electroporation system is not feasible and the different devices are used in for specific applications.

Among all applications, there is a growing scientific interest in research of the high-power and high-frequency submicrosecond and nanosecond (nsPEF) pulses. As a result, there are over 1500 references results on the high-voltage and high-frequency generators for electroporation in 2019 on Google Scholar. The number of references is steadily increasing and correlates with researchers' interest since 1990. Provision of the flexible high-voltage and high-frequency square-wave electroporation system, covering a wide and the least studied pulse parameters range, would allow to expend the experimental nsPEF electroporation research area and investigate of newly proposed concepts. It can be used to reach a deeper understanding of the individual pore formation process, which will allow better control and optimization of the electroporation protocols and, thus, the refinement of the biotechnological and biomedical methods.

Therefore, the results presented in this thesis provide bases for applied research and contribute to the better coordination of electroporation research work. The development of the high-frequency square-wave electroporation system will be used in further investigation of electroporation biomedical techniques and medical applications.

The Object of Research

The object of the research is high-frequency square-wave electroporation system.

The Aim of the Thesis

The aim of the thesis is to develop a high-frequency square-wave electroporation system by researching pulse transient and compensation circuits.

The Tasks of the Thesis

To solve the stated problem and reach the aim of the thesis, the following objectives are formulated:

1. To develop the simulation model for high-frequency square-wave electroporation system using by applying the best practices of transient process compensation and investigate the circuit parasitic elements influence on the generated pulse shape.
2. To propose the planar electrodes topology for single cell real-time manipulation and develop a model to investigate the electric field distribution and homogeneity.
3. To develop the prototype of the submicrosecond electroporation system and investigate the applicability for *in vitro* electroporation.
4. To compare the simulation results of a pulse forming circuit with the obtained experimental results and provide an uncertainty assessment.

Research Methodologyt

The numerical and experimental methods were applied in the development and application phases. Transient processes were investigated using numerical methods by application of SPICE model using LTspice program package. The electric field distribution analysis has been performed using finite element method provided by the COMSOL Multiphysics software package. A verification of the numerical results has been performed using experimental comparison and the statistical evaluation methods.

Scientific Novelty of the Thesis

The aspects of scientific novelty in the field of Electrical and Electronic Engineering are as follows:

1. Developed simulation model of submicrosecond electroporation system suitable for the transient processes and parasitic elements influence analyses.
2. Proposed planar electrode topology for real-time electroporation applications and developed simulation model suitable for the electric field distribution analyses.
3. Proposed control crowbar circuit ensures a load independent pulse fall time.
4. Developed electroporation system prototype, which can deliver adjustable square-wave electric pulses with a predefined amplitude (up to 3 kV), frequency (from 1 Hz to 3.5 MHz), pulse duration (from 100 ns to 1 ms).

Practical Value of the Research Findings

The developed novel submicrosecond high-frequency electroporation system can generate single and bursts of high-amplitude (up to 3 kV) square-wave electric pulses of variable duration (from 100 ns to 1 ms) and predefined repetition frequency (1 Hz to 3.5 MHz). The proposed synchronized controllable crowbar ensures a constant pulse rise and fall times, wich are independent from the load, thus highly relevant in electroporation research due to the accurate control of delivered energy.

The electroporator was successfully applied and tested in interdisciplinary experiments in Nature Research Centre (Vilnius, Lithuania) for the inactivation of the human pathogen *Candida albicans*. The test showed, that the new system is compatible with standard commercial electroporation cuvettes.

The proposed submicrosecond high-frequency square-wave electroporation system enables further study of the electroporation phenomenon in the least investigated electric field frequency and strength range.

The Defended Statements

1. The proposed simulation model of pulse forming circuit is suitable for transient processes analyses and provides generated electric pulse parameters results with uncertainty of ±21% (95.4% confidence level) for the submicrosecond pulse range.

2. The developed high-frequency square-wave electroporation system is capable to ensure 18 ns pulse fall time, which is independent from the load.
3. The developed pulse forming circuit ensures a delivery of adjustable up to 3 kV square-wave electric pulses with a predefined frequency (1 Hz to 3.5 MHz). The duration of the pulse can be varied in a range from 100 ns to 1 ms.
4. The proposed topology of the planar electrodes ensures more than 1 kV/cm strength and homogenic of electric field for single cell electroporation analyses.

Approval of the Research Findings

Research results are published in six scientific articles: three – in scientific journals included in Clarivate Analytics Web of Science database with impact factor (Novickij et al. 2016; Butkus, Tolvaisiene 2020; Butkus, Murauskas, et al. 2020), two – in international conference publications which are referred by Clarivate Analytics Web of Science database Proceedings (Butkus et al. 2017; Butkus, Tolvaisiene 2020), one article is printed in peer-reviewed scientific journal listed in Index Copernicus database (Butkus 2018).

Research results on the subject of the thesis have been announced in ten scientific conferences in Lithuania and abroad:

- 20th Conference for Junior Researchers "*Science – Future of Lithuania. Electronics and Electrical Engineering*". 2017. Vilnius, Lithuania.
- 60th international conference for students of physics and natural science "*Open Readings 2017*". 2017. Vilnius, Lithuania.
- VGTU Electronics Faculty cycle of seminars. 2017. Vilnius, Lithuania;
- 5th IEEE Workshop on "*Advances in Information, Electronic and Electrical Engineering (AIEE)*". 2017. Riga, Latvia.
- KTU PhD week "*What do PhD students do*?". 2018. Kaunas, Lithuania.
- Second International Conference "*Electrical, Electronic and Information Sciences – eStream 2018*". 2018. Vilnius, Lithuania.
- 21th Conference for Junior Researchers "*Science – Future of Lithuania. Electronics and Electrical Engineering*". 2018. Vilnius, Lithuania.
- 62th international conference for students of physics and natural science "*Open Readings 2019*". 2019. Vilnius, Lithuania.
- Third International Conference "*Electrical, Electronic and Information Sciences – eStream 2019*". 2019. Vilnius, Lithuania.

- 7th IEEE Workshop on "*Advances in Information, Electronic and Electrical Engineering (AIEE)*". 2019. Liepaja, Latvia.

Structure of the Dissertation

The dissertation contains: introduction, three chapters, general conclusions, list of references with separately presented list of scientific publications by the author and summary in Lithuanian.

The total scope of dissertation consists of 125 pages, where displayed 40 figures, 8 tables, 1 equation and 209 references are used.

Acknowledgements

This work was performed using the joint facilities of the High Magnetic Field Institute of Vilnius Gediminas Technical University (Vilnius, Lithuania), the Laboratory of Biodegradation Research of Nature Research Centre (Vilnius, Lithuania) and Laboratory of Microbiology at the Centre of Laboratory Medicine of Vilnius University Hospital Santaros Clinics (Vilnius, Lithuania).

I wish to express my deepest gratitude to my supervisor Assoc. Prof. Dr Sonata Tolvaišienė for her immense support to move forward. Special thanks are owed to Dr Vitalij Novickij and Dr Audrius Grainys for their remarkable help and advise received. I would also like to thank all my colleagues in the Department of Electrical Engineering and State Research Institute Center for Physical Sciences and Technology for all the time given to have valuable discussions on topics related to the dissertation. All the scientific, professional and specific competences I acquired during my PhD is the result of all of yours.

I am grateful to my family for support during these years.

1

Pulsed Electric Fields Generation and Application Review

This Chapter reviews the most relevant scientific literature related to the main subjects of this dissertation. The electroporation phenomena, frequency response of cells and effects of the submicrosecond and nanosecond pulsed electric fields (nsPEF) are introduced. The review of nsPEF generators and transient process compensation circuits are presented. Different approaches in development and application of electroporation systems have been observed. This Chapter concludes in formulating of main objective and tasks of the thesis.

Two scientific publications were published on the section topic (Butkus, Tolvaisiene 2020; Butkus, Murauskas, et al. 2020).

1.1. Electroporation Phenomena and Applications

High intensity pulsed electric fields (PEF) can trigger increased permeability of biological cells to exogenous molecules to which the cells were initially impermeable (Cemazar et al. 2018). PEF polarizes the cell membrane, which causes reorientation of lipids and formation of pores (Denzi et al. 2015; Dutta

et al. 2015), thus increasing molecular transport across the cell membrane (Bennett et al. 2014; Tsong 1991). In case of reversible electroporation (depends on pulse parameters), the cell membrane is then resealed (Sundararajan 2009). As a result, there is a variety of electroporation applications, which include cancer treatment (Miklavčič et al. 2014), gene delivery (Shi et al. 2018), food processing (Sitzmann et al. 2016), biorefinery (Golberg et al. 2016) and many other (Yarmush et al. 2014; Wagstaff et al. 2016). In each case, various PEF parameters are required, which establishes a challenge in generator design in terms of universality. The straightforward distribution of applications in the pulse amplitude–duration space is summarized in Figure 1.1 (Venslauskas et al. 2015; Miklavčič et al. 2017; Reberšek et al. 2010; Batista et al. 2016; Buchmann et al. 2019; Kotnik et al. 2019; Chopinet et al. 2013).

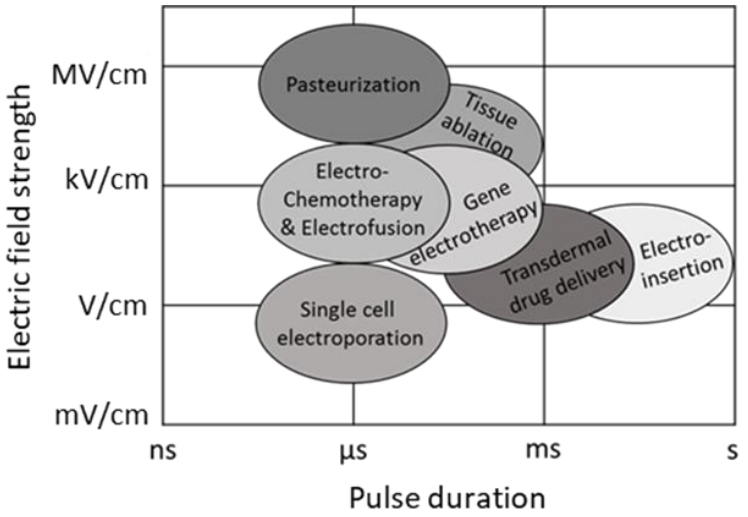

Fig. 1.1. Generalized representation of pulse parameters for different electroporation applications (Butkus, Murauskas, et al. 2020)

From figure above, it can be seen that the majority of applications lie in the micro-millisecond range. Indeed, the range of longer but lower amplitude pulses dominated the field for decades, however, in the recent years the number of works focusing shorter (submicrosecond and nanosecond) pulses increased significantly. The reason lies in the limitations of conventional microsecond range methodologies such as bioimpedance-dependent field distribution (Neal et al. 2012), Joule heating (Garcia et al. 2011), muscle contractions (Mi, Xu, et al. 2018), electrical breakdown (Guenther et al. 2015) and oxidative stress (Rodaite-Riseviciene et al. 2014). Nanosecond pulses cannot solve all the problems

completely, however, in many cases the negative factors are diminished. However, state-of-art pulsed power electronics are required for generators to form pulses up to tens of kV and hundreds of amperes in the nanosecond range. Therefore, the price and engineering complexity of such generators is high, nevertheless, the trends in applications of nanosecond PEF make it viable (Figure 1.2).

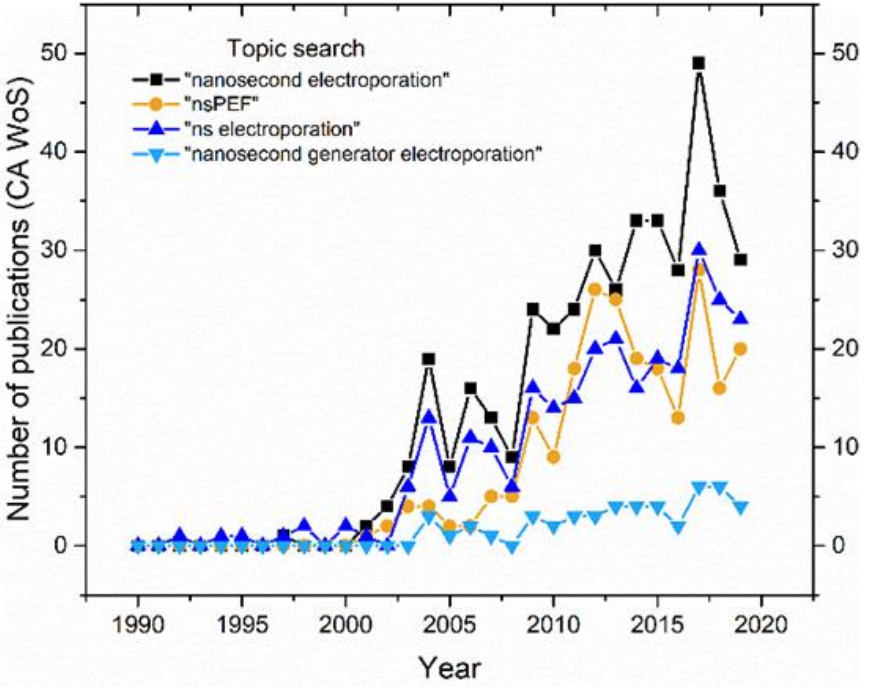

Fig. 1.2. The trends in the number of publications on the topics of nanosecond electroporation according to Clarivate Analytics Web of Science (2020-05-25) (Butkus, Murauskas, et al. 2020)

As it can be seen in Figure 1.2, there is a definitive rise in publications in the last decade, which partially is a consequence of better availability of pulse forming switches on the market. Development of laboratory grade generators for electroporation has intensified with the development of better semiconductors (i.e., silicon-carbide technology) (Das et al. 2012). Nevertheless, the number of papers focusing nanosecond pulse generators for electroporation is still low. A similar trend is observed in the frontier of short microsecond or sub-microsecond pulses using high frequency bursts (Figure 1.3), which possibly is a natural transition step from long micro-millisecond to the nanosecond range.

.

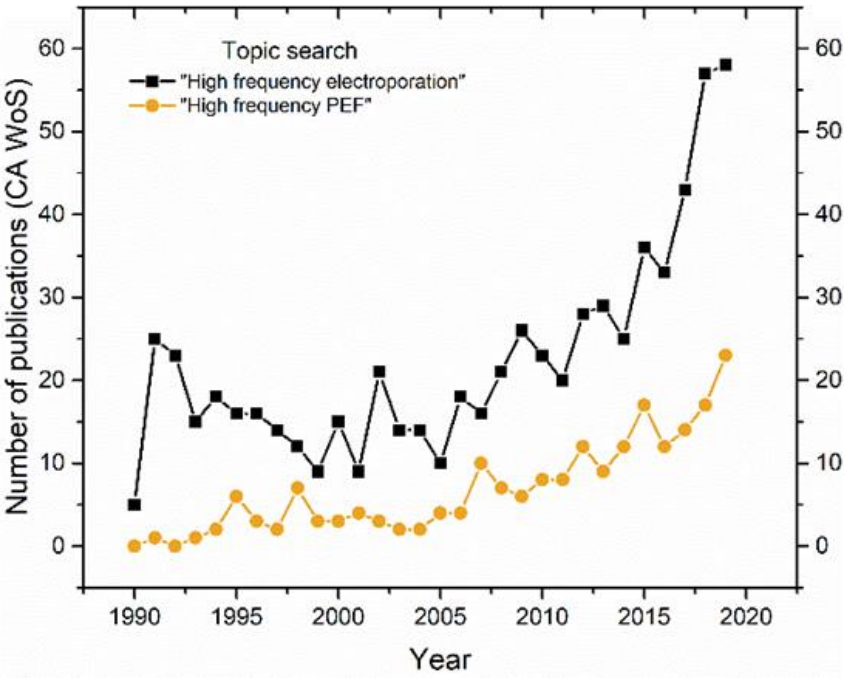

Fig. 1.3. The trends in the number of publications on the topics of high frequency electroporation according to Clarivate Analytics Web of Science (2020-05-25)(Butkus, Murauskas, et al. 2020)

Independently on the selected pulse range or electroporation application, for the optimal effectiveness of the treatment, not only the pulse amplitude and duration, but also other parameters like repetition frequency, waveform and number of pulses must be carefully selected. As a result, universality of electroporators is important when study of new phenomena and biological effects of PEF are established. Therefore, before selecting or developing any new electroporation system (also often called electroporator), all the required pulse parameters must be known in advance for desired applications, which in case of electroporation research is not trivial.

1.2. State of Art Requirements for Pulse Forming

To develop a flexible pulsed power device for electroporation of biological cells, the required parameters for the output electric pulse must be determined. Due to the transdisciplinary nature of the scientific field, the selection of the parameters

is influenced by biological processes that are induced in biological objects in high electric fields. Therefore, the pulse waveform amplitude, duration, repetition frequency and other output pulse parameters must be carefully selected in terms of their intended applicability in the experiments.

1.2.1. Waveform

There can be many pulse waveforms applied for the electroporation technique: square (rectangular), exponential decay and Gaussian or bell-shaped as represented in Figure 1.4. These pulses are monopolar, but the bipolar pulse configuration can be used as well.

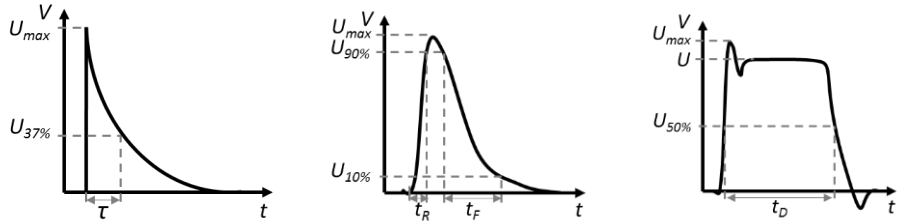

a) b) c)

Fig. 1.4. Pulse waveforms: a) Exponential decay pulse, where τ is the exponential decay time constant; b) Gaussian or bell-shaped pulse t_R and t_F is pulse rise and fall time accordingly measured between 10% and 90% of the pulse amplitude; c) square (rectangular) wave pulse, where t_D is pulse duration, measured at 50% of the pulse amplitude

It is essential to well define the pulse shapes and polarity as it is known to have an effect on the cellular response (Kotnik et al. 2003; Miklavcic et al. 2010). For instance, the pulse amplitude, rise-time and fall time of the bell-shaped voltage pulse are important and are recommended to be clearly specified (Cemazar et al. 2018). There are also several studies performed, which suggests, that the square-wave and exponential decay pulses have higher efficiency in comparison with other type of pulses (Chicaybam et al. 2017; Miklavcic et al. 2010).

For research activities, next to the application efficiency, it is necessary to control the experiment and precisely estimate the impact of the pulse to the biological load. In comparison with square-wave pulse, the exponentially decaying pulse (Figure 1.4) is more difficult to describe, because the exponential decay time constant is dependent on the impedance of a biological load, which is often unknown precisely, varies from sample to sample and is also dependent on the pulse delivery frequency (Reberšek et al. 2014; Bhonsle et al. 2018).

Moreover, the precise impedance of the biological load is often unknown. In some cases, to limit the exponential pulse decay dependence on the load impedance, the resistor could be connected in parallel to the load. However, it will reduce the overall efficiency of energy delivery to the biological load, since most of the energy would be disputed on the resistor instead. Furthermore, for higher range of experimental applications, the pulse shape should provide independency between the pulse amplitude and length. This is not achievable with exponentially decaying pulse with the same time constant, but different amplitude. As a result, the square-wave pulses are more common in the electroporation research applications.

The parameters characterizing the square-wave pulse are presented in Figure 1.5. Similar to the exponentially decaying pulse, the square-wave pulse fall time is also often dependent on the biological load impedance. However, in this case it can be solved with the pulse forming circuit design and proper application of transient process compensation circuits (e.g. with controlled crowbar circuits (Stankevic et al. 2020)).

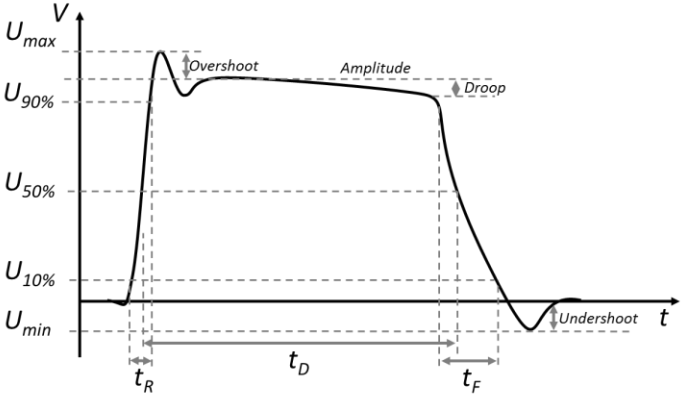

Fig. 1.5. The parameters characterizing the square-wave pulse

To sum up, the square-wave pulses are more practical to use in industrial or research activities, because it is more trivial to estimate impact of the pulse to the biological load and to control the experiment or application. Further in this work, more attention will be given to the application and development of square-wave pulses.

1.2.2. Pulse Duration

For electroporation application an individual duration of square-wave pulses is reported in range from approximately picoseconds to milliseconds. The submicrosecond (from picosecond to nanosecond) pulsed electric fields (nsPEF)

pulses are used to induce electroporation of an intracellular organelle while the integrity of plasma membrane in a biological cell remains intact (Semenov et al. 2015; Semenov et al. 2016; Mao et al. 2018; Pirc et al. 2019; Tang et al. 2020), while longer pulse up to milliseconds are used to enhance the transfer of large charged molecules (proteins, DNA, RNA) into the cells (Kulbacka et al. 2016; Cervia et al. 2018; Kašėta et al. 2020).

Although, more than two decades have passed since the first experimental *in vitro* study was reported with nsPEF pulses (Schoenbach et al. 1997), the nsPEF effects are still poorly studied, not entirely understood and uncommercialized (Pirc et al. 2019; Chalovich et al. 2012). One of the main obstacle for nsPEF application is the required complex experimental infrastructure (Novickij, Švedienė, et al. 2017). Indeed, due to very short pulses durations and required integrated with the high-voltages, it is not a trivial task to design and build a compact and successfully functioning nsPEF electroporation system, which could ensure high-quality pulse with minimum oscillations and reflections in the waveform (Pirc et al. 2019). As a result, most of electroporation clinical and experimental applications as well as commercially available electroporation systems are dominated with the use of pulse duration from tens of μs to tens of ms range, while the nsPEF is poorly covered.

To sum up, the individual pulse duration varies for different electroporation type in range from subnanoseconds to milliseconds. The different phenomena can be researched by applying differ duration pulses. The capability of pulse generator to produce pulses in a wide pulse duration range is important for wider research application range and higher flexibility. However, the conceptual PEF generators design for micro- and milli- second pulses differ from the ones design to deliver submicrosecond pulses. For this reason, some specific pulse duration range must be selected, which could cover the current gaps of electroporation research.

1.2.3. Number of Pulses and Repetition Frequency

In most cases, the series of pulses are applied for electroporation application. For instance, in almost all the electrochemotherapy treatments, eight pulses are applied instead of one (Silve et al. 2014). As another example, it has been demonstrated, that in case of irreversible electroporation, the transmembrane voltage threshold for a single 1 μs long pulse is 2.1 times higher in comparison with the bursts of 100 μs long pulses (Sano et al. 2015; Scuderi et al. 2019). In addition, number of studies have confirmed, that the effects of electroporation are not only depended on the number of pulses applied, but in general the electroporation is a frequency-dependent phenomena (Silve et al. 2014; Sano et al. 2014; García-Sánchez et al. 2018; Bhonsle et al. 2018; Novickij, Ruzgys, Grainys, et al. 2018; De Angelis et al. 2019). This dependence could be used to

increase the treatment efficiency as some additional studies, have suggested that high-frequency fields ranging from 500 kHz to 1 MHz are best suited to penetrate epithelial layers, since only a minor Joule heating is induced (Novickij, Ruzgys, Grainys, et al. 2018; Arena et al. 2011).

While some studies had proposed numerical methods to compare the permeability induced by the high-frequency monopolar and bipolar bursts of electrical pulses (Sweeney et al. 2016; Chiapperino et al. 2020), in general researchers notice that the available experimental contributions dealing with high-frequency electroporation (>0.5 MHz pulse repetition frequency range) are focusing mainly on the bipolar pulsing protocols, presumably due to the technological challenges of generating high-power and high-voltage monopolar MHz pulse repetition frequency (Novickij, Ruzgys, Grainys, et al. 2018). The coverage of research on the influence of pulse repetition frequency during monopolar electroporation is limited to the kHz range (Nesin et al. 2011; Lamberti et al. 2015; Steelman et al. 2016). The need for electroporation research at the MHz pulse repetition frequency range is still identified (Novickij, Ruzgys, Grainys, et al. 2018; Zou et al. 2015).

In fact, the researchers have suggested, that the high-frequency pulse burst can reach the threshold pulse repetition frequency, which supposed to be unique for each cell type and electroporation medium, since the induced transmembrane voltage relaxation (discharge) duration will be higher than the delay time between the pulses (Novickij, Ruzgys, Grainys, et al. 2018). In some previous studies, this electroporation saturation phenomenon was name cell sensitization and de-sensitization (Silve et al. 2014; Dermol et al. 2016; Muratori et al. 2016). More recent studies have investigated the relation between pulse number and the observed outcomes, which is complex and difficult to fully characterize. It was observed that the increased number of pulses always evolves to a saturation or at least a reduction in the electric field effects (García-Sánchez et al. 2019). These developments indicate the promising future for high-frequency (>0.5 MHz) electroporation systems. The new devices must be able to electroporation frequency manipulation, which is expected to lead to the more effective applications and achieve specific aims in electroporation protocols (Novickij, Ruzgys, Grainys, et al. 2018).

Following this overview results, it is indicative that the new system should be capable to produce unipolar pulses with wide range of frequency. There is a demand for the electroporation systems capable to cover the high-frequency range from 0.5 kHz to 1 MHz with adaptable number of repeated pulses. This capability can reflect the latest findings of the electroporation studies and contribute to further research of frequency dependence of electroporation phenomena.

1.2.4. Pulse Amplitude and Electric Field Strength

The electric field parameters depend on the geometry of the experimental system and on the heterogeneity of the sample (tissue or cell density) in terms of conductivity and permittivity (Cemazar et al. 2018). In general, the electric field strength for PEF applications ranges approximately from 0.1 kV/cm up to 100 kV/cm.

In the micro–millisecond range the electric field strength from 0.1 kV/cm to 10 kV/cm is sufficient for transfection (Kotnik et al. 2000; Buchmann et al. 2019). However, the usage of nsPEF requires the application of even higher electric field strength (up to 100 kV/cm) since the amplification of the external electric field in the cell membrane is frequency dependent and decreases in the sub-megahertz range (Kotnik et al. 2000; Zou et al. 2015; Silve et al. 2014; Novickij, Ruzgys, Grainys, et al. 2018). This indicates, that in case nsPEF pulses are used to trigger the induced transmembrane voltage, the applied voltage (using the same setup) could be hundreds times higher compared to conventional micro-millisecond protocols (Novickij, Ruzgys, Grainys, et al. 2018).

However, some studies also suggest, that the higher pulse repetition frequency (kHz range) might result the decrease of the electroporation efficiency (Steelman et al. 2016; Sersa et al. 2010). On the other hand, the generated Joule heating by the shorter length pulses increases the temperature only by few degrees and does not by itself cause hyperthermia effects (Chalovich et al. 2006) or create significant poration (Chalovich et al. 2012). As a result, the most efficient electric field strength selection depends on other pulse parameters, the biological cell parameters and the protocols applied.

It was already indicated above, that the new electroporation system is intended to be applied for the *in vitro* electroporation research. The *in vitro* electroporation of organelles, bacteria or yeasts require even higher voltage (Rebersek et al. 2011) than in comparison during *in vivo* research. For instance, a well-established protocol for the *in vitro* electroporation of the mammalian cells is to use a burst of microsecond pulses (e.g. 8 pulses of 100 μs duration) in the kV/cm PEF range (Gowrishankar et al. 2006; Moisescu et al. 2013; Son et al. 2016). To generate such the electric field intensity, high pulse voltage amplitude is required if standard 1 mm electroporation cuvettes are used. The electric field homogeneity is also an important factor. In case new type of electrodes are applied, it is additionally recommended to evaluate the electric field distribution via numerical modelling (Cemazar et al. 2018).

To sum up, the design electroporation systems must be compatible with standard 1 mm electroporation cuvettes. The pulse amplitude must be adjustable and able to reach few kV, which would ensure the sufficient (tens of kV/cm) electric field strength.

1.2.5. Result of the State of Art Requirements for Pulse Forming

Due to the transdisciplinary nature of the scientific field, the selection of the PEF parameters is influenced by intended electroporation applications. In this section, the summary of PEF parameters is provided and presented in Table 1.1, which is based on the state of art analyses of electroporation applications described above.

Table 1.1. The summary of the state of art requirements for pulse forming

Pulse parameter	Scientific demand
Pulse waveform	Square-wave
Pulse duration	From ns to ms
Pulses repetition frequency	From Hz to MHz
Number of pulses	From single to hundred
Electric field strength	Tens of kV/cm
Pulse amplitude	Adjustable and up to few kV

For the electroporation scientific research, it is essential to have good control of the pulse energy, which is ensured if the square-wave pulse is used. The device must be capable of generating repeated electrical pulses of identical form independent of the load type, which is relevant in electroporation experiments.

The most of electroporation protocols are designed for microsecond range devices, while there is a scientific interest in research of the high-power and high-frequency nsPEF pulses due to the primarily non-thermal effects and ability to target cell internal organelles. Therefore, to be able to cover most of the electroporation applications as well as to support the demand of the electroporation research, this work will focus on the develop of the high-frequency electroporation system, which can generate single and burst of PEF pulses of variable duration from microseconds to submicroseconds (nsPEF). This range of PEF pulse duration would ensure that the device is flexible and therefore applicable in a wide area of the experimental applications.

The efficiency of electroporation application can be dependent on the pulse frequency. To be able to investigate the electroporation frequency dependence and propose new electroporation protocols, the device should be capable of altering the pulse frequency over an extensive range. Thus, it was decided that the PEF frequency range must be adjustable from Hz to MHz range.

The high-frequency pulse burst can reach the threshold pulse repetition frequency, which supposed to be unique for each cell type and electroporation medium, since the induced transmembrane voltage relaxation (discharge) duration will be higher than the delay time between the pulses (Novickij, Ruzgys, Grainys,

et al. 2018). Hence, the designed system should be able to produce single as well as a wide range of burst pulse (up to hundred). This capability can reflect the latest findings of the electroporation studies and contribute to further research in this area.

The selection of a short pulse duration means, that the trade-off with the PEF amplitude must be made (Schoenbach et al. 2015; Rems et al. 2016; Leguèbe et al. 2014). A short pulse duration (in range of nsPEF) increases the required electric field strength needed to reach the transmembrane voltage threshold due to the amount of energy involved. Consequently, the application of submicrosecond pulses requires an electric field strength of at least tens of kV/cm. In the case wherein standard 1 mm electroporation cuvettes are planned to be used. As a result, a high-voltage power supply (in the range of at least 2–3 kV) should be applied to reach a sufficient electric field strength described before. However, as the overall aim of a variable and controllable PEF typically remains. Due to this, the pulse forming circuit should be able to deliver adjustable power PEF pulses with a voltage level ranging from up to few kV.

The described requirements impose additional consideration for the current control. The usual biological loads vary from 50 Ω to 500 Ω during experimental applications. In case of the maximum amplitude of high-voltage pulses, the pulsed electric current might reach tens of amperes. The device must be able to withstand high currents. However, other than nsPEF applications, the high-energy pulses are rarely used, because of the Joule heating, which takes place due to the high current flow and negatively impact the electroporation process (Pliquett et al. 2014).

1.3. The Principle Circuits for Pulse Generators

For electroporation research it is essential to have a pulse generator suitable to deliver controllable energy to biological tissue via application of repetitive electrical pulses with the predefined pulse waveform, voltage amplitude and pulse widths. The pulse forming circuits of the electroporator can be based on relatively simple circuits, which are discussed in the following works (Reberšek et al. 2014; Puc et al. 2004; Bernal et al. 2015; Redondo 2017; Pirc et al. 2017; Schoenbach et al. 2010; Rebersek et al. 2011; Behrend et al. 2003; Reberšek et al. 2010; Lucia et al. 2019) and summarized in this section. The energy delivery can be provided by capacitor, inductor or transmission lines with the control of the switching element. These circuits can be enhanced by the application of modular approach, application of transformers, diodes or even by merging two concepts into a hybrid one. In this section, the common designs of pulse forming circuits used for electroporation application are presented and discussed.

1.3.1. Capacitor Discharge Pulse Generator

A direct capacitor discharge pulse forming circuit concept is one of the most common, simple and oldest concepts for PEF pulse forming (Schmitt et al. 2019; Reberšek et al. 2010). It is based on the transfer of energy stored in the capacitors into the load throughout well-defined voltage pulses. The pulse delivery is normally controlled with a semiconductor switch. Depending on the switch type or driving mode, the waveform is either square (using metal–oxide–semiconductor field-effect transistors (MOSFETs) and insulated-gate bipolar transistors (IGBTs) (Rubin et al. 2019)) or exponential decay wave (older concept typically used with thyristors (Ping et al. 2003)). In case of exponential decay pulses, the duration of the pulse (decay time) is defined by RC parameters of the discharge circuit, while in the case of square-wave pulses the parameters are mostly limited by the switch capabilities and the discharge capacitor value. The principle pulse forming circuit of capacitor discharge pulse generator is represented in Figure 1.6.

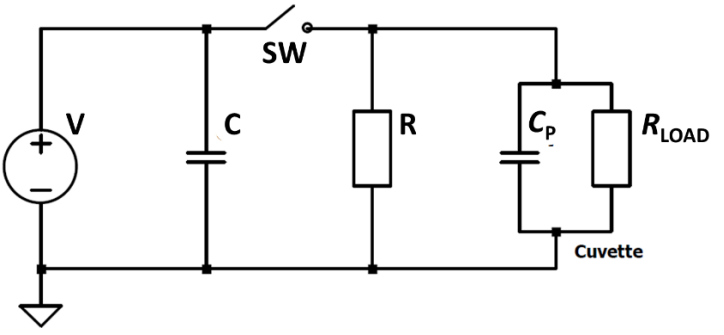

Fig. 1.6. The principle circuit of a direct capacitor discharge pulse generator (Butkus, Murauskas, et al. 2020)

As it can be seen in Figure 1.6, the capacitor discharge pulse generator is composed of a variable high-voltage power supply V, a discharge capacitor C, a switch SW and optionally a resistor R. The direct capacitor discharge circuit topology benefits from a simple and inexpensive design (Rebersek et al. 2011; Schmitt et al. 2019). However, to ensure the square-wave delivery and limiting the pulse amplitude droop, a high capacity (μF to mF range) capacitor bank is required and the switch must withstand the full voltage amplitude. It limits the selection of available switches in case of high-voltage builds. In such a case, several series switches must be used, which results in increased complexity of the generator due to challenges in switch synchronization.

To overcome the limitations of the direct capacitor discharge concept, a more complex modular circuit topology can be used (A. A. Elserougi et al. 2016). It provides voltage distribution between several switches and gives additional flexibility for the output pulse shape and amplitude. A simple example of a modular structure is presented in Figure 1.7.

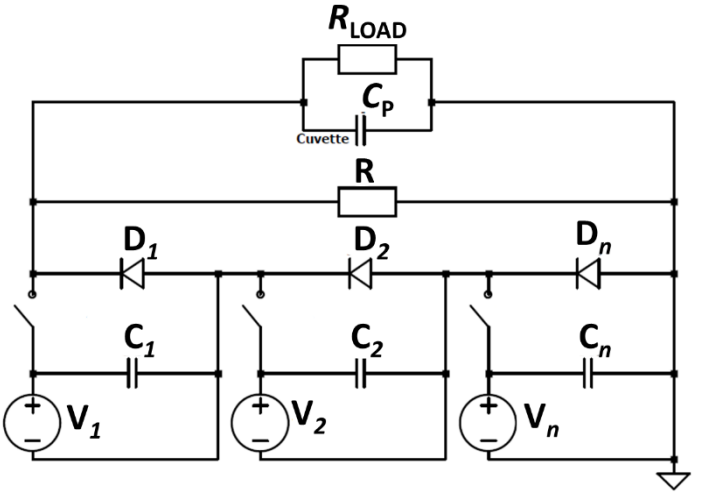

Fig. 1.7. The principle circuit of modular direct capacitor discharge pulse generator (Butkus, Murauskas, et al. 2020)

The modular direct capacitor discharge pulse forming circuit includes several galvanically isolated high-voltage power supplies V_1, V_2, …, V_n. Each is controlled individually and can be set to a different amplitude. The voltages of the individual circuits contribute to the generation of a single output pulse at any time. The output voltage will be the sum of the voltages from separate stages, so adjusting the output voltage is possible. However, many stages are required to have enough output voltage levels, which consequently increases the cost of the device (Redondo 2017; Rebersek et al. 2011).

Other popular design of modular direct capacitor discharge pulse forming circuits is a Marx generator topology, which is an example of a modular circuit, however, due to high applicability is often separated as an independent circuit topology. Originally it was developed to test power grid high-voltage components and provide a capability to produce high-voltage pulses using a low-voltage DC supply. This circuit topology has been adopted for PEF generation and widely used in electroporation applications (Elgenedy et al. 2019; Sack 2017). The simplified circuit is represented in Figure 1.8.

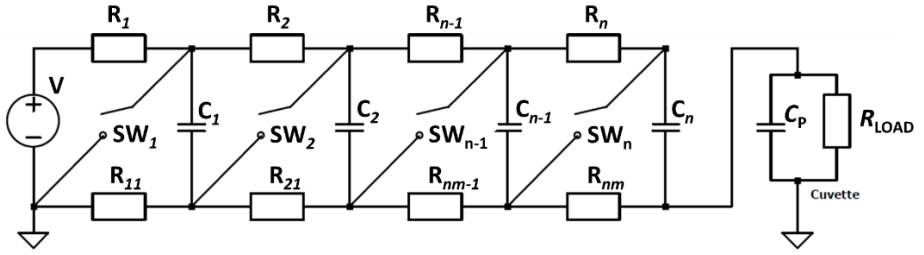

Fig. 1.8. The circuit of pulse generator based on Marx circuit topology (Butkus, Murauskas, et al. 2020)

As it is seen from the figure above, the full Marx circuit topology is based on separate stages/cells, where each stage has an energy storing capacitor C, two resistors R and a switch SW. The stages are charged in parallel from a direct current power supply V and subsequently connected in series with a load when the switches are triggered. In case of spark gaps the capacitors are fully discharged (decaying pulse), however the current and voltage flexibilities are high. For such a design, the pulse repetition rates are frequently in the order of several Hz, but the total charging voltage can reach tens or even hundreds of kV (Camp et al. 2008; Foshee et al. 2007; Hahn et al. 2001). The voltage levels between 50 and 100 kV are most commonly used in industrial application (Sack et al. 2010; Sack, Mueller 2017). In case when the semiconductor switches are used, a partial discharge of the capacitors can be achieved. The output voltages are frequently determined by the switch breakdown voltage and the number of stages, however, devices in the range of 1–6 kV are common (Muratori et al. 2016; Sack 2017; Redondo 2017).

In case the bipolar pulses are required to optimize the electroporation applications (e.g., food products treatment) (Wandel et al. 2016; Kurcevskis et al. 2020), the direct capacitor discharge pulse generator concept can be enhanced with half-bridge or full-bridge circuit (Cronjé et al. 2013) as presented in Figure 1.9.

In both cases the generator can produce positive and/or negative high-voltage pulses. However, the half bridge circuit topology has limitations in operation with capacitive-type of loads, hence full-bridge concept is more common. The increase of the number of the switches in a full-bridge concept brings additional operational flexibility similarly to the direct capacitor discharge circuit topology. Moreover, to enhance the pulse control and scalability several half-bridge or full-bridge pulse forming circuits can be stacked in a modular approach (Abdelsalam et al. 2017; Elgenedy et al. 2019; A. Elserougi et al. 2016). Additionally, Marx

generators can be arranged in a bridge configuration to enable the generation of bipolar pulses (Dong et al. 2017; Sack 2017; Elgenedy et al. 2019).

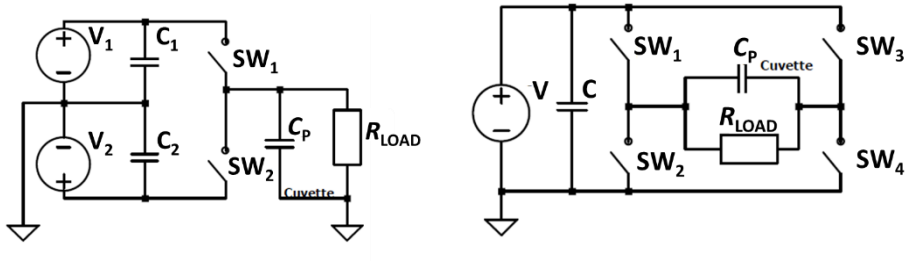

a) b)

Fig. 1.9. The conceptual circuits of direct capacitor discharge pulse generators: a) bipolar half-bridge; b) full-bridge (Butkus, Murauskas, et al. 2020)

Nevertheless, independently on the topologies described above the capacitor discharge circuits are limited by switching dynamics of semiconductor devices, thus the minimal pulse durations are typically in the sub-microsecond range. In order to form shorter pulses (i.e., less than 100 ns) other electroporator topologies are required.

1.3.2. Pulse Forming Circuit Topology Based on Transmission Lines

The other group of pulse forming circuits is based on the charge and discharge of the transmission lines. This is a common type of circuit topology for generation of high-voltage pulses with less than 100 ns duration (Redondo 2017; Deshpande et al. 2019). As illustrated in Figure 1.10, the pulse forming circuit is composed of coaxial cable, which is used as a conductor of length *l* and charged through a resistor R to a voltage V. The transmission line discharge and pulse forming are controlled by the switch SW.

In order to form square-wave pulses the impedance of the load must match the characteristic impedance of the transmission line. However, load matching requirement by design limits the generator's compatibility with dynamic loads since the impedance of the transmission line is dependent on the parameters of the cable. The pulse amplitude of a single transmission line generator is limited to the half of the power supply voltage, while two or more lines must be used to match the pulse amplitude voltage to the power supply voltage (Figure 1.11).

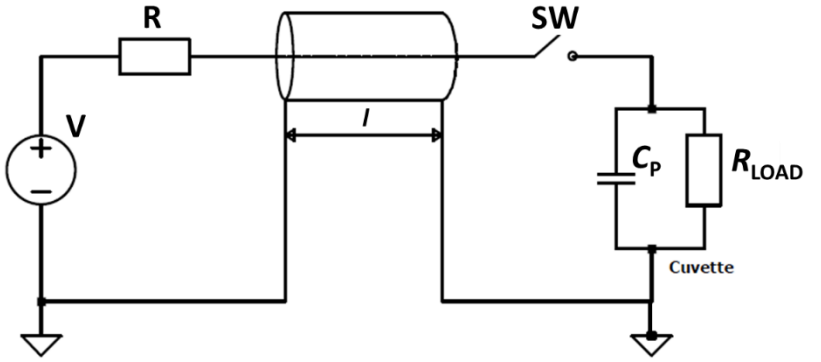

Fig. 1.10. The conceptual circuit of a transmission line pulse generator (Butkus, Murauskas, et al. 2020)

This type of configuration is known as a Blumlein transmission line pulse generator. Blumlein pulse generator is one of the most popular designs for the generation of square-wave high-voltage nsPEF pulses (Mi, Zhang, et al. 2016; Mi, Wan, et al. 2016; Mi et al. 2017). The generator is based on the two transmission lines of identical length *l*. Both transmission lines are electrically connected at one end to a load and discharged by closing the switch. If the load is mismatched (i.e., the load resistance is larger or smaller than the transmission line impedance), reflections of the voltage step at the load and at the open end of the transmission line will lead to a strain of consecutive decaying pulses (Romeo et al. 2013; Kolb et al. 2006; Schoenbach et al. 2010). Hence, to generate square-wave pulse without any pulse reflections, the impedance of the load must be twice the impedance of the transmission line. This is not always an easy task to achieve, since the electrical impedance of biological tissue is often unknown, can vary from sample to sample and can be even dynamic during the pulse delivery (Warindi et al. 2017; Rebersek et al. 2011).

The control of pulse duration in a Blumlein circuit is non-flexible. It is defined by the length of the transmission line and the dielectric between the conductors, while the switch-off time determines the rise time of the generated voltage pulse. When the switch is closed, a voltage pulse is generated across the load for the time it takes the voltage step to propagate along the transmission line (Schoenbach et al. 2010). The switching element must withstand full high-voltage, which can be a challenge. On the other hand, in case of a spark gap switch, the output amplitudes can reach tens or hundreds of kV and a few kA.

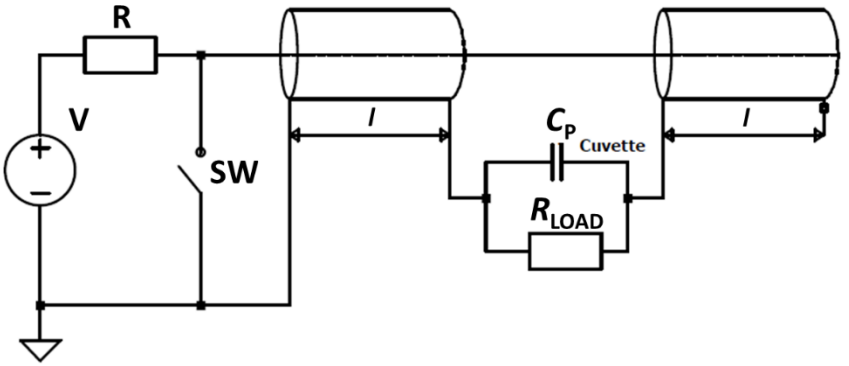

Fig. 1.11. The conceptual circuit of a Blumlein pulse generator (Butkus, Murauskas, et al. 2020)

Lastly, the Blumlein generators are large dimension devices and have high demands for the electrical components. The usual concepts have a relatively short lifetime and operate in low repetition rate, while a square-wave pulse is typically delivered with a jitter (Romeo et al. 2013; Rebersek et al. 2011). However, with the latest modifications, Blumlein generators can now generate also a high-frequency (range of up to few MHz) output pulses with variable duration, amplitude and even polarity (Mi, Zhang, et al. 2016; Rebersek et al. 2009; Romeo et al. 2013; Rebersek et al. 2011).

1.3.3. The Inductive Energy Discharge Pulse Generators

The third group of pulse generators is based on inductive energy discharge circuits, which transfer energy stored in the magnetic fields of coils into well-defined voltage pulses. The circuit concept is shown Figure 1.12.

The generator uses an AC power supply, a low voltage capacitor bank C for a primary electric energy storage and an inductor for secondary magnetic energy storage. When the switch SW1 is closed, the electric energy is discharged from the capacitor bank C into the inductor L. Hence, during the first quarter period of the sinusoidal AC-current, the magnetic energy stored in the inductor increases and the electric energy stored in the capacitor bank decreases. At the peak of sinusoidal current, the magnetic energy stored in the inductor reaches its maximum. At this point, the opening switch SW2 is activated and the current is abruptly interrupted influencing high rate of change of the magnetic flux (dB/dt). Such a transient process induces voltage in the inductor, which is further discharged by a spark gap through the load (Lindblom 2006).

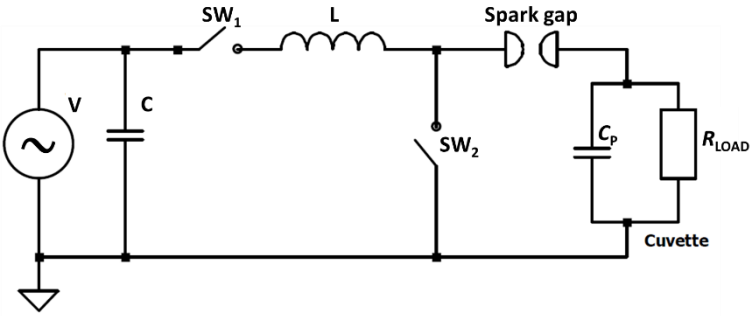

Fig. 1.12. The conceptual circuit of an inductive energy discharge pulse generator (Butkus, Murauskas, et al. 2020)

The inductive energy discharge pulse generator has many drawbacks and is not used for electroporation research. Instead, improved circuits are applied (i.e., the diode opening switch (DOS) circuit topology). This is a commonly used concept for generation of high voltage (several kV) pulses in the nsPEF range (Pirc et al. 2019). The diode opening switch circuit is presented in Figure 1.13.

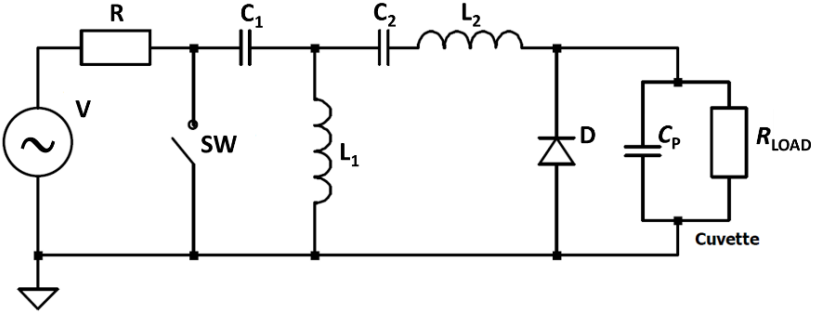

Fig. 1.13. The conceptual circuit of a diode opening switch generator (Butkus, Murauskas, et al. 2020)

The DOS circuit is based on the DC voltage power supply V, which charges the capacitor bank C1 through the resistor R. When the capacitor is fully charged, the switch SW is closed and the energy in the capacitor C1 starts circulating in the resonant network (C1, C2, L1 and L2). After completing half of the period, the resonant network starts pumping the current through the diodes in the reverse direction. Ideally, the diode abruptly stops conducting and commutates the L2 current into the load. Therefore, this type of circuit is based on the saved energy transfer from inductor L2 to the load with a good repeatability (Pirc et al. 2019).

Beside the application of diodes, it is also common that the inductive energy discharge pulse generator can be improved with the step-up pulse transformer. In this case the amplitude of the voltage pulse did not affect the opening switch (Redondo 2017). A simplified transformer-based pulse forming circuit is presented in Figure 1.14. The generator produces positive voltage pulses in the load.

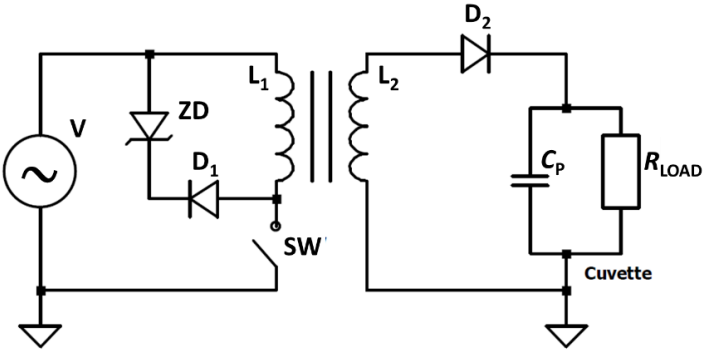

Fig. 1.14. The conceptual circuit of a transformers based pulse generator (Butkus, Murauskas, et al. 2020)

Despite the advantages, the transformer-based pulse generator also has several issues, like core saturation, reset time after pulse delivery and more often the distorted pulse shape because of higher effects of the parasitic circuit elements. All these issues must be considered during the design of the pulse forming circuit (Redondo 2017). On the other hand, the transformer based circuit topology can be combined with the modular approach discussed before providing additional flexibility and pulse control (Darwish et al. 2019). This topology, and all others discussed before, can also be coupled with half-bridge and full-bridge circuits to enable bipolar pulse generation.

1.3.4. Summary of Conceptual Pulse Generators

The presented concepts of pulse generators demonstrate the diversity of techniques used for high-voltage pulse generation suitable for electroporation applications. All the techniques are summarized in the Figure 1.15.

As it can be seen from the Figure 1.15, following the principle used for the energy storage, the pulse generators discussed above can be divided into three groups: direct capacitors discharge, transmission line discharge and inductive storage discharge. Each has advantages and disadvantages (Reberšek et al. 2010; Bernal et al. 2015; Redondo 2017; Rebersek et al. 2011; Davies et al. 2019), which

are summarized in the Table 1.2. It is also common, to use hybrid concepts, which would result the better performance of these devices and would allow to overcome the limitations imposed by a single concept.

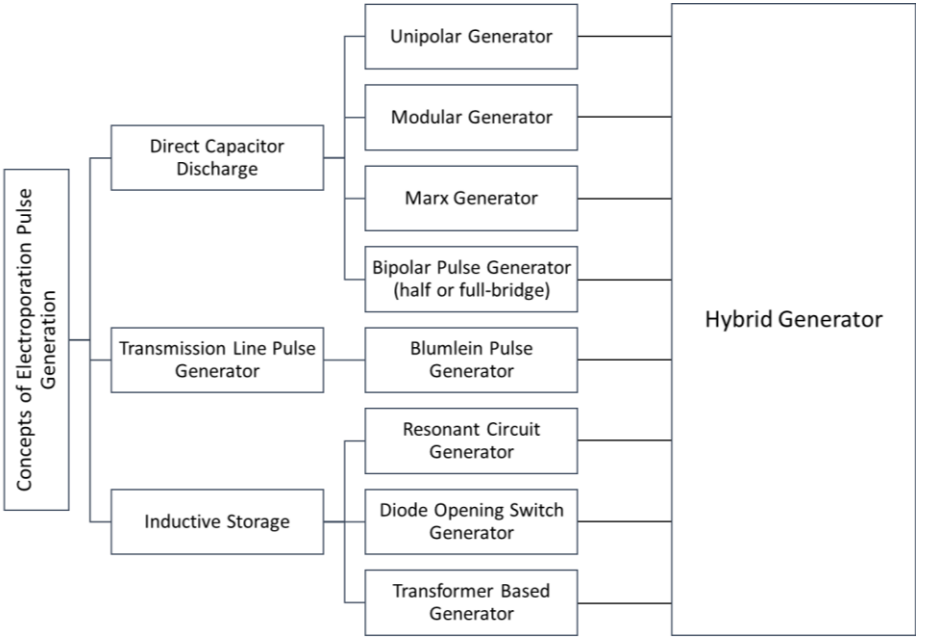

Fig. 1.15. The conceptual diversity of pulse generators for electroporation applications (Butkus, Murauskas, et al. 2020)

There is high diversity of techniques used for the development of the PEF generators for electroporation applications. Some are well commercialized and a first comprehensive list of commercially available electroporators has been collected in 2004 (Puc et al. 2004), which was later updated in 2010 (Reberšek et al. 2010) and in 2017 (Pirc et al. 2017). It can be seen, that commercial approach had followed the most common demands of electroporation application. As a result, most of commercial electroporators were developed with the pulse amplitude up to few kV and duration from tens of μs to seconds. In comparison, the selection of commercial high-voltage nanosecond or submicroseconds Pulsed Electric Field (nsPEF) electroporators is significantly lower (Pirc et al. 2017).

Table 1.2. The comparison between conceptual pulse generators for electroporation applications (Butkus, Murauskas, et al. 2020)

Concept			Advantage	Disadvantage
Direct Capacitor	Non-Modular	Unipolar	Simple and inexpensive construction for systems up to 1 kV; Very flexible pulse shape control in the sub-microsecond–millisecond range; Can operate in a high frequency range.	High-voltage supply required; Amplitude droop during the pulse; High capacity capacitor banks are required for square-wave delivery into high loads; Switch must withstand full voltage amplitude or complex synchronization circuits are required; Not yet suitable for sub-100 ns pulses.
		Bipolar	Positive and/or negative high-voltage pulses; Highest pulse forming flexibility; Capability to use asymmetrical pulses; Wider application capabilities.	Switch synchronization is needed; Complex control systems; Limited voltage handling capability; Not suitable for sub-100 ns pulses.
	Modular		Applicable with low voltage switches and voltage supplies; Wide flexibility of pulse parameters; Arbitrary signal shape; Easy to achieve high currents; Can operate in high frequency range.	Limited amplitude resolution; Complex control system; Switch synchronization is needed; Not suitable for sub-100 ns pulses.
	Marx Generator		Applicable with low voltage switches and voltage supplies; High voltages up to hundreds of kV; High currents; Can generate sub-100 ns pulses.	Bulky structure; Voltage droop is common when high loads are used; Limited high frequency capability; Electrode degradation in case of spark-gaps.
Transmission line	Blumlein		Simple design; Commonly used for short pulse generation (sub-100 ns); High-voltages and currents; Can be used for bipolar pulses	Load impedance matching requirement; Pulse width inflexibility (limited to transmission line); Relatively short lifetime; Most of the usual concepts operate in low repetition rate; Big dimensions of the generator.
Inductive Storage	Resonant Circuit		High energy density pulsing can be ensured.	Not applicable for electroporation directly; Parasitic parameters affect the waveform; Switch synchronization is needed; Complex control system.
	Diode Opening Switch		High energy density; Accessible electrical components; Variable load impedance; Commonly used for short pulse generation (sub-100 ns); Fast repetition frequency.	Complicated design; Low output power; Switch synchronization is needed; Complex control system; Complex switching and poor control of pulse durations.
	Transformer based		High pulse amplitude; Applicable with low voltage switches; Flexible pulse amplitude.	Transient processes have higher effects on pulse waveform; Core saturation and reset after pulse.

Also, it is common, that the commercial devices have limited range of available pulse durations and repetition frequencies, thus limiting device application flexibility. This is one of the main reasons, why the commercial electroporators are also not perfectly suited for electroporation research applications, where a wide parameters selection is desired. To sum up, the there is a growing scientific demand for submicrosecond and high-frequency electroporators, which can, but are not limited, to deliver submicrosecond range adjustable energy pulses. To cover the demand, the researchers develop in-house electroporators (Pirc et al. 2019; Elgenedy et al. 2019; Sack 2017; A. Elserougi et al. 2016; Stankevic et al. 2020). While the up to date review of commercial available PEF generators is available (Pirc et al. 2017), there is only one (at our knowledge) extensive overview of in-house built submicrosecond and nanosecond and high-frequency electroporators (Butkus, Murauskas, et al. 2020). Currently, the works are mainly focused on the review of the general topologies used for generator design (Bernal et al. 2015; Elgenedy et al. 2018; Xiao et al. 2018; Butkus, Tolvaisiene 2020; Rebersek et al. 2011; Redondo 2017; Elgenedy et al. 2019; Behrend et al. 2003; Lucia et al. 2019).

Further, the in-house built nsPEF generators were analysed and classified based on the switching type. The review focused only on nsPEF pulse generators, which were reported specifically for the application in the field of electroporation. We have included only the references where the reported duration of the pulse is in the sub-microsecond range (below 1 μs). In total 63 nsPEF generators for electroporation matched the requirements and are listed in Table 1.3 including the one later deigned, presented and discussed in this work. The devices are grouped based on the pulse forming circuit with the following parameters reported: pulse form, pulse duration, maximum pulse amplitude, pulse repetition frequency, switch type, switch model and additional remarks on the pulse form and circuit topology in case the divergence from the usual performance is noticed.

1.4. Classification In-House Built Generators for nsPEF Electroporation

It was identified, that the traditional transmission line (including Blumlein-type) pulse forming circuits are no longer dominating in the nsPEF electroporation applications. The progress of semiconductor technologies enabled the development of cost effective, small-size and flexible sub-microsecond generators based on direct capacitor discharge circuit topology. The Marx generator circuit topology with new ultra-fast semiconductor switches forms a new leading technology trend now. In addition, there were few successful attempts to develop resonant-circuit nsPEF generators, which at the end were not followed by other

researchers. Unpopularity of this circuit topology is driven by the limited pulse duration flexibility and resulting Gaussian pulse shape.

All topologies demonstrate the possibility to produce high-voltage pulses, however, the transmission line (including Blumlein-type) topologies, which use spark gap switches, demonstrate a possibility to produce very high amplitude (peak voltages exceeding 10 kV) nsPEF square-wave pulses. Yet there is complexity associated with these designs and recent developments of Marx-bank (Liu et al. 2019; Zeng, Yao, et al. 2020) and other direct capacitor discharge circuits (Novickij et al. 2014) indicate the growing availability of the off-the-shelf components fulfilling the high-voltage pulse delivery requirements. It is expected that the transmission line topologies will be pushed out of the sub-microsecond range due to a lack of flexibility, requirement of impedance matching and distorted waveforms. These drawbacks are not associated with the reported direct capacitor discharge circuits (including Marx-bank). However, the sub-100 ns pulses in the range of tens of kV are still yet hardly achievable by the direct capacitor discharge technology.

Indeed, for the high-voltage sub nsPEF pulse delivery, the switch performance and characteristics are crucial. The spark gap switches are fast and cost-effective for nsPEF generation, but these switches have a short lifetime due to electrode erosion, poor pulse duration control and can be frequently associated with turn-on jitter (Xiao et al. 2018). In contrast, the semiconductor switches offer high flexibility of pulse control, but are more constrained by high-voltage or current withstand limits as well as switch opening and closing times. A series connected switches can solve high-voltage limitation issues, but this increases the stray inductance, which is making the circuit slower.

One of the latest comparison between typical MOSFET, IGBT and bipolar junction transistor (BJT) switches was made in 2019 (Davies et al. 2019). It was demonstrated that all three could ensure the breakdown voltage (collector–emitter or drain–source voltage) higher than 1 kV. However, the BJT switches, which among all would be the most cost-effective option, are slower than MOSFETs or IGBTs and cannot fulfil the nsPEF pulse forming requirements. It was demonstrated that only the high power MOSFETs can form pulses within the 100–300 ns range with the transition times (rise and fall time) faster than 100 ns (Davies et al. 2019). More than a half of reported nsPEF electroporators (Table 1.3) use the MOSFET switch as a main pulse forming component.

The review indicates that the direct capacitor discharge topology is taking a lead in the nsPEF applications when the sub-microsecond pulse is required. In addition, the MOSFET switches are now the main technology to produce high-voltage nsPEF pulses in various circuit topologies. The spark gap switches are still applicable in case of a very high-voltage amplitude or ultra-short pulse duration (a few nanoseconds) (Kolb et al. 2006).

Table 1.3. List of in-house developed nsPEF generators for electroporation application

	Reference	Pulse form	Polarity	t_D	U_{max}	f	Switch	Remarks
Blumlein-type	(Deng et al. 2000)	Gaussian	Unipolar	8 ns	30 kV	-	Spark gap	Pressurized switch
	(Behrend et al. 2003)	Gaussian	Unipolar	3–15 ns	>10 kV	-	Spark gap	Erratic pulse shape
	(Kolb et al. 2006)	Square	Unipolar	10 ns	40 kV	-	Spark gap	Erratic pulse shape
	(Kolb et al. 2006)	Square	Unipolar	10–300 ns	1 kV	0–50 MHz	MOSFET	-
	(Foshee et al. 2007)	Gaussian	Unipolar	50 ns	65 kV	10 Hz	Spark gap	Distorted pulse shape
	(Kolb et al. 2008)	Square	Unipolar	8–300 ns	1 kV	-	MOSFET	-
	(Rebersek et al. 2009)	Square	Unipolar & bipolar	20, 50, 75, 150, 230 ns	<0.3 kV	0–1.1 MHz	MOSFET	High pulse amplitude droop
	(Pavliha et al. 2011)	-	-	40–200 ns	1 kV	0–100 kHz	-	No pulse shape
	(Romeo et al. 2013)	Gaussian	Unipolar & bipolar	10, 20, 60 ns	2 kV	-	Transistor	Erratic pulse shape
	(Chuan et al. 2014)	Gaussian	Bipolar	2 ns	650 kV	-	Oil switch	Hybrid with resonant
	(Mi, Zhang, et al. 2016)	Square	Unipolar	50–100 ns	2 kV	0–(~3) kHz	MOSFET	Erratic pulse shape
	(Mi, Wan, et al. 2016)	Square	Unipolar	100 ns	1.7 kV	0–(~3) kHz	MOSFET	Erratic pulse shape with long tail; Modular circuit
	(Mi et al. 2017)	Gaussian	Unipolar	20 ns	2.5 kV	0–10 kHz	MOSFET	-
	(Mi, Bian, et al. 2018)	Gaussian	Unipolar & bipolar	30 ns	10 kV	0–200 kHz	MOSFET	Modular; Erratic pulse shape
	(Achour et al. 2019)	Square	Unipolar	30 ns	4 kV	1 kHz	IGBT & spark gap	Erratic pulse shape; With transformer
	(He et al. 2020)	Square	Unipolar	5 ns	0.5 kV	0–10 MHz	MOSFET	Fixed pulse duration

Continued Table 1.3

	Reference	Pulse form	Polarity	t_D	U_{max}	f	Switch	Remarks
Transmission line	(Behrend et al. 2003)	Gaussian	Unipolar	150 ns	12 kV	-	Spark gap	Erratic pulse shape
	(Merla et al. 2010)	Square	Bipolar	2 ns	1.6 kV	0–10 Hz	PCSS	Erratic pulse shape and laser triggering
	(Balevicius et al. 2013)	Square	Bipolar	10, 40, 60, 92 ns	12.5 kV	-	Spark gap	Laser triggering
	(Xiao et al. 2018)	Square	Bipolar	10, 60, 300 ns	10 kV	-	Spark gap	Erratic pulse shape; Hybrid with resonant
	(Deshpande et al. 2019)	Square	Unipolar	120, 160, 200, 300, 400 ns	10 kV	-	Spark gap	Erratic pulse shape
Direct capacitor discharge	(Hahn et al. 2001)	Gaussian	Unipolar	2 ns	2.6 kV	-	Spark gap	Erratic pulse shape
	(Behrend et al. 2003)	Square	Unipolar	12 ns	1 kV	-	MOSFET	Erratic pulse shape
	(Chaney et al. 2004)	Square	Unipolar	75 ns – 10 ms	0.400 kV	600 kHz	MOSFET	-
	(Yao et al. 2004)	Exponential	Unipolar	100 ns – 100 µs	0.3 kV	0–2 kHz	IGBT	-
	(Sunkam et al. 2004)	Exponential	Unipolar	-	3.4 kV	0–1 kHz	BJTs	Pulse rise time – 2 ns
	(Leveque et al. 2012)	Gaussian	Bipolar	2.5 ns	1.66 kV	-	Optoelectronic	-
	(Novickij et al. 2014)	Square	Unipolar	200 ns – 5 µs	8 kV	0–30 Hz	MOSFET	-
	(Krishnaveni et al. 2015)	Square	Unipolar	38 ns – 7 µs	0.5 kV	-	MOSFET	-
	(Novickij et al. 2016)	Square	Unipolar	100 ns – 1 ms	3 kV	0–1 MHz	MOSFET	-
	(Davies et al. 2019)	Square	Unipolar	80 ns – 1 µs	1.4 kV	0–50 Hz	MOSFET	-
	(Zajc et al. 2019)	Square	Unipolar	80 ns	0.5 kV	-	MOSFET	-

Continued Table 1.3

	Reference	Pulse form	Polarity	t_D	U_{max}	f	Switch	Remarks
Marx-bank/Modular	(Hahn et al. 2001)	Gaussian	Unipolar	6 ns	6 kV	-	Spark gap & MOSFET	Erratic pulse shape
	(Foshee et al. 2007)	Gaussian	Unipolar	200 ns	6 kV	-	Spark gap	Single pulse
	(Krishnaswamy et al. 2007)	Gaussian	Unipolar	1.3 ns	1.1 kV	0–200 kHz	Diode opening	-
	(Camp et al. 2008)	Gaussian	Unipolar	135–220 ps	20–120 kV	0–15 Hz	Peaking	-
	(Mendes et al. 2011)	Square	Bipolar	100 ns	1 kV	1 kHz	MOSFET & JFET[1]	Hybrid with Blumlein
	(Yao et al. 2012)	Square	Unipolar	200 ns – 1 µs	8 kV	0–1 kHz	MOSFET	-
	(Sakamoto et al. 2013)	Square	Bipolar	300 ns – 10 µs	4 kV	0–40 kHz	IGBT	-
	(Yao et al. 2015)	Gaussian	Unipolar	600 ps	31.2 kV	-	Spark gap	Erratic pulse shape
	(Dong et al. 2016)	Square	Unipolar	100 ns – 1 µs	8 kV	0–1 kHz	MOSFET	-
	(Li et al. 2016)	Gaussian	Unipolar	620 ps	1 kV	10 kHz	Avalanche transistors	Hybrid with transmission line
	(Redondo et al. 2017)	Square	Unipolar	200 ns – 100 µs	10 kV	0–1 kHz	MOSFET	-
	(Yao, Dong, Zhao, Mi, et al. 2016)	Square	Bipolar	100 ns – 1 µs	3 kV	0–1 kHz	MOSFET	Voltage droop
	(Yao, Dong, Zhao, Zhou, et al. 2016)	Square	Unipolar & bipolar	100 ns – 100 µs	3 kV	0–2 MHz	MOSFET	-
	(Li et al. 2017)	Gaussian	Unipolar	300 ps	1.6 kV	0–10 kHz	Avalanche transistors	Marx with gradient transmission
	(Dong et al. 2017)	Square	Bipolar	100 ns – 1 µs	3 kV	1 kHz	MOSFET	-

End of Table 1.3

	Reference	Pulse form	Polarity	t_D	U_{max}	f	Switch	Remarks
Marx-bank/Modular (continue)	(Garner et al. 2017)	Gaussian	Unipolar	400 ns – 20 µs	6 kV	0–100 MHz	IGBT	-
	(Li et al. 2018)	Gaussian	Unipolar	350 ps	3.1 kV	0–10 kHz	Avalanche transistors	-
	(Ke et al. 2018)	Square	Bipolar	200 ns – 1 µs	2 kV	0–1 kHz	MOSFET	-
	(Liu et al. 2019)	Square	Bipolar	500 ns – 1 ms	15 kV	10 kHz	MOSFET	-
	(Pirc et al. 2019)	Gaussian	Unipolar & bipolar	8 ns	6 kV	0–3.5 kHz	MOSFET	Fixed pulse duration
	(Redondo et al. 2019)	Square	Bipolar	500 ns – 10 µs	5 kV	0–0.5 MHz	MOSFET	-
	(Zeng, Yu, et al. 2020)	Square	Bipolar	500 ns – 5 µs	10 kV	0–0.5 MHz	MOSFET	-
	(Zeng, Yao, et al. 2020)	Square	Unipolar	200 ns – 1 µs	15.3 kV	0–10 kHz	MOSFET	Integrated with DOS circuit
Inductive storage	(Kuthi et al. 2005)	Gaussian	Unipolar & bipolar	3.5 ns	1.2 kV	0–100 kHz	MOSFET	DOS
	(Tang et al. 2007)	Gaussian	Unipolar	20 ns	4.5 kV	20 Hz	IGBT	Erratic pulse shape; With transformers
	(Tang et al. 2007)	Gaussian	Unipolar	5 ns	7.5 kV	20 Hz	MOSFET	-
	(Sanders et al. 2009)	Gaussian	Unipolar	5 ns	4.4 kV	0–3 MHz	MOSFET	Resonant circuit
	(Sanders et al. 2009)	Gaussian	Unipolar	2.6 ns	1 kV	0–3 MHz	MOSFET	Resonant circuit
	(Akiyama et al. 2010)	Gaussian	Unipolar	50 ns	30 kV	0–0.5 kHz	Magnetic	-
	(Kranjc et al. 2012)	Gaussian	Unipolar	50 ns	1 kV	-	MOSFET	DOS
	(Ma et al. 2019)	Square	Unipolar	23 ns	8.2 kV	-	MOSFET	Hybrid with Blumlein

Other types of switches (like photoconductive semiconductor, optoelectronic switch or even IGBT) are rarely applicable even if they also provide a capability to deliver ultra-short pulses. In all cases, the transient processes are triggered during the switch turn-on and turn-off, which negatively influence the pulse parameters. The proper compensation circuits must be applied to ensure system protection and the precise pulse waveform with constant pulse rise and fall times independently on the load/electrodes type (Dermol-Černe et al. 2020).

In all cases, the transient processes are triggered during the switch turn-on and turn-off, which negatively influence the pulse parameters and can breach the system safe operation limits. The proper compensation circuits must be applied to ensure system protection and the precise pulse waveform with constant pulse rise and fall times.

1.5. Transient Process Compensation in High-Frequency Circuits

The electroporation systems described above require an application of the high-voltage and current pulses at high-frequency. As it was showed, the operation of such devices in most cases is managed by high-power semiconductor switches like MOSFET. These switches are highly sensitive for operation mode beyond the safe operation limits. The voltage and current spikes, caused by switch turn-on or turn-off, may result permanent failure of the device. In such case, an application of snubber, clipping, crowbar and clamping circuits is necessary to protect the switch and ensure the safe operation of electroporation system.

The poorly design compensation circuits may lead to over-damped or under-damped response and reduce the overall pulse generation performance. Hence, to estimate the required compensation for the individual devices, the transient processes must be analysed. The switching impact on the pulse shape is influenced by the parasitic circuit parameters such as the contact capacitance, resistance of the pulse forming circuit transmission line and the stray inductance.

1.5.1. Snubber Circuits

Snubber circuits are used to protect switches (e.g. MOSFETs) from excessive voltage or current change and overvoltage during the switch turn on/off moments in circuits with inductive load. There are several types of snubber circuits, but most commonly used are resistor – capacitor (RC) and resistor – capacitor – diode (RCD) snubber circuits (Grainys 2014; Kadia et al. 2019). Snubber circuits are usually connected across the switch to limit the peak voltage during transient turn-on and turn-off (Zhong et al. 2014; Xiao et al. 2018; Kadia et al. 2019; Jørgensen

et al. 2020). An RCD snubber circuit can be forward or reverse polarized or non-polarized.

As an example, the switch SW protecting, forward-polarized RCD snubber circuit connected with an anti-parallel fast recovery diode is shown in the Figure 1.16. R2 limits the forward d*V*/d*t* and R1 limits the discharge current of the capacitor when the switch is turned on. Such design is used as an overvoltage snubber to clamp the voltage.

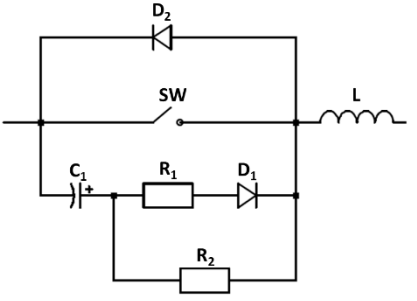

Fig. 1.16. Forward-polarized resistor – capacitor – diode (RCD) snubber circuit

Other type snubber circuits, like the reverse polarized snubber circuit can be used to limit the reverse-biased voltage occurring in the circuit due to the energy accumulation in the inductive coil. A non-polarized snubber circuit is used when a pair of switching devices is used in anti-parallel (Khan 2017).

In case the snubber circuits are applied, first, it is important that energy stored in RC snubber circuit capacitor is higher than the energy stored in the circuit's inductance. Second, the time constant of snubber circuits should me small compared to shortest expected switch turn on time. Finally, the snubber circuit's resistor must have a low self-inductance in order to reduce the pulse overshoot voltage. In such combination, the snubber RC circuits could be applied to protect the switches from high d*I*/d*t* and overvoltage (Novickij, Grainys, et al. 2017; Xiao et al. 2018) during the switching process.

1.5.2. Voltage Clamping Circuits

Voltage clamping circuits are design to limit the maximum or the minimum pulse amplitude and used to protect the switching components from operation in voltage which is out of the safe operation limits (Makarov et al. 2016). In addition, these circuits can also be used to improve the overall efficiency of the switching circuit and to recover otherwise wasted energy (Pollock 2019). They are can also be designed to ensure the square-wave pulse.

For instance, in the field of electroporation, the clamping circuits have been designed and used in modular (Abdelsalam et al. 2017; Darwish et al. 2019) or Marx-bank based pulse forming circuit designs (Sack et al. 2016; Sack et al. 2017). It provided the switch protection against over-voltage and was based on combined capacitive and avalanche-diode coupling between the switch collector and gate. In such way, the clamping circuit ensured, that the gate voltage of the switch is controlled and cannot over-cross the safe operation limits.

As another example, the diode clamped gate driver circuit was developed and applied to increase the energy utilization efficiency and pulse forming capabilities. The circuit design is represented in Figure 1.17 (Krishnaveni et al. 2017).

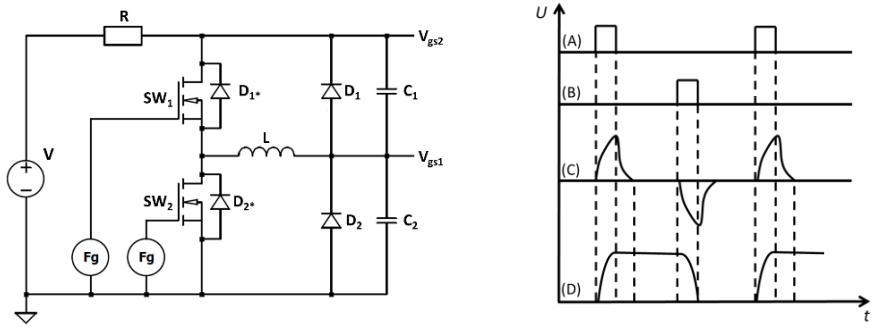

a) b)

Fig. 1.17. Voltage clamping circuit: a) design of diode clamped gate driver; b) the key waveforms where (A) is SW1 gate pulse; (B) is SW2 gate pulse; (C) is current through the resonance inductor; and (D) is capacitor voltage (Krishnaveni et al. 2017)

This type of clamping circuit was specifically proposed for high-frequency operation (Krishnaveni et al. 2017) and latter adapted for the development of the resonant circuit based high-voltage pulse generator with adjustable frequency for electroporation applications (Subramani et al. 2018). The authors showed, that it reduces the gate driving circuit losses and improves the pulse forming capabilities by providing square-wave pulses in the resonant circuit topology.

1.5.3. Crowbar and Controlled Crowbar Circuits

Crowbar circuits are frequently employed in direct capacitor discharge pulse forming circuits topologies (Novickij, Grainys, et al. 2017; Stankevic et al. 2020). They are used to form a very low-impedance short circuits, which provide a freewheel path for the load and prevent an excessive reverse voltage building up on the capacitor (Jin et al. 2004). As such, the lifetime of capacitor bank can be

increased, the capacitor discharge time prolonged and the energy transfer efficiency increased. In addition, the crowbar circuits can be used for unipolar current pulse forming, which might be needed for some electroporation applications (Tinschmann et al. 2008; Stankevic et al. 2020).

There are many configurations of crowbar circuits. In case of pulse forming circuits, the most common type is the active crowbar and controlled crowbar circuits. The active crowbar circuits are used to improve the pulse form and protect the device elements against the high-voltage and current transients. The active crowbar circuits, in comparison with the clamping circuits described before, can handle a higher fault current with small power dissipation. On the other hand, it is more likely than the clamp will trigger the deactivation of the pulse forming circuit and will bring the attention to the faulty operation.

However, for the electroporation research applications, it is essential to ensure the same pulse shape and duration for different biological samples. Therefore, the controlled crowbar circuits are used to ensure the pulse fall time independence from the load. As presented in Figure 1.18, the simply controlled crowbar circuit is integrated into the pulse forming circuit of capacitor discharge pulse generator described in Section 1.3.1.

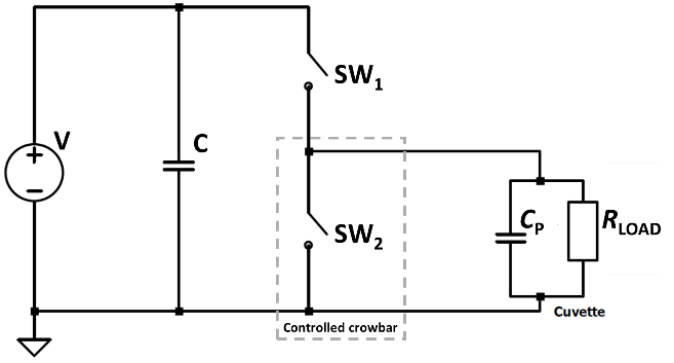

Fig. 1.18. Design of controlled crowbar circuit

In Figure 1.18, the switch SW_2 is open during pulse delivery and closed at the end of the pulse duration in order to create an alternative path for the current flow to the ground. In such case, the pulse forming circuits in synchronized operation with a controlled crowbar circuits are used to achieve a short pulse fall time independent of the load, by removing the pulse characteristic tail (Dong et al. 2016; Stankevic et al. 2020; Novickij, Grainys, et al. 2017). The impact of the controlled crowbar circuit is showed in Figure 1.19.

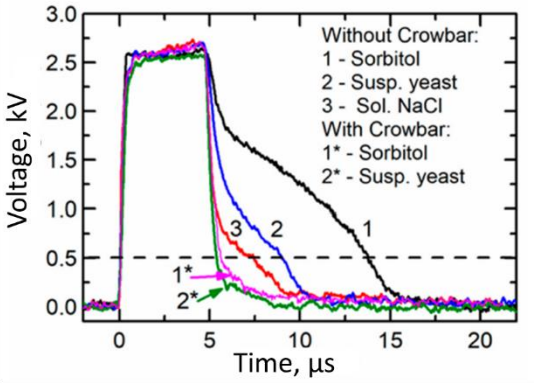

Fig. 1.19. The electric pulse form achieved on different loads with and without the controlled crowbar circuit (Stankevic et al. 2020)

The pulse form obtained on different biological loads without a controlled crowbar circuit (curve 1, curve 2 and curve 3) is compared with pulse generated using controlled crowbar circuit (curve 1* and curve 2*). It can be seen, that the controlled crowbar ensures the pulse fall time independence from the load impedance, which ensures an equal pulse duration and experimental treatment of different biological loads (Stankevic et al. 2020).

1.6. Conclusions for the Chapter 1 and the Formulation of the Thesis Tasks

1. The usage of electrical pulses for various electroporation applications has a high-potential and the scientific interest in submicrosecond pulses is increasing. This leads to the growing demand for the nsPEF electroporators.
2. The biological effects of the electrical pulses strongly depend on the pulse waveform, duration, repetition frequency, amplitude, number of pulses and electric field strength applied. The pulse waveform of majority electroporation systems is still load dependent, while there is a strong need to ensure the delivery of precise energy independent on the experimental load used.
3. Different techniques to design the pulse forming circuits for the nsPEF electroporation systems exists, mostly with narrow range of parameters. To cover the wide range of electroporation research needs, future design

development must ensure, that pulse forming circuits are capable to handle high-voltage and currents pulses at high-frequency as well as provide a wide selection of pulse parameters.

4. The recent years developments of SiC MOSFET technology resulted the new wave of Marx-bank, modular and direct capacitor discharge based nsPEF electroporators with adjustable pulse parameters and decline in Blumlein and transmission line based electroporators.
5. The transient processes are triggered during the switch turn-on and turn-off, which negatively influence the pulse parameters and can breach the system safe operation limits. The proper compensation circuits must be applied to ensure system protection and the precise pulse waveform with constant pulse rise and fall times.

The following tasks must be solved to achieve the aim of this research:

1. To develop the simulation model for high-frequency square-wave electroporation system using by applying the best practices of transient process compensation and investigate the circuit parasitic elements influence on the generated pulse shape.
2. To propose the planar electrodes topology for single cell real-time manipulation and develop a model to investigate the electric field distribution and homogeneity.
3. To develop the prototype of the submicrosecond electroporation system and investigate the applicability for in vitro electroporation.
4. To compare the simulation results of a pulse forming circuit with the obtained experimental results and provide an uncertainty assessment.

2

The Simulation Model of Electroporation System

In this Chapter, simulation models of the high-voltage, high-frequency nsPEF generator and planar electrodes for real-time electroporation on a microscope stage are presented. The nsPEF generator performance and the influence of the parasitic electrical circuit elements to the generated electric pulse are investigated using SPICE model and LTspice simulation software. The planar electrodes chip topology is analysed using finite element method (FEM) analysis in COMSOL Multiphysics environment to ensure a homogeneous cell exposure.

Four scientific publications were published on the section topic (Novickij et al. 2016; Butkus et al. 2017; Butkus 2018; Butkus et al. 2019).

2.1. The Development of High-Frequency nsPEF Electroporation System

In this section the research and development of the high-voltage, high-frequency submicrosecond electric pulse forming circuit using Simulation Program with Integrated Circuit Emphasis (SPICE) model is presented.

2.1.1. The Definition of the Pulse Forming Circuit Parameters

The designing of high-voltage, high-frequency nsPEF pulse forming circuit is a challenging and multidisciplinary task. It requires application of numerical methods to investigate the electrical circuit's transient processes and parasitic elements, such as the contact capacitance, resistance of the transmission line and stray inductance. Inappropriate application of compensation circuits may lead to the appearance of overvoltage, overcurrent or waveform distortion, as well as over-damped or under-damped responses. These would result in a poorly performing pulse forming circuit. Hence, proper compensation circuits must be developed to compensate the transient processes that occur during pulse turn-on and turn-off time as a result of the parasitic circuit parameters (Novickij, Stankevic, et al. 2015). Moreover, other issues, like load matching, driving circuit topologies for the semiconductor switches etc., should be solved.

To select the most optimal pulse forming circuit design, the pulse requirements must be clearly defined. Therefore, the pulse waveform amplitude, duration, repetition frequency and other output pulse parameters must be carefully selected in terms of their applicability in the experiments (Novickij et al. 2016). In previous Chapter 1, it was identified, that the high-frequency nsPEF electroporation has a growing scientific interest. Following this discussion and provided state of art electroporation system parametric assessment, the summary of the suggested pulse forming requirements are presented in Table 2.1.

Table 2.1. The summary of the state of art requirements for pulse forming

Pulse parameter	Scientific demand
Pulse waveform	load-independent and square-wave
Shortest pulse duration, s	from 1×10^{-7} to 1×10^{-3}
Pulses repetition frequency, MHz	up to 1
Number of pulses	from 1 to 100
Electric field strength, kV/m	30
Pulse amplitude, kV	From 0 to 3
Maximum (pulsed) current, A	up to 60

Following the pulse forming circuit requirements listed in Table 2.1, it can be seen, that the desired novel electroporation system must be flexible and be capable of delivering load-independent and adjustable square-wave electric pulses of duration ranging from 100 ns to 1 ms. The pulse repetition frequency must have a wide range from 1 Hz to 1 MHz, with the voltage amplitude up to 3 kV (30 kV/cm in a 1 mm gap cuvette). Taking into consideration, that the typical biological load

resistance is expected to variate in range from 50 Ω to 500 Ω the device should be able to handle the maximum (pulsed) current up to 60 A.

2.1.2. The Conceptual Designing of Pulse Forming Circuit

As it was discussed in previous chapter, there are several pulse generators conceptual circuits: direct capacitors discharge, transmission line discharge and inductive storage discharge. All are suitable for nsPEF applications. However, it was demonstrated that due to the recent developments of SiC MOSFETs, the direct capacitor discharge circuit topology forms a leading trend to provide a high-quality square-wave pulse shape with the wide range of the pulse parameters flexibility. Thus, is a preferred design in recent developments of the nsPEF electroporation systems. Moreover, to ensure the load independent pulse shape, the controlled crowbar circuits are used. As a result, the conceptual direct capacitors discharge pulse forming circuit integrated with the controlled crowbar circuit is represented in Figure 2.1.

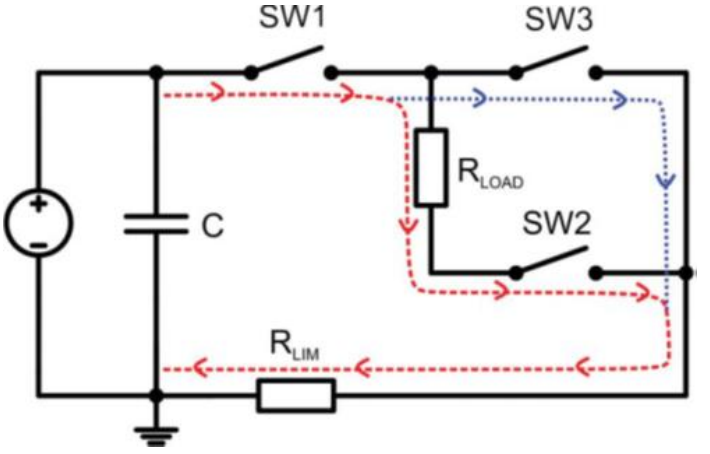

Fig. 2.1. Simplified equivalent circuit of the generator (Novickij et al. 2016)

For the simplicity, the biological load (cuvette) is approximated as parallel connected resistor (R_{LOAD}) without expressing the parasitic load capacitance C_p. Same applies for all other parasitic elements. As a result, the pulse forming circuit itself is composed for a variable high-voltage power supply, a capacitor (C) and the maximum current limiting resistor (R_{LIM}). Different from the direct capacitor discharge circuit topology, in this case three switches (SW1, SW2, SW3) are used instead of one to form additional current path and enable controlled crowbar integration.

The SW1 and SW2 switches belong to main power line and are responsible of commutation of the power source voltage over the load. When these switches are turned on, a high-voltage pulse is over the load and the current contour is shown as a dashed line. Consequently, these two switches operated in a synchronized mode, thus, are opened and closed at the same time. The pulse rise time is dependent on the switching characteristics of the switches and the parasitic circuit stray inductance and capacitance (Butkus et al. 2019). The maximum current in case of $R_{LOAD} = 0\ \Omega$ is limited by the current limiting resistor (R_{LIM}).

The switch SW3 represents controllable crowbar circuit which is triggered at the same moment when the main power line switches SW1 and SW2 are closed (Butkus et al. 2017). In this way, the controlled crowbar circuit could be opened to create a new path for the high current to flow to the ground (blue line), avoiding a path through the cuvette (red line), since this path is closed at the same time by SW1 and SW3. As a result, the pulse fall time became independent of the load and is only dependent on the type and the switching characteristics of the switches that were used and the parasitic parameters of the overall circuit. As shown in previous chapter, without the synchronized controlled crowbar circuit (SW3), the characteristic tail dependent on the load would appear and, thus, it would be impossible to generate a nsPEF pulses with the high impedance buffers (Novickij et al. 2016; Butkus et al. 2019).

In such design, the pulse length is controlled by the switches SW1 and SW3. To ensure the proper operation of the switches, the snubber circuits like resistive-capacitive (RC) should be applied to balance the voltage in each switch during the steady state and transient operation. In addition, since the series of square-wave pulses are required, the energy stored in the capacitor has to be several order of magnitude higher than the energy delivered to the load (Redondo 2017). Since all energy is stored in the capacitor bank, this impose some addition safety requirements. For instance, the capacitor bank directly defines the pulse voltage amplitude, which is required to be in several of kilovolt range and the switches must be able to withstand this voltage.

For the nsPEF electroporation applications, the switching speed must be in the range of nanoseconds. This can be achieved with the application of fast switches, which offer the switch-on and switch-off times on the order of in the range of ns. In recent works authors have demonstrated, that MOSFET switches in comparison with IGBTs and BJTs are cheaper and better suited to produce pulses within the 100–300 ns regime with transition times (rise and fall time) faster than 100 ns, although all three have breakdown voltages (collector–emitter or drain–source voltage) in excess of 1 kV (Davies et al. 2019). As a result, it was decided to focus only on MOSFET switches and the comparing of typical high-voltage and high-frequency MOSFETs is provided in Table 2.2.

Table 2.2. Comparing typical high-voltage and high-frequency MOSFET switches parameters

Made	Model	Breakdown voltage, V	Turn-On Delay, ns	Rise time, ns	Turn-Off Delay, ns	Fall time, ns	I_D, A	I_{DM}, A	Reference
CREE	C2M0160120D	1200	7	9	13	14	18	40	(CREE Inc. 2019)
	C2M0080120D	1200	15	22	24	14	36	80	(CREE Inc. 2015a)
	C2M1000170D	1700	6	10	11	60	5	90	(CREE Inc. 2015b)
IXYS RF	DE375-102N12A	1000	5	3	5	8	12	72	(IXYS RF 2018)
	DE275-102N06A	1000	3	2	4	5	6	48	(IXYS RF 2001)
Microsemi	APT10035JLL	1000	12	10	36	9	25	100	(Microsemi 2003a)
	APT10035LLLG	1000	12	10	36	9	28	112	(Microsemi 2003b)
ON Semiconductor	2SK3747	1500	12	37	152	592	2	4	(ON Semiconductor 2013a)
	NDFP03N150C	1500	15	20	148	44	2.5	5	(ON Semiconductor 2013b)
	WPH4003	1700	19	21	200	55	3	6	(ON Semiconductor 2013c)
STMicroelectronics	STH2N120K5-2AG	1200	10.3	7.8	34	39	1.5	2.5	(STMicroelectronics 2018)
	STFW3N170	1700	25	9	51	53	2.6	10.4	(STMicroelectronics 2015)
Vishay Siliconix	IRFPG50	1000	19	35	130	36	6.1	24	(Vishay Siliconix 2014)
	IRFBG20	1000	9.4	17	58	31	1.4	5.6	(Vishay Siliconix 2016)

From the Table 2.2, it can be seen that the latest developments of the SiC based semiconductor technologies enabled the commercial MOSFET switches to handle a voltage pulses up to of 1.7 kV, thus the series connected array of MOSFET switches are still needed to reach the sufficient level of pulse voltage in direct capacitor discharge circuit topology. In addition, the offered pulse rise time is between few to tens of ns, while the pulse fall time can go up to several hundreds of ns, hence, it is one of the limiting factor during the selection of the switches for desired nsPEF electroporation system. While, to ensure the safe operation of the pulse forming circuit, an important factor is also a continuous and a pulsed drain currents. It was noted, that the large portion of high-voltage commercial MOSFET switches can offer sufficient breakdown voltage and speed performance, but are limited with a continuous and a pulsed drain currents. As a result, it was concluded, that the series connected array of MOSFET (C2M0080120D, Cree Inc., Durham, NC, USA) switches with the 1.2 kV breakdown voltage, 36 A continuous I_D and 80 A pulsed drain currents I_{DM} is the most practical choice for the required nsPEF electroporation system.

Since the MOSFET is a voltage controlled device, it can be driven easier and with a lower cost than a BJT which is a current controlled device. However, the MOSFET switching time is largely determined by how fast the input capacitance is charged during the turn-on transient and discharged during the turn-off transient. This mainly depends on the gate current at the start of conduction, meaning, that the MOSFET switching speed is still dependent of the gate current that charges the parasitic capacitances of the semiconductor device (Kim et al. 2016; Manias 2017). Therefore, a higher gate currents will be required in high switching frequency operation (Kim et al. 2016).

For the power MOSFET switches control and synchronization, gate drive circuits (DR) are used, which accepts a low power input from a controller and produces the appropriate voltage and current for the switch control. Moreover, to prevent the short-circuit, a galvanic isolation is applied, where the magnetic (transformer) or optical coupling drivers are mainly used (Manias 2017). However, the optical coupling-based gate drivers mainly use light-emitting diodes, which results a disadvantage of rapid aging. In addition, the commercial products usually have restricted dV/dt robustness, that contributes to longer dead-time and affects overall operating frequency and efficiency (Kreutzer et al. 2015). Therefore, the high current magnetic gate drivers are preferred.

As a result, a 4 A isolated, half-bridge ADuM42231 gate driver was selected (Analog Devices 2017). It is suitable for the high-frequency applications at range up to 1 MHz and uses the Analog Devices, Inc., iCoupler® technology, which has advantage of 5 kV rms reinforced isolation and up to 0.7 kV galvanic isolation between the drivers' high-side and low-side outputs. As a result, the potential for cross conduction is minimized and the equipment reliability and safety are

improved. Thus, the selected gate driver will ensure the high-frequency operation and the reliable control over the switching characteristics of selected MOSFET switches.

2.1.3. The SPICE Model of the Pulse Forming Circuit

One of the main tasks during the development of the nsPEF electroporation system is the evaluation of circuit parasitic elements influence and compensation of the transient processes in the pulse forming circuit during the rise and fall time of the generated pulse. This ensure the control of pulse parameters and the smooth square-wave pulse form, which was noted as an issue for more than one-third of in-house developed nsPEF generators (Table 2.2). To ensure the compensation of the transient processes, $R_{S1}C_{S1}$– $R_{S6}C_{S6}$ snubber circuits were implemented into the pulse forming circuit and connected in parallel with the semiconductor MOSFET switches (Figure 2.2). As an advantage, the $R_{Si}C_{Si}$ snubber circuits provide an additional support for the synchronization of the series-connected switches.

In the prototype development phase, the design of optimal RC snubber circuits can be a time consuming and costly task if the different set-ups of RC snubber circuits are experimentally tested directly on the prototype system. On the other hand, this task can be more easily solved via application of a proper simulation model (such as a SPICE model) (Butkus et al. 2019). As a result, to investigate the transient processes and design the measures needed to compensate the parasitic circuit parameter's influence on the PEF generator, the commercially free LTSpice simulation software was used to create a SPICE model of the pulse forming circuit.

The developed SPICE model of the pulse forming circuit for the PEF generator is presented in Figure 2.2. It is divided into several main groups: control; power supply; cuvette, controlled crowbar; power circuit and compensation circuit (both not identified in the figure). The power supply part consists of a high-voltage DC power supply supported by the capacitor array, for energy accumulation.

The control part of the generator is responsible for precise triggering operations of the semiconductor switches. The main component of the control part is the microprocessor, which can provide the user with the ability to precisely define the electric field strength, duration range, pulse number and frequency. Thus, the PEF generator is able output either a single short square-wave pulse or a defined number of multiple pulses.

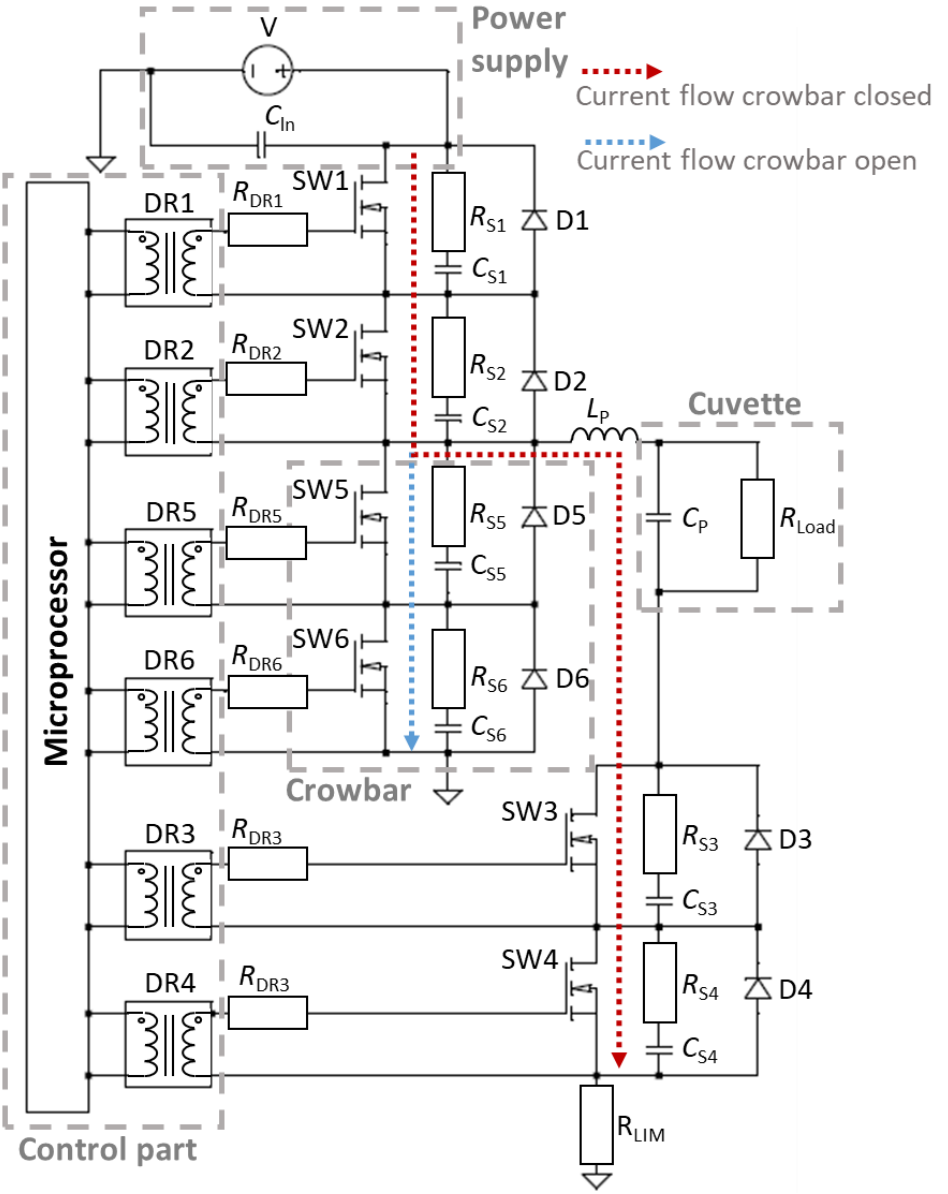

Fig. 2.2. A SPICE model of the pulse forming circuit for high-frequency square-wave electroporation system (Butkus et al. 2019)

The control part is represented by six driver circuits DR1–DR6. To imitate the galvanic isolation, the MOSFET switches were connected to the pulse control unit throughout the power transformers (transformation ratio equal to 1) and driver circuit current limiting resistance R_{DR1}–R_{DR6}. To imitate the performance of actual driving circuits selected in previous section, the implemented driving circuit is set to drive semiconductor switches with peak output current up to 4 A, and have an output voltage from 4.5 V to 18 V. The boundary conditions for simulation parameter selection are assumed to be a 5 kV isolation capability at the maximum frequency of 1 MHz. As a result, this driving circuit is suitable to provide a precise and a reliable imitation of synchronized control over the switching characteristics of MOSFET switches.

The power circuit part of the generator consists from the six high-speed, high-voltage and low capacitance C2M0080120D SiC power MOSFET switches SW1–SW6 manufactured by CREE (Durham, USA). These switches are expected to ensure the delivery of the high-voltage square-wave pulses at the high switching frequency. To match the switching characteristics, a manufacturer developed SPICE model of C2M0080120D SiC power MOSFET switch was used for the simulation model development. All switches were connected to the driving circuit throughout current limiting resistance R_{DR1}–R_{DR6}.

Each C2M0080120D switch can withstand voltages up to 1.2 kV and pulsed drain currents up to 80 A. In order to handle commutation voltages up to 3 kV, in the pairs of MOSFET switches are connected in series. Following the conceptual circuit design described in previous section, the pairs of SW1–SW2 and SW3–SW4 switches belong to main power line and are responsible of commutation of the power source voltage over the load. When these MOSFET switches were turned on, a high-voltage pulse was over the load. Consequently, these four switches operated in a synchronized mode by two channel galvanically isolated DR1–DR2 and DR3–DR4 MOSFET drivers and, thus, were opened and closed at the same time. The switches in the pair of SW5–SW6 represent controllable crowbar circuit which is triggered by the DR5–DR6 at the same moment when the main power line switches SW1–SW4 are closed (Butkus et al. 2017). In this way, the controlled crowbar circuit creates a new path for the high current to flow to the ground, avoiding a path through the cuvette, since this path was closed at the same time by SW1–SW2 and SW3–SW4.

For the compensation circuit, snubber diodes D1 to D6 were implemented in parallel to each MOSFET switch to provide reverse voltage protection. In addition, energy absorbing RC snubber circuits were connected in parallel to each MOSFET switch in order to eliminate sudden voltage surges in the pulse forming circuit created by stray inductance and to ensure MOSFET synchronization. This type of compensation circuit ensures proper surge voltage damping during turn-

on and turn-off time, thereby protecting the power MOSFET switches and other devices in its vicinity.

Parasitic inductance of the Printed Circuit Board (PCB) circuit is implemented as an inductor L_P. To represent the electroporation cuvette and imitate the cell and the suspension charging constant, the parasitic load capacitance C_p, together with load resistance R_{LOAD} were used. In this way, the presented pulse forming circuit offered flexibility for different experimental applications, while the SPICE model itself was suitable for the electrical pulse forming circuit transient processes and analysis of the parasitic elements (Butkus et al. 2019). As will be demonstrated below, the SPICE model was also able to optimize prototype development and reduce the time and cost needs during the prototype development phase (Butkus et al. 2019).

The generation of 3 kV square-wave electric pulses for nsPEF electroporation applications is complicated and a multidisciplinary engineering task, which cannot be solved without a proper set-up of RC snubber circuits. To suppress the transient processes of the pulse forming circuit, the parameters shown in Table 2.3 were selected based on knowledge of previous developments (Grainys 2014; Novickij 2015) and were swept from the minimum to the maximum values. The impact of each parameter was evaluated to find the optimal RC snubber circuit parameters under different load conditions. In fact, to imitate the real electroporation experiment parameters, where low conductivity buffers are used and the R_{LOAD} was varied from 50 Ω to 500 Ω.

Table 2.3. Requirements for electroporation system (Butkus et al. 2017)

Symbol	Pulse parameter	Min. value	Max. value	Final value
R_S	Snubber resistance, Ω	0.1	20	10
C_S	Snubber capacitance, pF	200	900	500
R_{LOAD}	Load resistance, Ω	50	500	50–500
C_P	Parasitic load capacitance, pF	10	100	50
L_p	Parasitic circuit inductance, μH	1	5	1.2

Parasitic line inductance L_p and parasitic load capacitance C_P have a high impact on the performance of pulse forming circuits and can impose transient processes of overvoltage and overcurrent. In addition, other undesirable pulse distortions, like circuit ringing, can be triggered. To illustrate the pulse forming circuit parasitic elements impact on the pulse form without the application of the snubber and crowbar circuits, the parasitic line inductance was variated from 1 μH to 5 μH. The impact on the pulse shape is presented in Figure 2.3.

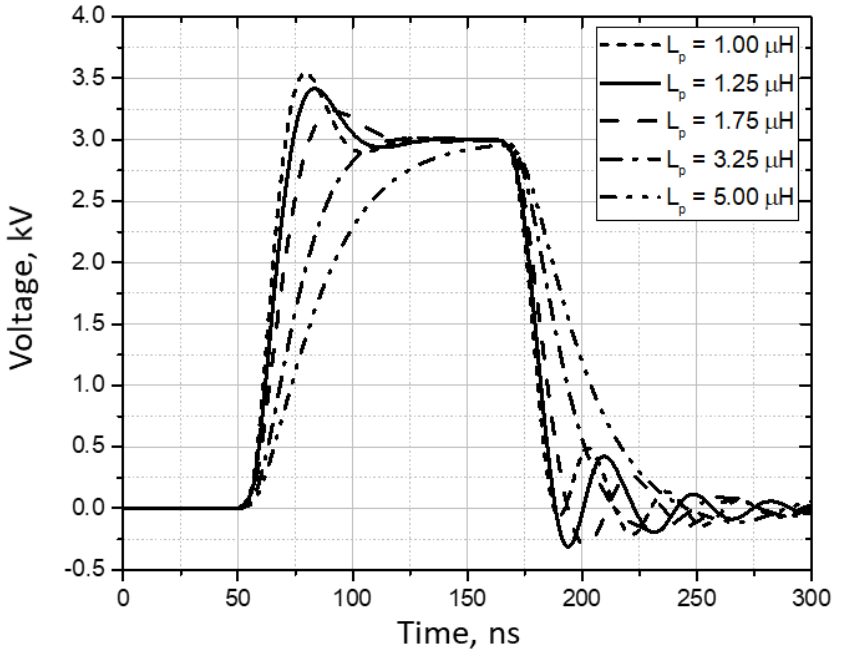

Fig. 2.3. The output voltage pulse on the load of 150 Ω (C_P = 50 pF) without the snubber and crowbar circuits (Butkus et al. 2019)

As it can be seen in the Figure 2.3., the parasitic circuit inductance influence on the pulse, which resulted in overvoltage during turn-on and turn-off of the semiconductor MOSFET switches (Butkus et al. 2019).The voltage overshoot and undershoot up to 0.5 kV as well as voltage ringing's after the pulse turn off were detected, which may cost the overvoltage of the MOSFET switches. Due to this the RC snubber circuits were implemented into the circuit. The resulting pulse on the load of 100 Ω with implemented RC snubber circuit is shown in the Figure 2.4 (Butkus et al. 2017).

As seen in the Figure 2.4, the rise time of the generated pulse depends only on switching parameters of the semiconductor. The implemented RC snubber circuits allow to limit the reverse overvoltage during the turn-off phase of the semiconductor switches. To ensure fastest turn-off time and the minimum reverse overvoltage, the snubber resistance R_s was set to 10 Ω and the snubber capacitance C_s to 500 pF (Butkus et al. 2017). This optimal set-up of RC snubber circuit is further applied, for all following simulations.

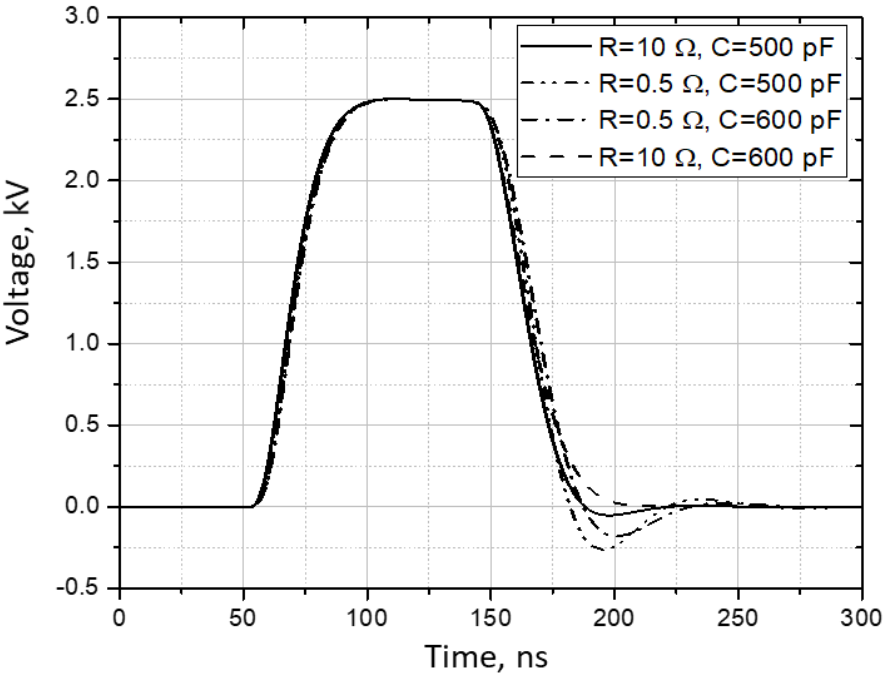

Fig. 2.4. The output voltage pulse on the load of 100 Ω (L_P = 1.2 μH) with different snubber circuit parameters (Butkus et al. 2017)

To minimize the fall-time of the produced waveform also to neglect the pulse tail influenced by the load the controlled crowbar circuit was implemented into the system. The influence of the controlled crowbar circuit to the generated pulse form can be seen in the Figure 2.5. As it is shown, in case the synchronized controlled crowbar circuit is not applied, the characteristic tail appears, resulting the pulse fall-time dependence on the load. If the load is increased, the characteristic tail impact on the pulse fall-time is also increased. However, in case of the activation of the controlled crowbar, the pulse fall-time dependance on the load resistance reduce significantly. With such change, the pulse fall-time can be generally assumed to be time independent on the load resistance, thus resulting better pulse forming circuit performance. However, it was also noted, the controlled crowbar impacts the pulse undershoot, which depends on the load and can increase up to –0.7 kV in case of the load of 500 Ω.

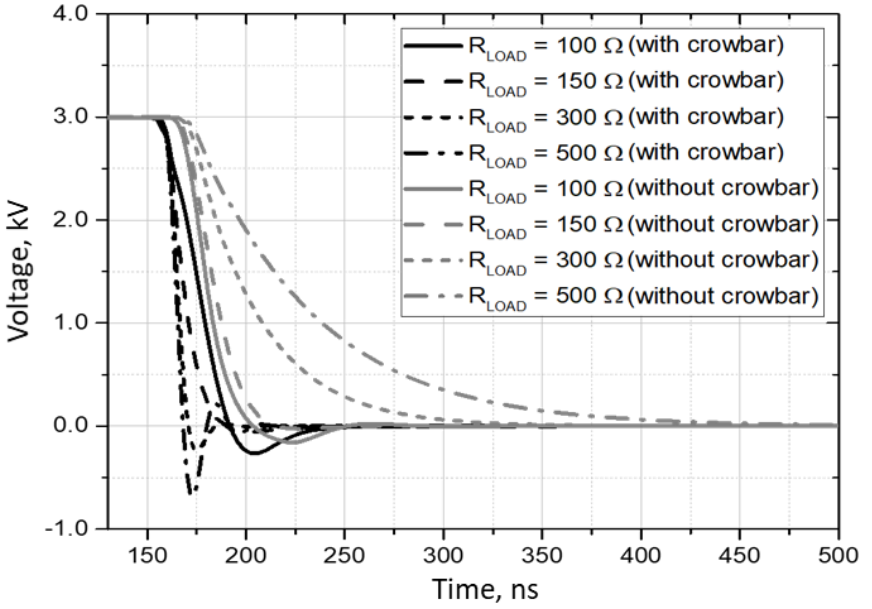

Fig. 2.5. The controlled crowbar circuit impact on the pulse turn-off time and the load resistance dependence

For delivering the constant pulse amplitude in repetitive pulsing performance, the power supply unit must be connected with the sufficient capacitor bank. The remaining maximum pulse amplitude after single pulse delivery can be evaluate following the capacitor discharge formula below:

$$U_{\text{series}} = U_{\max} e^{-t_D / R_{\text{LOAD}} C}, \tag{2.1}$$

where C is capacitance of capacitor bank, R_{LOAD} – load resistance, t_D – pulse duration and $U_{\max}$ – initial voltage. In case the initial voltage is fixed, the capacitor discharge voltage depends on pulse duration and load resistance. The longer pulse duration is used, the more the capacitor will discharge as well as the smaller resistance of load are used, the faster capacitor is discharged. For the illustration purpose, the pulse amplitude dependence on the pules duration in series delivery is presented in Figure 2.6.

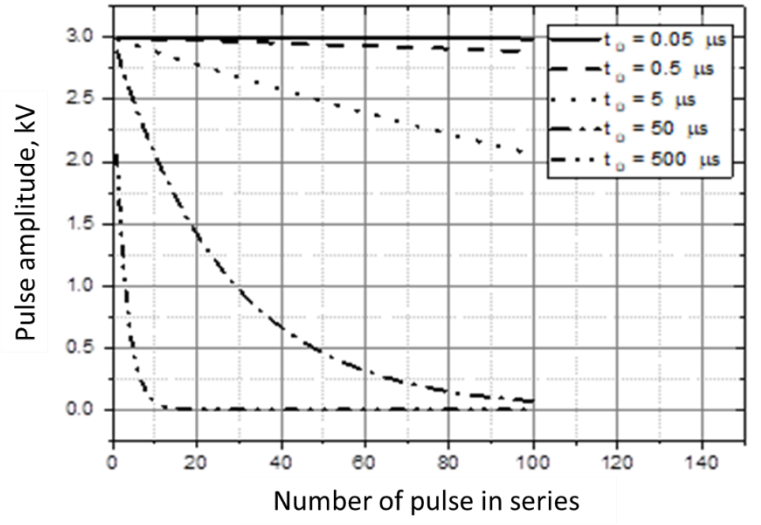

Fig. 2.6. Pulse amplitude dependence on the pules duration in series delivery

In Figure 2.6, the pulse amplitude dependence on the number of pulses was estimated for the capacitor bank of 13.3 μF with the load resistance of 100 Ω. For the pulse duration from 50 ns to 500 ns, the constant voltage supply with less than 10% drop is ensured, however in case of longer pulses, either the bigger load resistance or larger capacitor bank must be used to ensure constant voltage supply.

Although the simulation results indicate the proper performance of designed pulse forming circuit, the actual performance and the impact of RC snubber circuits and the controlled crowbar circuit still needs to be validated with the comparison of simulation and measurement results of actual pulse. This task is covered in the following chapter.

2.2. The Simulation Model of Planar Electrodes for Electroporation

In this section the concept of planar electrodes for real-time electroporation on a microscope stage is presented and the topology is analysed using finite element method (FEM) analysis. A multiparametric investigation of the chip topology is performed in COMSOL Multiphysics environment to define the configuration of electrodes, electric field distribution and other electroporation parameters to ensure a homogeneous cell exposure. Based on the simulation results, an optimal

electrode configuration, for investigation of the single cell permeabilization thresholds during the real-time *in vitro* electroporation, is proposed.

2.2.1. Planar Electrodes for Electroporation

The most common way of investigating electroporation *in vitro* is to study the cell uptake of dyes: either fluorescent molecules (fluorophores) or color stains (such as trypan blue) (Batista Napotnik et al. 2018). The cells are put into a cuvette with electrodes and after pulsing procedures the release or loading of the dye is observed (Novickij, Tabasnikov, et al. 2015). For this research, the most common electroporation systems use a standard cuvette with metal electrodes. The usual distance between electrodes vary from 1 mm to 4 mm. However, this method does not allow to research and monitor the dyes dynamic in real-time, due to the required cell handling from the cuvette to the microscope slide (Novickij, Tabasnikov, et al. 2015). As a result, the observation of the dye release dynamics is not possible during pulsing procedures.

In order to overcome the drawbacks of the standard cuvette electroporators, the microfluidics-based electroporation technique is rapidly developing (Geng et al. 2013). Even though this technique is advanced with its unique characteristics of miniaturization and integration, it is still difficult to study fast, nanoscale pore formation dynamics using real-time fluorescent microscopy. In order to perform such experiments, the electrode structures, which are capable of delivering uniformly distributed electric field to the biological cells, is required.

The planar electrode structures proved to be advantageous for this type electroporation experiments (Geng et al. 2013; Novickij, Tabašnikov, et al. 2017), but various issues, such as the spatial non-uniformity of the electric field distribution, complexity of electrode fabrication, biological compatibility issues, and the voltage breakdown occurrence between the electrodes has to be solved (Novickij, Tabašnikov, et al. 2017). Due to this, the variety of available planar electrodes for electroporation is currently limited due to the complexity, price and the electrodes fabrication challenges. As a result, the need to research the various electrodes configurations and their parameters (such as thickness, electrode gap, finger width) influence on the generated electric field intensity and homogeneity still exists.

In addition, to enable the planar electrodes for real-time electroporation applications at least several (more than two) electrodes must be used for the structure. The electrodes must be made only from the biocompatible and highly conductive metals. In the sections below, the detailed parametric analyses were performed. The finite element method simulations were applied for the evaluation of electrical field distribution to support the development of the required planar electrodes structure. As a result, the generated electric field intensity and

homogeneity dependency on the electrodes configuration was evaluated and the optimal configuration was proposed.

2.2.2. The Simulation Model of Planar Electrodes

In order to investigate an electric field distribution and make preparation works for the electrodes prototype development, the planar electrodes computer model was developed using COMSOL Multiphysics software (COMSOL Inc., USA) (Butkus 2018).

The requirements for the electrodes were defined, which are enforced by the biological objects. The gap between the electrodes must be big enough to ensure sufficient field of view to accommodate multiple cells (for statistical analysis of the observed effect). The typical mammalian cell size in the range of 8–10 μm and the permeabilization threshold is in the range of 0.3–1 kV/cm (Krassowska et al. 2007; V. Novickij et al. 2016), therefore it was defined that the minimum effective gap should be at least 80 μm. On the other hand, to have more flexibility during the experiment, the gap between the electrodes should be wider than the effective gap. For this reason, the gap between electrodes is selected to vary from 150 μm to 500 μm, while the generated electric field should be at least 1 kV/cm.

In addition, the biocompatibility of the electrodes is a concern. Cells are sensitive to oxidation and the pH changes in the electrode/medium interface (Li et al. 2015), thus only biocompatible and highly conductive metals should be used. As a result, the choice is limited to gold and platinum, however, taking into account future availability of infrastructure and the specifics of fabrication process, platinum has been selected.

Lastly, electroporation is highly dependent on the parameters of the electric field (i.e. direction, pulse form, duration etc.), therefore the structure should support bipolar pulses and delivery of pulses with different angles of electric field, which will allow a more flexible study the spatial distribution of pores in the cell membranes by real-time fluorescent dye diffusion. As a result, at least several (more than two) electrodes must be present in the structure, while we limited the topology to four.

For the Multiphysics environment simulations, the Electric Currents interface of the COMSOL Multiphysics software has been selected. The selected interface provides a solution of the current conservation equation which is based on Ohm's law using the scalar electric potential as the dependent variable. For the results resolution fine element resolution, the free tetrahedral mesh was selected with a minimum and maximum finite element size of 1.65 μm and 38.5 μm, respectively. The specific size of each element is influenced by the geometry of the electrodes. The simplified electrodes mesh structures are represented in Figure 2.7 (Butkus 2018).

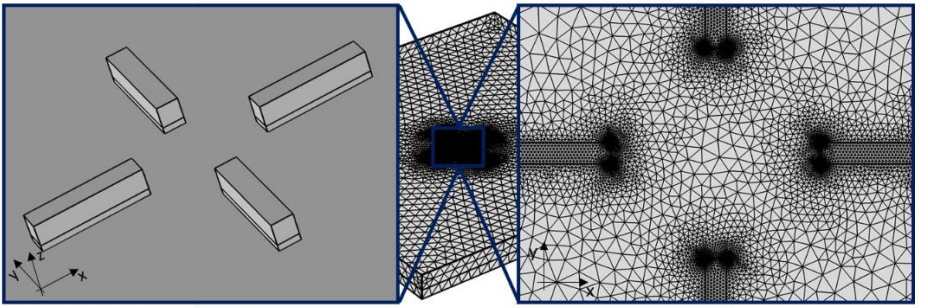

Fig. 2.7. 3D simplified electrodes (left) and free tetrahedral mesh (right) structures of planar electrodes for electroporation (Butkus 2018)

As it can be seen from Figure 2.7, the topology consists of 4 symmetrical electrodes, which form 2 pairs (vertical, horizontal). The aim is to estimate the influence of electrode geometry (gap) on the electric field homogeneity both in vertical and horizontal planes, which will ensure equal exposure of cells to pulsed electric field (Butkus 2018). The Table 2.4 shows the summary of the main simulation parameters used to develop a model of planar electrodes in COMSOL Multiphysics environment (Butkus 2018).

Table 2.4. Summary of main simulation parameters (Butkus 2018)

Model parameter	Value
Electrode width, μm	10
Electrode length, μm	50
Electrode thickness of titanium layer, μm	0.01
Electrode thickness of platinum layer, μm	0.1
Distance between electrodes, μm	150–500
Applied voltage, V	30
Water electrical conductivity, S/m	0.1
Water relative permittivity, S/m	78
Platinum electrical conductivity	8.9×10^{6}
Platinum relative permittivity	2.6
Titanium electrical conductivity, S/m	2.6×10^{6}
Titanium relative permittivity	100
Silica glass electrical conductivity, S/m	1×10^{-14}
Silica glass relative permittivity	2.09

Four platinum electrodes with titanium layer on the top were positioned on the 1.1 mm width (and the same depth) 0.03 mm height silica glass plate. On the top of the silica glass plate, the electrode structures are surrounded by 0.05 mm height water container. Both represent the typical medium in which the electrodes are used. The electrode gap was changed during simulation from 150 μm to 500 μm in order to determine the optimal value for homogeneous electric field distribution, which must be at least 1 kV/cm (Butkus 2018).

2.2.3. The Modelling Results and Electric Field Distribution

The example of electric field distribution between two planar electrodes pairs in YZ and XY planes is presented in Figure 2.8. Since the electrodes represent identical pairs, the only of one pair is presented, but the same results are applicable for second pair of the electrodes.

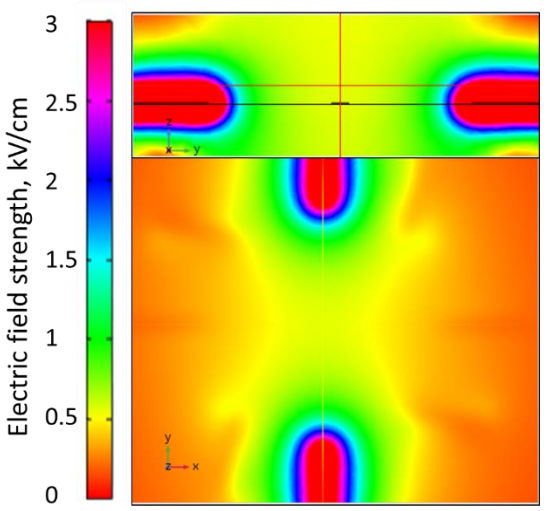

Fig. 2.8. The electric field distribution of planar electrode pair in YZ plane (top) and XY plane (bottom) when electrode gap is equal to 350 μm (Butkus 2018)

The distance between electrodes is set to 350 μm and the applied voltage is 30 V (Butkus 2018). If the gap between electrodes is set to 150 μm, the electric field in the middle is 1.1 kV/cm, which is applicable for reversible electroporation procedures of the biological cells and tissues (Pucihar et al. 2011). The influence of electrode gap on the electric field amplitude in the middle of the chip is summarized in Figure 2.9 (Butkus 2018).

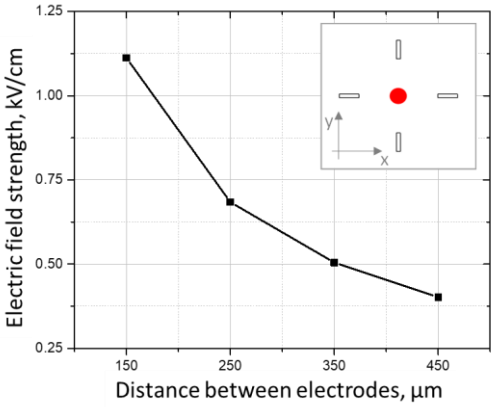

Fig. 2.9. The electric field strength dependence on the distance between electrodes (Butkus 2018)

Therefore, the distribution of electric field values in the effective gap (80 µm) is presented in Figure 2.10. As it can be seen the electric field is homogeneous when the 250–450 µm gap between electrodes are used. As a trade-off, the electric field amplitude is reduced. However, the fabrication process allows application of voltage higher than 30 V, thus the drop of amplitude can be compensated by increase of voltage (Butkus 2018).

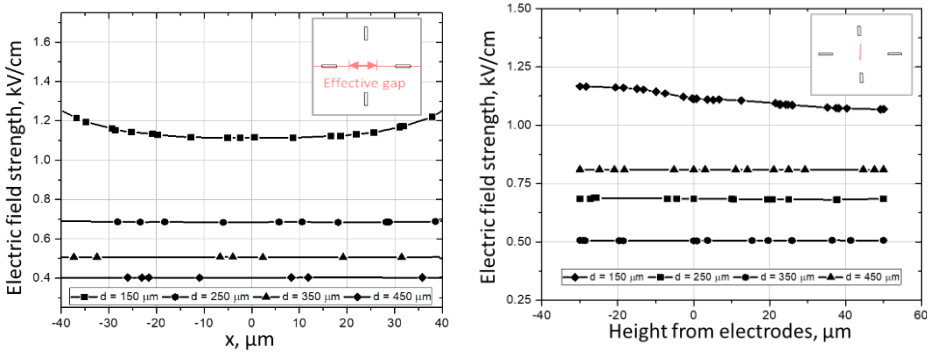

a) b)

Fig. 2.10. The electric field strength distribution dependence on the distance between electrodes: a) field strength distribution in x-plane; b) field strength distribution in z-plane (height from electrodes) (Butkus 2018)

Another important parameter is the electric field homogeneity in the vertical plane (z-plane). The electric field strength distribution (z-plane) dependence on the distance between electrodes is summarized in Figure 2.10. Like x-plane distribution in the z-plane the 250–450 μm gap electrodes offer the best homogeneity. Heights up to 60 μm from the electrodes where investigated, which is sufficient since the cells are small (8–10 μm) (Butkus 2018).

Based on the results, it was concluded that the 250–350 μm gap between electrodes has the most potential since it ensures homogeneous distribution and provides an optimal trade-off between the applied voltage (less than 100 V) and acquired electric field parameters (more than 1 kV/cm). The results also demonstrate, that the planar electrodes topology of 4 symmetrical electrodes, which form 2 pairs (vertical, horizontal), is simple and yet sufficient for real-time electroporation applications.

2.3. Conclusions of Chapter 2

1. The high-voltage and high-frequency nsPEF pulse forming circuit was developed and investigated using SPICE model. The RC snubber circuits were implemented to limit the reverse overvoltage during the turn-off phase of the semiconductor switches. To ensure fastest turn-off time and the minimum reverse overvoltage, the snubber resistance has to be set to 10 Ω and the snubber capacitance to 500 pF.
2. The pulse forming circuit ensures pulse rise time of 25 ns, while the proposed controlled crowbar circuit based on the semiconductor switches ensures relatively load-independent electric pulse fall-time of 18 ns.
3. Based on the selected MOSFET switches and gate drivers datasheets, the shortest pulse duration is in range of 75 ns, while the repetition frequency can be variated from 1 Hz to 1 MHz, with the voltage amplitude up to 3 kV, which ensure a 30 kV/cm electric field strength in a 1 mm gap cuvette and the maximum drain pulsed current up to 80 A.
4. The planar electrodes model in COMSOL Multiphysics was developed to analyse electrodes topology and electric field distribution for real-time electroporation. The electrodes structure of two pairs (vertical, horizontal) of symmetrical electrodes produced from platinum with additional titanium layer was proposed. The 250–350 μm gap between the electrode pairs ensure the homogeneous electric field distribution.

3

Research and Development of the Electroporation System

In this Chapter, the development of novel high-frequency square-wave electroporation system which can produce single and bursts of high-amplitude (up to 3 kV) pulses of variable duration (100 ns to 1 ms) with predefined repetition frequency (1 Hz to 3.5 MHz) is presented. The simulation and the prototype results are compared. The prototype system is successfully tested for the inactivation of the human pathogen *Candida albicans*.

Two scientific publications were published on the section topic (Novickij et al. 2016; Butkus et al. 2019).

3.1. The High-Frequency Electroporator for *In Vitro* applications

In this section, the development of square-wave electroporation system prototype is presented. The prototype is based on the simulation model and pulse forming circuit design presented in Chapter 2. The prototype production and performance are discussed.

3.1.1. The Development of the Prototype System

The crucial part of the electroporator is the pulse forming circuit. Following the transient processes analyses and circuit design detailed in the Chapter 2, the prototype of the square-wave electroporation system was developed.

The device features a compact design (18×29×22 cm) which provides advantage for portability and for reduction of the total parasitic inductance of the pulse forming circuit. As it can be seen, the power circuit and the pulse transmission line were chemically etched on a double sided FR4 PCB (Mega Electronics, Cambridge, UK). The 3 kV switching voltage supply MS3P/C (Spellman High Voltage Electronics Corp., Hauppauge, NY, USA) was used as the high-voltage source. In addition, the capacitor bank of 13.3 μF was used to ensure the pulse quality during the repetitive delivery. If more capacitance is needed to ensure pulse amplitude, the device was has built in plugin for external capacitance. The developed prototype of the system is based on isolated precision half-bridge drivers ADUM4223CRWZ (Analog Devices Inc., Norwood, MA, USA), while the pulse-forming is limited by the high-frequency semiconductor MOSFET switches with high dV/dt. As presented in previous chapters, the IGBTs, relays or the transmission line implementations have frequency, rise/fall time or current/voltage handling limitations. It was considered advantageous to use the series connected array of silicon carbide power MOSFET C2M0080120D (Cree Inc., Durham, NC, USA) switches with the 1.2 kV breakdown voltage for the high-voltage handling support. The discrete modules featuring higher voltages and power are slower and are disadvantageous for the implementation of the high-frequency electroporator.

The simplified pulse forming circuit of the device is shown in Figure 3.1 (Novickij et al. 2016). The prototype model circuit features six MOSFETs switches. Following the results of Chapter 2, the S1–S4 switches belong to main power line, which provides of the square-wave power pulses over the load (red dotted line), while S5–S6 forms a controlled crowbar circuit (blue dotted line). The controlled crowbar circuit (S5 and S6) is synchronized with S3 and S4 and is implemented to achieve a short pulse fall time, which generally independent of the load.

The RC snubber circuits are introduced in parallel to each switch for the purpose of pulse forming circuit transient compensation, while the snubber diodes D1–D6 are introduced to protect the switches from the reverse voltage. The decoupled driving circuits (DR1–DR4) are synchronized and control the MOSFETs. It should be noted that the driving circuits DR1–DR6 of the MOSFET array are drawn for better clarity of perception of the working principle of the pulse generator and do not represent the real pulse-forming, synchronization and power circuits of the drivers.

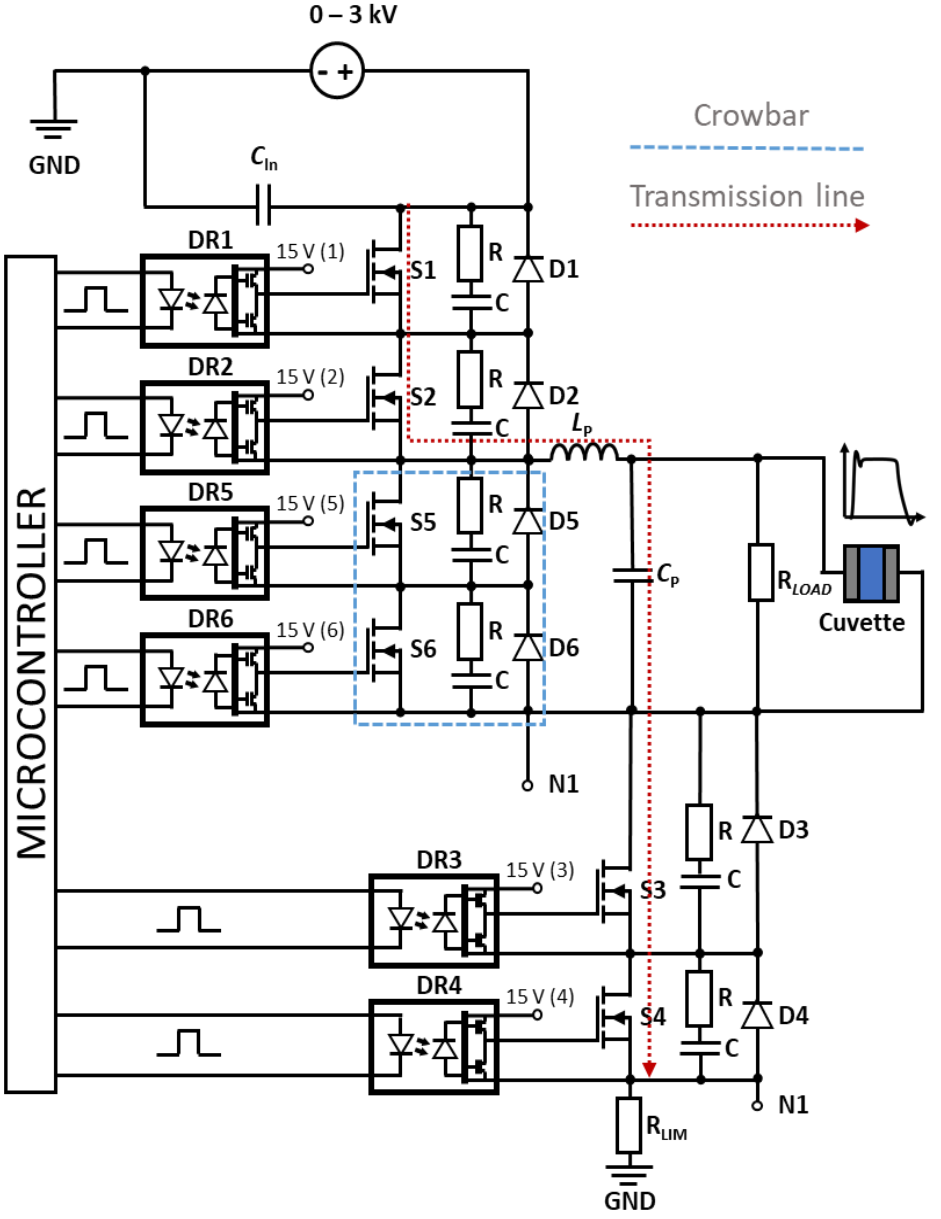

Fig. 3.1. Simplified schema of the high-frequency electroporator

The capacitor array, represented as C_P, is used for the energy storage. The C_s and L are introduced in the circuit diagram to highlight the influence of the contact capacitance and stray inductance respectively (Novickij et al. 2016). After validating model and experimental results, as presented in following section, the stray inductance was estimated as 1.2 μH (±21%), while the C_s was 50 pF (±21%) (Butkus et al. 2019).

The system performance is researched and presented in further chapter. The influence of the crowbar circuit was investigated by testing the generator performance using various resistive loads with and without the controlled crowbar. The maximum repetition frequency of the pulses was experimentally determined as a mean of five measurements (Novickij et al. 2016).

3.1.2. The Performance of the Prototype System

The generated pulse was measured using the 1:100 probe and a DPO4034 digital oscilloscope (Tektronix, Beaverton, OR, USA). The oscilloscope screenshot of shortest output pulse waveform is shown in Figure 3.2. As it can be seen, the transient compensation circuit of prototype device successfully minimized the influence of the parasitic inductance and capacitance. The pulse has only minor voltage overshoot and undershoot, which are respectively resulted of turn-on and turn-off of the switches. For further shortest pulse analyses, the experimental measurement results with detail pulse parameters are represented in Figure 3.8.

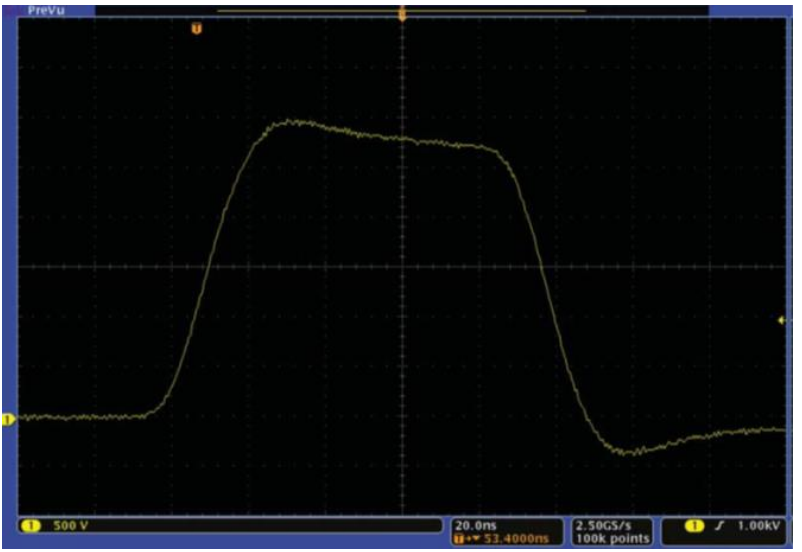

Fig. 3.2. DPO4034 digital oscilloscope screenshot of the shortest electrical pulse waveform generated by the electroporator (Novickij et al. 2016)

As seen in the Figure 3.8, the shortest pulse duration (measured at 50% of U_{max}) is 90 ns (±10%). The minimum pulse duration is limited by the MOSFET switching characteristics and the parasitic parameters of the circuit. The rise and fall times (10–90% of U_{max}) are <30 ns. The proposed synchronized controlled crowbar circuit ensured fast voltage switching. In addition, the output pulse waveform of the maximum 3 kV pulse amplitude can be found in following experimental applications (Novickij, Stanevičienė, et al. 2020).

The influence of the controlled crowbar circuit was investigated experimentally with various resistive loads. The investigation results are presented in Figure 3.3. As seen in the figure, without the activation of the controlled crowbar circuit, the pulse fall time depends on the load impedance. In case of high loads (<500 Ω) the pulse fall time would extend from few ns to hundreds of ns, which is disadvantageous in electroporation. Even in case of smaller load, the pulse fall time is still affected and is longer than the MOSFET switch manufacture specified (24 ns) fall time. On the other hand, when the controlled crowbar is activated, the pulse fall time is only dependent on the MOSFET switch opening time. Therefore, the pulse fall time is reduced to 18 ns and the prototype system allows ensuring an identical electric field treatment intensity independent of the load type (Novickij et al. 2016).

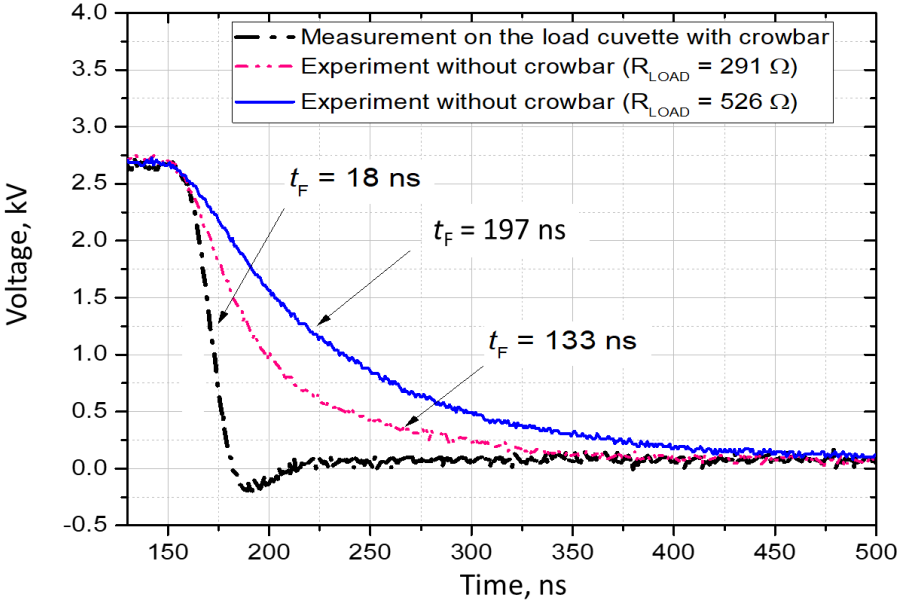

Fig. 3.3. Falling edge of generated electrical pulse for the cases with and without crowbar

The maximum pulse repetition frequency of the device was tested and experimentally determined as a mean of five measurements. It was determined that a maximum repetition frequency of 3.5 MHz could be achieved, which is higher than expected, thus an additional advantage of the system. The 3.5 MHz pulse burst is shown in Figure 3.5.

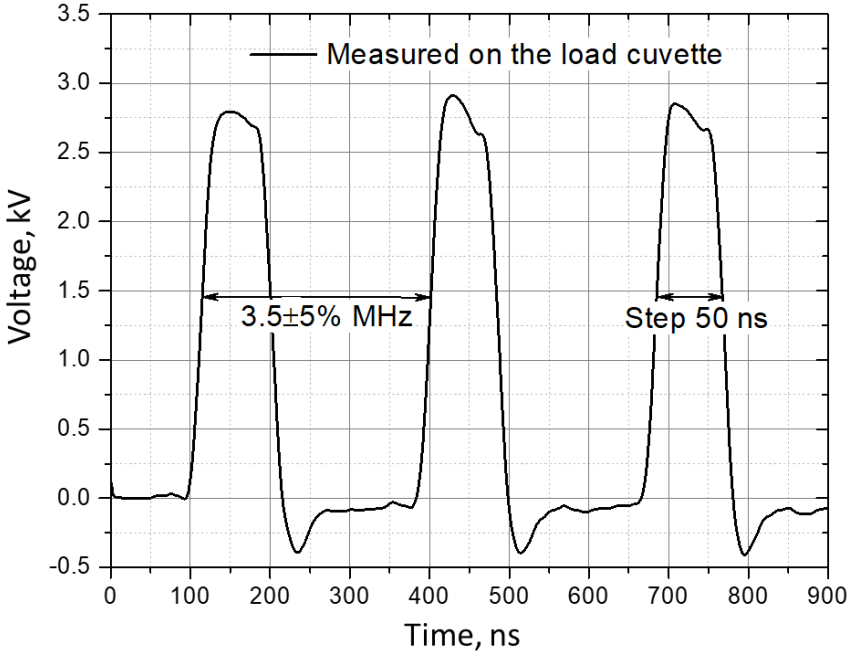

Fig. 3.4. High-frequency burst of 100 ns pulses generated by the developed electroporator (Novickij et al. 2016)

The maximum pulse repetition frequency is highly influenced by the switch type. In our case, it was CREE C2M0080120D (Cree Inc., Durham, NC, USA), which additionally ensures 36 A continuous and 80 A pulsed drain currents. However, the following maximum current measurement results for single switch, it was concluded, that the maximum pulsed current value was limited to 60 A for the support of the 50 Ω load (at maximum voltage). In any case, high-energy pulses are rarely used because of the Joule heating which takes place due to the high current flow. Therefore, high impedance buffers are preferable and the device must be capable of generating electrical pulses of identical form independent of the buffer type, which is relevant in electroporation experiments. Further switching dynamics can be investigated in advance using the methodology proposed by Ahmed et al. (Ahmed et al. 2015; Novickij et al. 2016).

To sum up, it was confirmed that the resulting high-frequency electroporator is capable of delivering adjustable up to 3 kV pulses with a predefined wide range of frequency (1 Hz to 3.5 MHz). The duration of the pulse can be varied in a broad range: 100 ns – 1 ms (Novickij et al. 2016).

3.2. The Comparison with In-House Built Generators for nsPEF Electroporation

The developed prototype of high-frequency square-wave electroporation system can be directly used in a wide range of electroporation applications as well as contributing to a research of the electroporation phenomenon in the least studied ranges of electric field strength and frequency. To highlight the novelty, the developed system is compared with other in-house developed nsPEF generators following the results Chapter 1 (Figure 3.5).

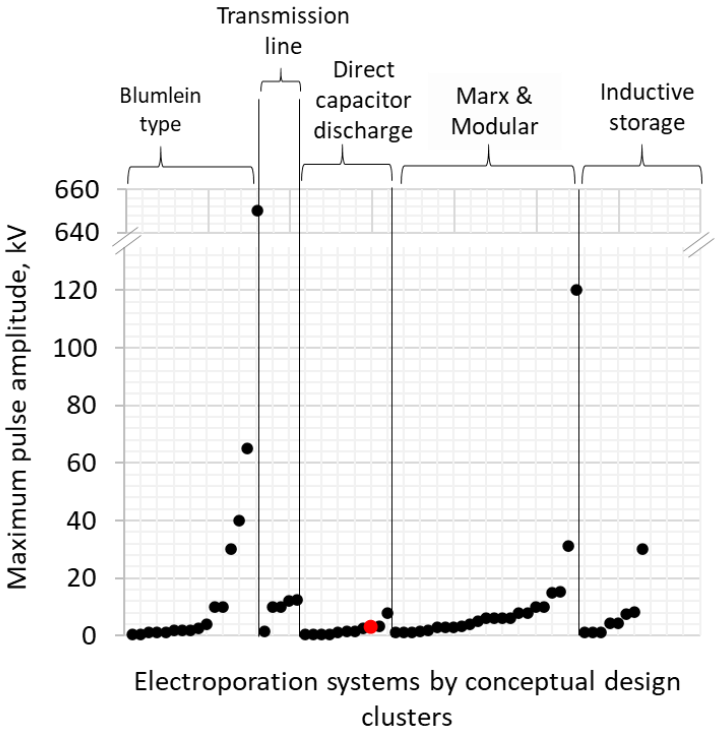

Fig. 3.5. The comparison of nsPEF electroporation systems according to the maximum amplitude of generated pulse

Figure 3.5 provides a comparison of in-house built nsPEF electroporation systems according to the maximum amplitude of generated pulse. It can be seen, that the majority of devices provides the maximum amplitude in range of few kV, while few Blumlein type devices can deliver the pulse up to hundreds of kV. The maximum amplitude of the developed square-wave electroporation system is up to 3 kV and is marked in red in Figure 3.5. It can be seen, that it is in top three in the class of direct capacitor discharge-based generators, but does not outstand the majority of nsPEF electroporation systems.

In most cases, series of pulses are applied for electroporation application, therefore, the pulse repetition frequency is an important parameter for different applications. It was mentioned, that high-frequency electroporation systems are required to reflect the latest findings of the electroporation studies and contribute to further research of frequency dependence of electroporation phenomena. Figure 3.6 provides a comparison of in-house built nsPEF electroporation systems according to maximum repetition frequency of generated pulse.

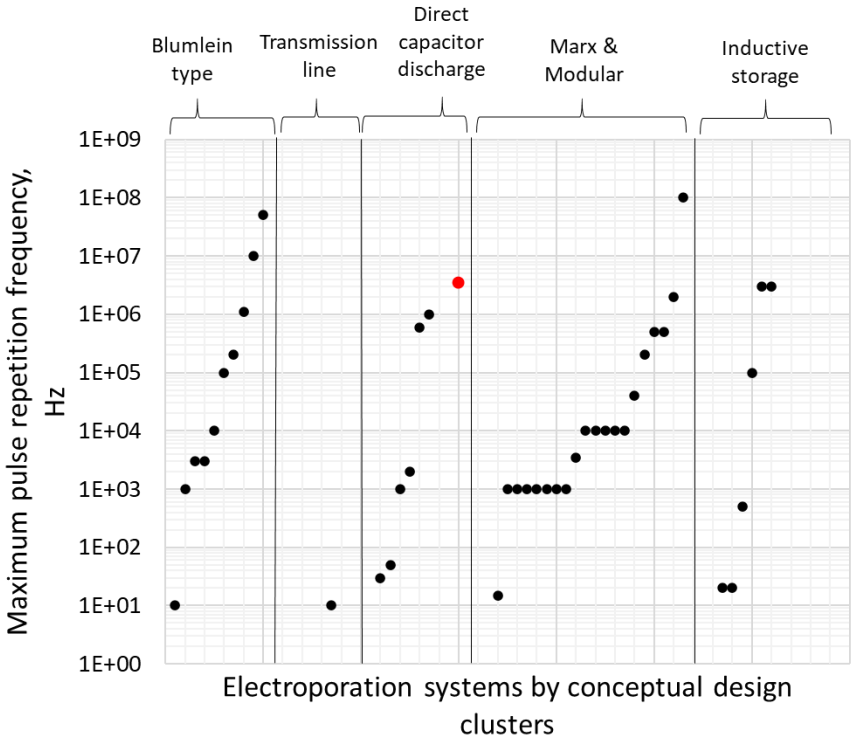

Fig. 3.6. The comparison of nsPEF electroporation systems according to the maximum repetition frequency of generated pulses

As it can be seen in Figure 3.6, the developed high-frequency square-wave electroporation system, with maximum repetition frequency up to 3.5 MHz, has the best frequency range in the category of direct capacitor discharge based electroporators. In addition, the device frequency range is among top four in-house built nsPEF electroporation systems. Therefore, the extensive range of frequency variation ensures of the developed system is suitable to investigate the electroporation frequency dependence in high-frequency range and propose new electroporation protocols.

Lastly, the potential electroporation application depends on the individual duration of square-wave pulse. It was indicated, that the majority of electroporation applications lie in the micro-millisecond range, while in recent years there is a growing interest to research and apply shorter (submicrosecond and nanosecond) pulses. Figure 3.7 compares currently in-house built electroporation systems based on available pulse duration range. It is noticeable, that about 60% of developed devices were reported with a fixed pulse duration. This is resulted by the pulse forming circuit design and most common for transmission line, Blumlein and inductive storage-based systems. Even about 40% of Marx or modular based nsPEF electroporators were also reported with fixed pulse duration. Therefore, the nsPEF electroporation system capability to deliver adjustable range of pulse is a highly desired feature for wide range electroporation research.

The pulse duration range of developed square-wave electroporation system can be adjusted from 100 ns to 1 ms. It is highlighted in red color in Figure 3.7. The shortest pulse duration of the system is one of the shortest among the direct capacitor discharge-based nsPEF electroporation systems, but falls behind the majority Blumlein, transmission line and inductive storage devices with shorter, but fixed (not adjustable) pulse duration. These nsPEF electroporation systems are specifically designed to deliver less than 100 ns pulses, but most often are not able to variate the pulse duration due to the switches used (e.g. spar-gap).

The longest pulse duration of the system is equal to 1 ms and place the system among top three devices, which can deliver both: submicrosecond and millisecond pulses. Taking into account all range of the pulse duration, it can be seen, that the developed electroporation system can deliver second widest range of pulse duration among all in-house built nsPEF electroporation systems.

These results show, that the developed prototype system features the most advanced pulse forming capabilities in nsPEF range. It confirms, that this system can be directly used in a wide range of electroporation applications. Thus, help to reach a deeper understanding of the individual pore formation process, which will allow better control and optimization of the electroporation protocols. It can also support research and application of the most popular electroporation protocols (microsecond range) for biomedical techniques and medical applications.

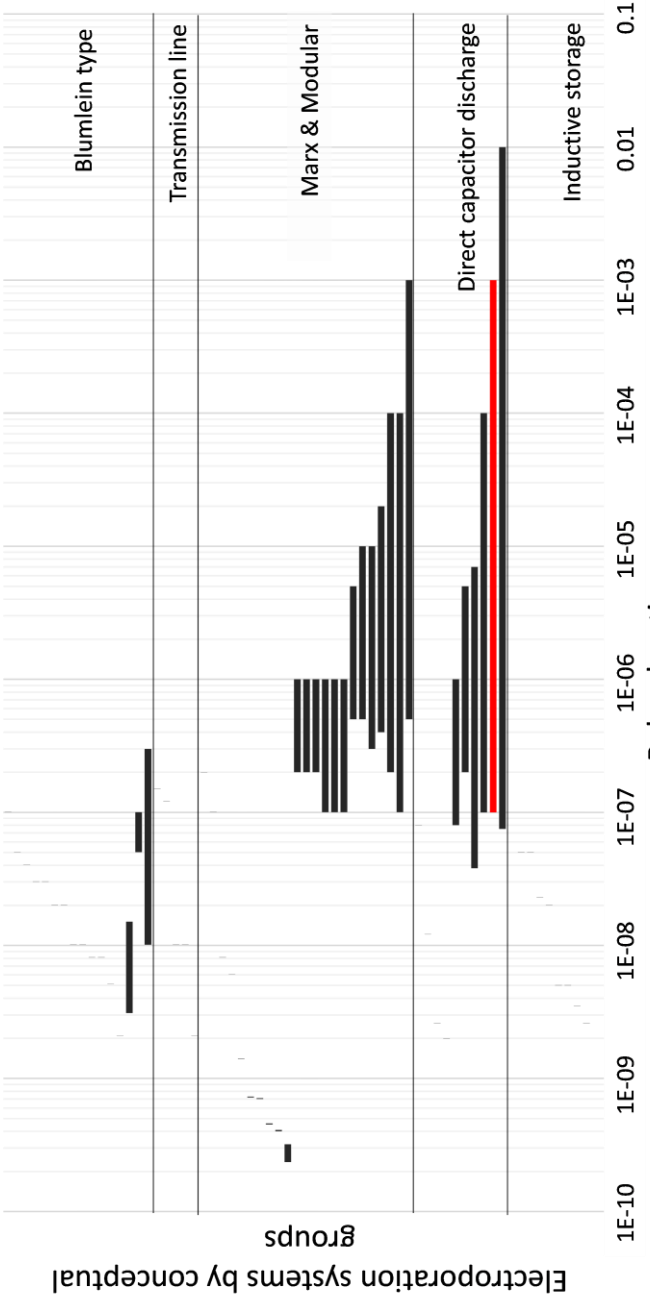

Fig. 3.7. The comparison of nsPEF electroporation systems according to the duration range of generated pulse

3.3. The Validation of the SPICE Model

In this section, a validation of the simulation results of a pulse forming circuit is provided. The SPICE model (presented in Chapter 2) was validated via a comparison of the simulation and experimental results obtained from the prototype system described above.

As a first step of validation, a single compensated output pulse on the load of 100 Ω was simulated with the SPICE model under different RC snubber circuit parameters and compared with the measured single output pulse of the nsPEF generator prototype system. The PEF generator output signal on the 100 Ω load cuvette was measured using the 1:100 probe and a DPO4034 digital oscilloscope (Tektronix, Beaverton, OR, USA). To capture the output waveform, the experimental results were recorded as a mean of five measurements (Butkus et al. 2019). The single pulse comparison results are presented in Figure 3.8.

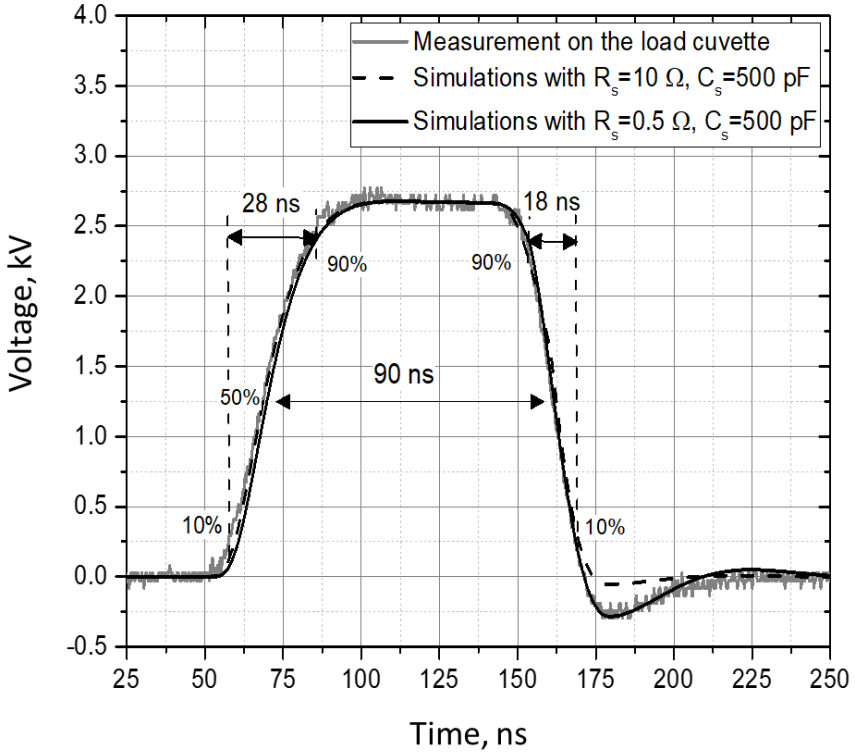

Fig. 3.8. The comparison of simulation and experimental results of a single electrical pulse waveform generated by the PEF generator (Butkus et al. 2019)

Figure 3.8 shows the measured output pulse of the developed PEF generator prototype system and two simulation curves with swept snubber resistance. The single 2.7 kV output pulse waveform at the minimum duration of the existing nsPEF generator was used for this comparison. As seen in Figure 3.8, the pulse duration (measured at 50% of the pulse amplitude) was 90 ns (±10%), which was well adjusted in the SPICE model to match the measurement results to estimate the pulse rise and fall time matching. A rise time of 28 ns and a fall time of 18 ns was measured (10–90% of the pulse amplitude). The measured values matched well with the simulation results, underlining the influence of the controlled crowbar circuit on output voltage (Butkus et al. 2019).

In addition, as seen in Figure 3.8, the snubber resistance of 10 Ω and the snubber capacitance of 500 pF resulted in a faster turn-off time and better minimization of the reverse overvoltage. However, the snubber resistance of 0.5 Ω with 500 pF snubber capacitance fit better with the measured signal. These results suggest that the RC snubber circuits used in the prototype system could be further improved. In any case, the implemented RC circuit helped to suppress a transient process and limit the reverse overvoltage during the fall time of the pulse. At the same time, the comparison results indicate that the developed SPICE model is sufficient for the prototyping of PEF generators (Butkus et al. 2019).

To evaluate the uncertainty of the simulation and experimental results of a single electrical pulse, the uncertainty evaluation histogram with the confidence level of two standard deviations (2σ), as presented in Figure 3.9, was used.

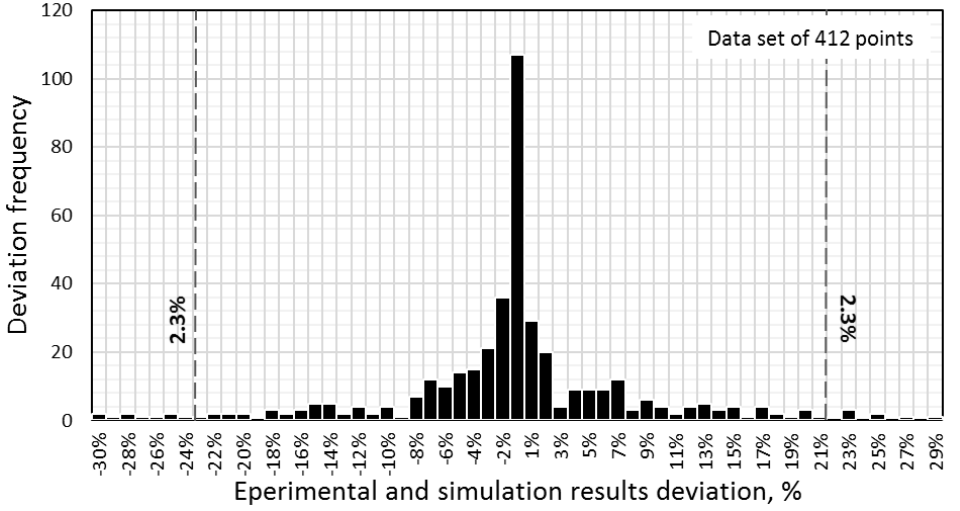

Fig. 3.9. The comparison of simulation and experimental results of a single electrical pulse waveform generated by the PEF generator (Butkus et al. 2019)

The Figure 3.9, presents the histogram composed of 412 simulation and experimental result deviation sample points. Each sample points represents a voltage value at the same timestamp. For each of these points, a deviation was calculated, which were later used to construct a histogram. The bins range of 1% was chosen with limit of the ±30%. Therefore, a vertical axis represents the frequency of the calculated deviation in each given range.

Figure 3.9 shows, that the largest frequency of deviation clusters is around the value of ±2%, thus, representing the mean value, but more importantly, due to the inherent error in simulation results, outcomes are scattered about the mean. The histogram shape is close to the normal distribution and the two vertical lines, at about ±21%, are placed to separate the 95.4% of the comparison data set from remaining 2.3% for each side. This shows, that the actual uncertainty of simulation results is ±21% (with 95.4% confidence level).

To evaluate the controlled crowbar circuit impact estimated in SPICE model and actual experimental result, the resulting pulse of the prototype system on the load of 100 **Ω** with the implemented crowbar circuit is shown in Figure 3.10. Therefore, the simulation results are in good match with the experimental measurement, thus validating the impact on the pulse fall time (Butkus et al. 2019).

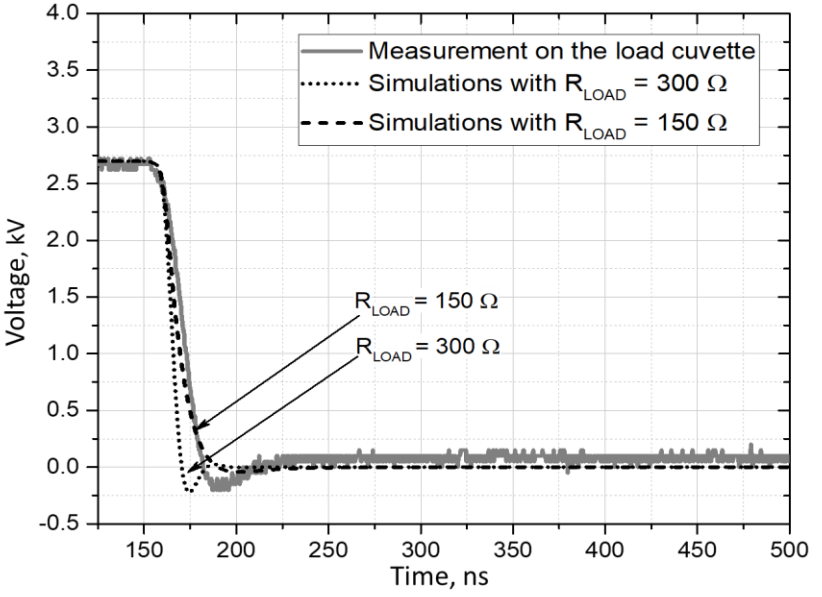

Fig. 3.10. Falling edge of generated and simulated electrical pulse for the cases with and without crowbar (Butkus et al. 2019)

The developed prototype system of the nsPEF generator was capable of generating pulses with a frequency up to 3.5 MHz. Figure 3.11 presents the measured 3 kV output pulse at highest pulse repetition frequency performance of the developed prototype of the nsPEF electroporation system. It appears that pulses with a duration of 80 ns (measured on 50% of the pulse amplitude) and a rise and fall time of 25 ns and 18 ns, respectively, were generated. In addition, the simulation results of the SPICE model at high-frequency performance is included for comparison reason.

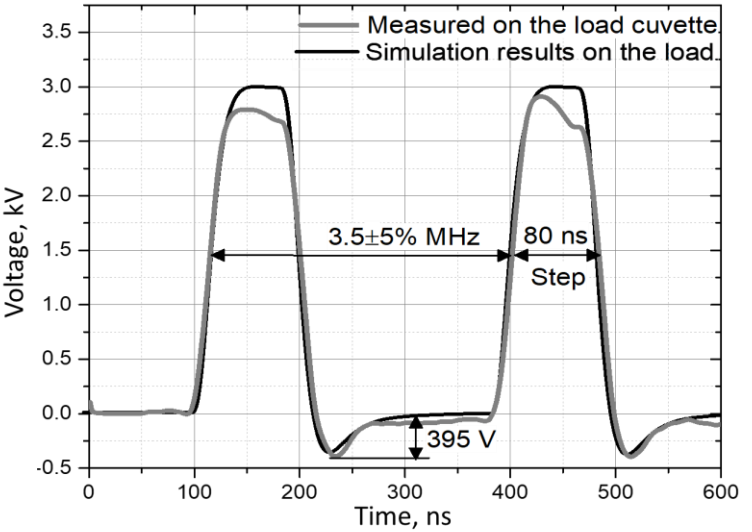

Fig. 3.11. Simulation and experimental results of the PEF generator's high-voltage submicrosecond output pulses on the load of 100 Ω with repetition frequency up to 3.5 MHz (Butkus et al. 2019)

As it can be seen in Figure 3.11, the high-frequency performance simulation results of the SPICE model were in good agreement with the measured output signal of the prototype system, except for the peak amplitude of the experimentally generated pulse. The high frequency and high voltage pulses creates a thermal impact on the load, which result the change of the electrical parameters. Therefore, pulse amplitude difference of measured and simulated results in high-frequency. In any case, the developed SPICE model may be considered sufficient for analysing transient processes in electroporation systems and can be used in the prototype design phase of new PEF generators (Butkus et al. 2019). In addition, the further works could be complemented by the additional model to reflect the thermal influence and change of the load electrical parameters during the treatment.

3.4. The Application of Prototype System for Electroporation

In this section the application of the developed novel high-frequency electroporation system for electroporation application is demonstrated. The electroporator was tested for *in vitro* inactivation of the human pathogen *Candida albicans* using electroporation. *C. albicans* was isolated from nail specimens in the Laboratory of Microbiology at the Centre of Laboratory Medicine, Vilnius University Hospital, Santariškės Clinics and identified by Vitek® 2 systems (bioMérieux, Marcy-l'Étoile, France). The strain was maintained on Sabouraud dextrose agar (SDA; Liofilchem, Roseto degli Abruzzi, Italy) slants at 28 ºC. The suspensions for the treatment were prepared by gently scraping the culture surface with a sterile glass rod and inoculating the cells into sterile deionized water. *C. albicans* cell density for each solution was OD_{610} = 0.2. The suspensions were incubated overnight. Aliquot samples (80 µL) were used for pulsed electric field treatment.

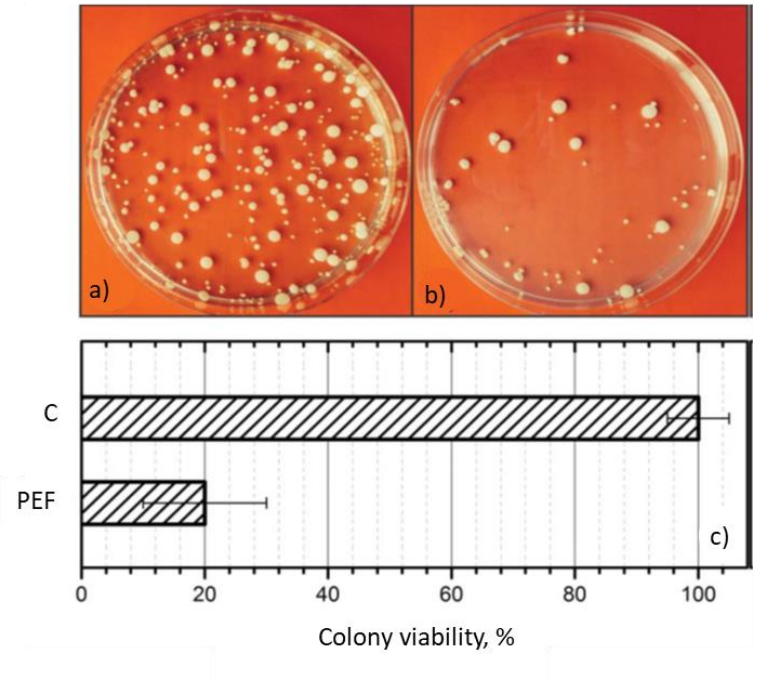

Fig. 3.12. Inactivation of *C. albicans* using electroporation: a) control (C) sample without PEF treatment; b) control (C) sample after PEF treatment (10×100 µs 30 kV/cm); c) colony plate counts (Novickij et al. 2016)

A burst of ten 30 kV/cm (10 Hz) 100 μs electrical pulses was applied. After PEF treatment, 3 μL samples were pipetted into 1 μL sterile distilled water and vortexed. Additional dilution by a factor of 100 was performed for each sample. Then, 100 μL samples were inoculated onto SDA Petri dishes. The cells were incubated at 28 °C for 72 h. After incubation, the number of viable cells was evaluated by calculation of the number of the colony-forming units and was expressed as a percentage in respect to the control sample (without PEF treatment). The colonies before and after the treatment are shown in Figure 3.12.

The obtained results demonstrated that the applied electroporation regime can be successfully used for inactivation of *C. albicans in vitro*. The colony viability was reduced to 20% after electroporation. Thus, it was confirmed that the developed electroporator is suitable for biological experiments and enables a flexible parametric study of the electroporation process, which was not possible previously to such an extent (Novickij et al. 2016).

Until the introduction of the new device, the latest electroporation phenomena studies were limited by the kHz range repetition rate pulses (Silve et al. 2014; Lamberti et al. 2015). However, it has been shown that even alteration of the frequency in a narrow 2–30 Hz range creates a changes in the bio-effects of the high electric field (Lamberti et al. 2015). As a result, the novel high-frequency square-wave electroporation system allows to investigate and propose new electroporation concepts. It had already successfully assisted many different research works, which are summarized in Table 3.1.

As indicated in Table 3.1, the device was successfully used to investigate the nsPEF effects, which resulted the proposal of new treatment methodologies and non-viral gene delivery methods proof of concept (Novickij, Rembialkowska, et al. 2020; Ruzgys et al. 2018; Novickij, Zinkevičienė, Perminaitė, et al. 2018; Novickij, Stanevičienė, et al. 2020; Novickij, Zinkevičienė, Valiulis, et al. 2018; Novickij, Zinkevičienė, Stanevičienė, et al. 2018; Novickij, Česna, et al. 2019), which confirmed, that nsPEF bursts can be used for eradication of bacteria. The developed square-wave systems application has also included the research in MHz pulse repetition frequency range (Ruzgys et al. 2019; Pakhomov et al. 2019). The authors have successfully used this electroporation system to develop a new methodology based on high frequency. So far, the system was also used to investigate the different permeabilization patterns in combination with magnetic field (Novickij, Zinkevičienė, Valiulis, et al. 2018), calcium (Novickij, Česna, et al. 2019) and conventional (Novickij, Lastauskienė, et al. 2018) electroporation treatments.

Table 3.1. Application of the developed high-frequency square-wave electroporation system

Research focus	Duration	Electric Field, kV/cm	Number of pulses	Frequency	Reference
Investigation of extracellular medium conductivity effects during electroporation in the nsPEF range	25, 100–900 ns,100 µs	0.6–60	8–1200	1 Hz–1 kHz	(Novickij, Rembialkowska, et al. 2020)
Excitation and electroporation by MHz bursts of nsPEF	11-500 ns and 1 ms	0.01-5	5–1000	1 Hz, 3-4 MHz	(Pakhomov et al. 2019)
C Comparison of electroporation efficiency and the amount of generated reactive oxygen species	200 ns and 5, 10, 100 µs	7–14	1, 8, 25, 50	1Hz, 1 MHz	(Ruzgys et al. 2019)
nsPEF application as a non-viral gene delivery method proof of concept	200 ns and 2, 100 µs	1.4, 10–18	1, 2, 10	1 Hz–1 MHz	(Ruzgys et al. 2018)
Development of new methodology based on high frequency nsPEF bursts for enabling the successful eradication of bacteria	300–900 ns and 100 µs	15–25	8, 500, 1000	15 kHz	(Novickij, Zinkevičienė, Perminaitė, et al. 2018)
Inactivation of *S. typhimurium* and *L. innocua* in stationary phase using ns and ms PEF in combination with nisin-loaded pectin nanoparticles.	200 ns – 500 µs	30	10–5000	-	(Novickij, Stanevičienė, et al. 2020)
Investigation of different permeabilization patterns in combination of pulsed electric and magnetic field treatments	300, 500 ns and 2, 100 µs	0–8	1, 5	1 kHz	(Novickij, Zinkevičienė, Valiulis, et al. 2018)
Inactivation of *Escherichia coli* using nsPEF and nisin nanoparticles	100–900 ns and 100 µs	0–30	8, 500	1 kHz	(Novickij, Zinkevičienė, Stanevičienė, et al. 2018)
Antitumor response and immunomodulatory effects using the combination of nsPEF irreversible and calcium electroporation	200, 500 ns	12	500	100 Hz	(Novickij, Česna, et al. 2019)
Dye concentration & transient permeability of Sp2/0 myeloma cells	100 µs	0.8–2	8	1 kHz	(V. Novickij et al. 2016)
Permeabilization of pathogenic yeast using nsPEF in combination with conventional electroporation	100 µs	8, 10, 13, 17	1	-	(Novickij, Lastauskienė, et al. 2018)
PEF-assisted sensitization of multidrug-resistant *C. albicans* to antifungal drugs	100, 200 µs	2.5–25	1, 25, 50	1 kHz	(Novickij, Švediene, Paškevičius, et al. 2018)
Increase of the inactivation of *S. aureus* and *P. aeruginosa* with PEF in combination with low concentrations of acetic and formic acids	100 µs	10–30	10, 20	1 kHz	(Novickij, Lastauskiene, et al. 2019)

Summarizing the prototype system performance and application results with the state of art comparison presented in Section 3.2, there are no currently published (at our knowledge) implementations of high-frequency (MHz range), high-voltage (up to 3 kV), electroporation systems that are capable of generating adjustable duration (from 100 ns to 1 ms) square-wave pulses with load-independent pulse fall times. The introduction of such high-frequency devices is advantageous for the study of the submicrosecond electroporation range. Due to the capacitive properties of the cytoplasm and the dielectric relaxation, the induced transmembrane potential dependence is not trivial in the high pulse frequency range (Zou et al. 2015), while the role of the pulse repetition rate in the nsPEF range is considered to be controversial and requires investigation.

The expansion of the study range by introduction of novel high-frequency square-wave electroporation system allows investigation of newly proposed concepts such as electro-desensitization (Silve et al. 2014; Novickij, Švediene, Paškevičius, et al. 2018) and helps to extend the understanding of the electroporation process even further.

3.4. Conclusions of Chapter 3

1. The developed high-frequency square-wave electroporation system ensures a delivery of adjustable up to 3 kV square-wave electric pulses with a predefined frequency (1 Hz to 3.5 MHz). The duration of the pulse can be varied in a range from 100 ns to 1 ms.
2. The proposed synchronized controllable crowbar circuit ensures a constant pulse fall time, which is independent from the load, thus highly relevant in electroporation.
3. SPICE model for a pulse forming circuit, which was introduced in previous chapter, was validated and proved to be in good agreement with the experimental results with uncertainty of ±21% (95.4% confidence level), for the submicrosecond pulse range.
4. The electroporator showed decent performance in electroporation experiments for inactivation of the human pathogen *C. albicans*. It was shown that a burst of ten 30 kV/cm (10 Hz) 100 μs pulses reduced the colony viability to 20% compared to the untreated samples.

General Conclusions

1. A novel high-frequency square-wave electroporation system, which can deliver adjustable high-amplitude (up to 3 kV) pulses with a predefined frequency (from 1 Hz to 3.5 MHz), has been developed and presented. The duration of the pulse produced by the system can be varied in a range from 100 ns to 1 ms.
2. The proposed synchronized controllable crowbar circuit has been proved to be efficient and capable to ensure a constant 18 ns pulse fall time, which is independent from the load, thus is highly relevant in electroporation.
3. The results of developed simulation model of the high-frequency square-wave pulse forming circuit are in compliance with experimentally determined results with uncertainty of ±21% (95.4% confidence level). The model is suitable for the evaluation of the influence of the circuit parasitic elements and transient processes on the submicrosecond pulse shape.
4. Based on the planar electrodes models results in COMSOL Multiphysics environment, it can be stated that, the proposed topology of the planar electrodes is suitable for real-time electroporation, while the 250–350 μm gap between electrodes ensures homogeneous distribution and electric field strength more than 1 kV/cm.

References

Abdelsalam I., Elgenedy M. A., Ahmed S., Williams B. W. 2017. Full-bridge modular multilevel submodule-based high-voltage bipolar pulse generator with low-voltage DC, input for pulsed electric field applications, *IEEE Transactions on Plasma Science* 45(10): 2857–2864. DOI: 10.1109/TPS.2017.2743822.

Achour Y., Starzyński J., Kasprzycka W., Trafny E. A. 2019. Compact low-cost high-voltage pulse generator for biological applications, *International Journal of Circuit Theory and Applications* 47(12): 1948–1962. DOI: 10.1002/cta.2708.

Ahmed M. R., Todd R., Forsyth A. J. 2015. Analysis of SiC MOSFETs under hard and soft-switching, *2015 IEEE Energy Conversion Congress and Exposition, ECCE 2015*: 2231–2238. DOI: 10.1109/ECCE.2015.7309974.

Akiyama M., Sakugawa T., Hosseini S. H. R., Shiraishi E., Kiyan T., Akiyama H. 2010. High-performance pulsed-power generator controlled by FPGA *IEEE Transactions on Plasma Science*. DOI: 10.1109/TPS.2010.2042463.

Analog Devices 2017. ADuM3223/ADuM4223 Isolated Precision Half-Bridge Driver, *Technical Datasheet*: 1–20.

De Angelis A., Denzi A., Merla C., Andre F. M., Garcia-Sanchez T., Mir L. M., Apollonio F., Liberti M. 2019. A Microdosimetric Realistic Model to Study Frequency-Dependent Electroporation in a Cell with Endoplasmic Reticulum *2019 49th European Microwave Conference, EuMC 2019*. Institute of Electrical and Electronics Engineers Inc. DOI: 10.23919/EuMC.2019.8910909.

Arena C. B., Sano M. B., Rossmeisl J. H., Caldwell J. L., Garcia P. A., Rylander M. N., Davalos R. V. 2011. High-frequency irreversible electroporation (H-FIRE) for non-thermal ablation without muscle contraction, *BioMedical Engineering Online* 10. DOI: 10.1186/1475-925X-10-102.

Balevicius S., Stankevic V., Zurauskiene N., Shatkovskis E., Stirke A., Bitinaite A., Saule R., Maciuleviciene R., Saulis G. 2013. System for the nanoporation of biological cells based on an optically-triggered high-voltage spark-gap switch, *IEEE Transactions on Plasma Science* 41(10): 2706–2711. DOI: 10.1109/TPS.2013.2280376.

Batista N. T., Reberšek M., Vernier P. T., Mali B., Miklavčič D. 2016. Effects of high voltage nanosecond electric pulses on eucaryotic cells (in vitro): A systematic review, *Bioelectrochemistry* 110: 1–12. DOI: 10.1016/j.bioelechem.2016.02.011.

Batista Napotnik T., Miklavčič D. 2018. In vitro electroporation detection methods – An overview, *Bioelectrochemistry* 120: 166–182. DOI: 10.1016/j.bioelechem.2017.12.005.

Behrend M., Kuthi A., Gu X., Vernier P. T., Marcu L., Craft C. M., Gundersen M. A. 2003. Pulse Generators for Pulsed Electric Field Exposure of Biological Cells and Tissues *IEEE Transactions on Dielectrics and Electrical Insulation*. DOI: 10.1109/TDEI.2003.1237331.

Bennett W. F. D., Sapay N., Tieleman D. P. 2014. Atomistic Simulations of Pore Formation and Closure in Lipid Bilayers, *Biophysical Journal* 106(1): 210–219. DOI: 10.1016/j.bpj.2013.11.4486.

Bernal C., Lucia O., Sarnago H., Burdio J. M., Ivorra A., Castellvi Q. 2015. A Review of Pulse Generation Topologies for Clinical Electroporation, *In Proceedings of the IECON 2015—41st Annual Conference of the IEEE Industrial Electronics Society*, Yokohama, Japan, 9–12 November 2015; pp. 625–630. DOI: 10.1109/IECON.2015.7392169.

Bhonsle S., Lorenzo M. F., Safaai-Jazi A., Davalos R. V. 2018. Characterization of nonlinearity and dispersion in tissue impedance during high-frequency electroporation, *IEEE Transactions on Biomedical Engineering* 65(10): 2190–2201. DOI: 10.1109/TBME.2017.2787038.

Buchmann L., Mathys A. 2019. Perspective on Pulsed Electric Field Treatment in the Bio-based Industry, *Frontiers in Bioengineering and Biotechnology* 7: 265. DOI: 10.3389/fbioe.2019.00265.

Camp J. T., Xiao S., Schoenbach K. H. 2008. Development of a high voltage, 150 ps pulse generator for biological applications *Proceedings of the 2008 IEEE International Power Modulators and High Voltage Conference, PMHVC*. DOI: 10.1109/IPMC.2008.4743653.

Cemazar M., Sersa G., Frey W., Miklavcic D., Teissié J. 2018. Recommendations and requirements for reporting on applications of electric pulse delivery for electroporation of biological samples, *Bioelectrochemistry* 122: 69–76. DOI: 10.1016/j.bioelechem.2018.03.005.

Cervia L. D., Chang C. C., Wang L., Mao M., Yuan F. 2018. Enhancing Electrotransfection Efficiency through Improvement in Nuclear Entry of Plasmid DNA, *Molecular Therapy - Nucleic Acids* 11: 263–271. DOI: 10.1016/j.omtn.2018.02.009.

Chalovich J. M., Eisenberg E., Weaver J. C., Smith K. C., Esser A. T., Son R. S., Gowrishankar T. R., Chalovich J. M., Eisenberg E. 2012. A brief overview of electroporation pulse strength-duration space: A region where additional intracellular effects are expected, *Bioelectrochemistry* 87(5): 236–243. DOI: 10.1016/j.bioelechem.2012.02.007.

Chalovich J. M., Eisenberg E. 2006. Nanosecond pulsed electric fields cause melanomas to self- destruct, *Biochem Biophys Res Commun* 343(2): 351–360. DOI: 10.1016/j.immuni.2010.12.017.Two-stage.

Chaney A., Sundararajan R. 2004. Simple MOSFET-based high-voltage nanosecond pulse circuit, *IEEE Transactions on Plasma Science* 32(5 I): 1919–1924. DOI: 10.1109/TPS.2004.835966.

Chiapperino M. A., et al. 2020. Experimental and Numerical Study of Electroporation Induced by Long Monopolar and Short Bipolar Pulses on Realistic 3D Irregularly Shaped Cells, *IEEE Transactions on Biomedical Engineering*: 1–1. DOI: 10.1109/tbme.2020.2971138.

Chicaybam L., et al. 2017. An Efficient Electroporation Protocol for the Genetic Modification of Mammalian Cells, *Frontiers in Bioengineering and Biotechnology* 4: 99. DOI: 10.3389/fbioe.2016.00099.

Chopinet L., Batista-Napotnik T., Montigny A., Rebersek M., Teissié J., Rols M. P., Miklavčič D. 2013. Nanosecond electric pulse effects on gene expression, *Journal of Membrane Biology* 246(11): 851–859. DOI: 10.1007/s00232-013-9579-y.

Chuan L., Wenchuan W., Lin Z., Mingjia L., Jianhua Z. 2014. Development of 650 kV 2 ns high voltage pulse generator, *High Power Laser and Particle Beams* 26(12): 3–7.

CREE Inc. 2015a. C2M0080120D Silicon Carbide Power MOSFET, *Technical Datasheet*: 1–9.

CREE Inc. 2019. C2M0160120D Silicon Carbide Power MOSFET, *Technical Datasheet*: 1–10.

CREE Inc. 2015b. C2M1000170D Silicon Carbide Power MOSFET, *Technical Datasheet*: 1–10.

Cronjé T. F., Gaynor P. T. 2013. High voltage and frequency bipolar pulse generator design for electroporation-based cancer therapy *2013 Australasian Universities Power Engineering Conference, AUPEC 2013*. DOI: 10.1109/aupec.2013.6725469.

Darwish A., Elgenedy M. A., Finney S. J., Williams B. W., McDonald J. R. 2019. A step-up modular high-voltage pulse generator based on isolated input-parallel/output-series voltage-boosting modules and modular multilevel submodules, *IEEE Transactions on Industrial Electronics* 66(3): 2207–2216. DOI: 10.1109/TIE.2017.2772189.

Das M., Grider D., Leslie S., Raju R., Schutten M., Hefner A. 2012. 10 kV SiC power MOSFETs and JBS diodes: Enabling revolutionary module and power conversion technologies *Materials Science Forum*. DOI: 10.4028/www.scientific.net/MSF.717-720.1225.

Davies I. W., et al. 2019. Push-pull configuration of high-power MOSFETs for generation of nanosecond pulses for electropermeabilization of cells *International Journal of Microwave and Wireless Technologies*. Cambridge University Press. DOI: 10.1017/S1759078719000576.

Deng J., Stark R. H., Schoenbach K. H. 2000. Nanosecond pulse generator for Intracellular Electromanipulation *IEEE Conference Record of Power Modulator Symposium*. IEEE. DOI: 10.1109/modsym.2000.896161.

Denzi A., et al. 2015. Assessment of cytoplasm conductivity by nanosecond pulsed electric fields, *IEEE Transactions on Biomedical Engineering* 62(6): 1595–1603. DOI: 10.1109/TBME.2015.2399250.

Dermol-Černe J., Pirc E., Miklavčič D. 2020. Mechanistic view of skin electroporation–models and dosimetry for successful applications: an expert review, *Expert Opinion on Drug Delivery*. DOI: 10.1080/17425247.2020.1745772.

Dermol J., Pakhomova O. N., Pakhomov A. G., Miklavčič D. 2016. Cell Electrosensitization Exists Only in Certain Electroporation Buffers P. McNeil, sud., *PLOS ONE* 11(7): e0159434. DOI: 10.1371/journal.pone.0159434.

Deshpande A., Prakash G. V., Goswami U., Singh R., Anitha V. P. 2019. Implementation of Line Type High Voltage Nanosecond Rectangular Pulse Generator with Adjustable Pulse Widths for Liquid Discharge Applications *IEEE International Pulsed Power Conference*. Institute of Electrical and Electronics Engineers Inc. DOI: 10.1109/PPPS34859.2019.9009998.

Dong S., Yao C., Mi Y., Li C., Zhao Y., Lv Y., Liu H. 2017. Design of bipolar pulse generator topology based on Marx supplied by double power *2016 IEEE International Power Modulator and High Voltage Conference, IPMHVC 2016*. Institute of Electrical and Electronics Engineers Inc. DOI: 10.1109/IPMHVC.2016.8012779.

Dong S., Yao C., Yang N., Luo T., Zhou Y., Wang C. 2016. Solid-State Nanosecond-Pulse Plasma Jet Apparatus Based on Marx Structure with Crowbar Switches, *IEEE Transactions on Plasma Science* 44(12): 3353–3360. DOI: 10.1109/TPS.2016.2627141.

Dutta D., Asmar A., Stacey M. 2015. Effects of nanosecond pulse electric fields on cellular elasticity, *Micron* 72: 15–20. DOI: 10.1016/j.micron.2015.01.004.

Elgenedy M. A., Massoud A. M., Ahmed S., Williams B. W. 2018. A High-Gain, High-Voltage Pulse Generator Using Sequentially Charged Modular Multilevel Converter Submodules, for Water Disinfection Applications, *IEEE Journal of Emerging and Selected Topics in Power Electronics* 6(3): 1394–1406. DOI: 10.1109/JESTPE.2017.2750244.

Elgenedy M. A., Massoud A. M., Ahmed S., Williams B. W., McDonald J. R. 2019. A Modular Multilevel Voltage-Boosting Marx Pulse-Waveform Generator for Electroporation Applications, *IEEE Transactions on Power Electronics* 34(11): 10575–10589. DOI: 10.1109/TPEL.2019.2899974.

Elserougi A., Massoud A., Ahmed S. 2016. Conceptual study of a Bipolar modular high voltage Pulse generator with sequential charging, *IEEE Transactions on Dielectrics and Electrical Insulation* 23(6): 3450–3457. DOI: 10.1109/TDEI.2016.005803.

Elserougi A. A., Massoud A. M., Ahmed S. 2016. A Modular High-Voltage Pulse-Generator with Sequential Charging for Water Treatment Applications, *IEEE Transactions on Industrial Electronics*. DOI: 10.1109/TIE.2016.2515055.

Foshee W. G., Kirkici H., Hung J. Y., Blythe E. K., Goel A., Wehtje G. R. 2007. Seedling emergence of smallflower morningglory and green foxtail subjected to a pulsed electric field, *International Journal of Vegetable Science* 13(1): 61–72. DOI: 10.1300/J512v13n01_05.

García-Sánchez T., Leray I., Ronchetti M., Cadossi R., Mir L. M. 2019. Impact of the number of electric pulses on cell electrochemotherapy in vitro: Limits of linearity and saturation, *Bioelectrochemistry* 129: 218–227. DOI: 10.1016/j.bioelechem.2019.05.021

García-Sánchez T., Merla C., Fontaine J., Muscat A., Mir L. M. 2018. Sine wave electropermeabilization reveals the frequency-dependent response of the biological membranes, *Biochimica et Biophysica Acta - Biomembranes* 1860(5): 1022–1034. DOI: 10.1016/j.bbamem.2018.01.018.

Garcia P. A., Rossmeisl J. H., Neal R. E., Ellis T. L., Davalos R. V. 2011. A parametric study delineating irreversible electroporation from thermal damage based on a minimally invasive intracranial procedure, *BioMedical Engineering Online* 10. DOI: 10.1186/1475-925X-10-34.

Garner A. L., Caiafa A., Jiang Y., Klopman S., Morton C., Torres A. S., Loveless A. M., Neculaes V. B. 2017. Design, characterization and experimental validation of a compact, flexible pulsed power architecture for ex vivo platelet activation, *PLoS ONE* 12(7). DOI: 10.1371/journal.pone.0181214.

Geng T., Lu C. 2013. Microfluidic electroporation for cellular analysis and delivery, *Lab Chip* 13(19): 3803–3821. DOI: 10.1039/C3LC50566A.

Golberg A., et al. 2016. Energy-efficient biomass processing with pulsed electric fields for bioeconomy and sustainable development, *Biotechnology for Biofuels* 9(1): 1–22. DOI: 10.1186/s13068-016-0508-z.

Gowrishankar T. R., Esser A. T., Vasilkoski Z., Smith K. C., Weaver J. C. 2006. Microdosimetry for conventional and supra-electroporation in cells with organelles, *Biochemical and Biophysical Research Communications* 341(4): 1266–1276. DOI: 10.1016/j.bbrc.2006.01.094.

Grainys A. 2014. *Microsecond High Magnetic Field Shaped Pulse Generators*. Vilniaus Gedimino technikos universitetas. DOI: https://doi.org/10.20334/2254-M.

Guenther E., Klein N., Mikus P., Stehling M. K., Rubinsky B. 2015. Electrical breakdown in tissue electroporation, *Biochemical and Biophysical Research Communications* 467(4): 736–741. DOI: 10.1016/j.bbrc.2015.10.072.

Hahn U., Herrmann M., Leipold F., Schoenbach K. H. 2001. Nanosecond, kilovolt pulse generators *PPPS 2001 - Pulsed Power Plasma Science 2001*. Institute of Electrical and Electronics Engineers Inc. DOI: 10.1109/PPPS.2001.1001863.

He Y., Ma J., Yu L., Dong S., Gao L., Zeng W., Yao C. 2020. 10MHz High-Power Pulse Generator on Boost Module, *IEEE Transactions on Industrial Electronics*: 1–1. DOI: 10.1109/TIE.2020.2994860.

IXYS RF 2001. DE275-102N06A RF Power MOSFET, *Technical Datasheet*: 1–4.

IXYS RF 2018. DE375-102N12A RF Power MOSFET, *Technical Datasheet*: 1–5.

Jin Y., Lee H., Kim J., Kim Y., Rim G. 2004. Novel Crowbar Circuit for Compact 50-kJ Capacitor Bank, *IEEE Transactions on Plasma Science* 32(2): 525–530. DOI: 10.1109/TPS.2004.826028.

Jørgensen A. B., Sønderskov S. H., Beczkowski S., Bidoggia B., Munk-Nielsen S. 2020. Analysis of cascaded silicon carbide MOSFETs using a single gate driver for medium voltage applications, *IET Power Electronics* 13(3): 413–419. DOI: 10.1049/iet-pel.2019.0573.

Kadia B. R., Parmar K., Srinivas Y. S. S., Kulkarni S. V. 2019. Design, fabrication and testing of 7 kV, 6 A series connected IGBTs switch for triode based 20 kW stage ICRF amplifier, *Fusion Engineering and Design* 138: 226–230. DOI: 10.1016/j.fusengdes.2018.11.038.

Kašėta V., Kaušylė A., Kavaliauskaitė J., Petreikytė M., Stirkė A., Biziulevičienė G. 2020. Detection of intracellular biomarkers in viable cells using millisecond pulsed electric fields, *Experimental Cell Research* 389(1): 111877. DOI: 10.1016/j.yexcr.2020.111877.

Ke Q., Li C., Yao Cheng, Du J., Yao Chenguo, Mi Y. 2018. Development of bipolar nano/microsecond pulse generator *2018 IEEE International Power Modulator and High Voltage Conference, IPMHVC 2018*. Institute of Electrical and Electronics Engineers Inc. DOI: 10.1109/IPMHVC.2018.8936842.

Khan A. A. 2017. *Analysis and Comparison of efficiency and voltage gain of SEPIC with IGBT and snubber circuit as switching device*. Military Institute of Science and Technology Repository.

Kim T., Jang M., Agelidis V. G. 2016. Ultra-fast MHz range driving circuit for SiC MOSFET using frequency multiplier with eGaN FET, *IET Power Electronics* 9(10): 2085–2094. DOI: 10.1049/iet-pel.2015.0491.

Kolb J. F., Scarlett S., Cannone J., Zhuang J., Osgood C., Schoenbach K. H., De Angelis A., Zeni L. 2008. Nanosecond pulse generator with variable pulse duration for the study of pulse induced biological effects, *Proceedings of the 2008 IEEE International Power Modulators and High Voltage Conference, PMHVC*: 61–64. DOI: 10.1109/IPMC.2008.4743577.

Kolb J. F., Kono S., Schoenbach K. H. 2006. Nanosecond pulsed electric field generators for the study of subcellular effects, *Bioelectromagnetics* 27(3): 172–187. DOI: 10.1002/bem.20185.

Kotnik T., Rems L., Tarek M., Miklavčič D. 2019. Membrane Electroporation and Electropermeabilization: Mechanisms and Models, *Annual Review of Biophysics* 48(1): 63–91. DOI: 10.1146/annurev-biophys-052118-115451.

Kotnik T., Pucihar G., Reberšek M., Miklavčič D., Mir L. M. 2003. Role of pulse shape in cell membrane electropermeabilization, *Biochimica et Biophysica Acta - Biomembranes* 1614(2): 193–200. DOI: 10.1016/S0005-2736(03)00173-1.

Kotnik T., Miklavcic D. 2000. Second-order model of membrane electric field induced by alternating external electric fields, *IEEE Transactions on Biomedical Engineering* 47(8): 1074–1081. DOI: 10.1109/10.855935.

Kranjc M., Rebersek M., Miklavcic D. 2012. Numerical simulations aided development of nanosecond pulse electroporators *Proceedings of 6th European Conference on Antennas and Propagation, EuCAP 2012*. DOI: 10.1109/EuCAP.2012.6206633.

Krassowska W., Filev P. D. 2007. Modeling Electroporation in a Single Cell, *Biophysical Journal* 92(2): 404–417. DOI: 10.1529/biophysj.106.094235.

Kreutzer O., Eckardt B., Maerz M. 2015. Optimum gate driver design to reach SiC-MOSFET's full potential - Speeding up to 200 kV/μs *WiPDA 2015 - 3rd IEEE Workshop on Wide Bandgap Power Devices and Applications*. Institute of Electrical and Electronics Engineers Inc. DOI: 10.1109/WiPDA.2015.7369313.

Krishnaswamy P., Kuthi A., Vernier P.T., Gundersen M.A. 2007. Compact subnanosecond pulse generator using avalanche transistors for cell electroperturbation studies *IEEE Transactions on Dielectrics and Electrical Insulation*. DOI: 10.1109/TDEI.2007.4286518.

Krishnaveni R. S., Veeraraghavalu R., Rangarajan R. 2015. Development of pef source in nanosecond range for food sterilization, *Journal of Electrical Systems* 11(4): 407–419.

Krishnaveni S., Rajini V. 2017. Resonant Gate Driver for Series Operation of MOSFETs *Energy Procedia*. Elsevier Ltd. DOI: 10.1016/j.egypro.2017.05.104.

Kulbacka J., Pucek A., Wilk K. A., Dubińska-Magiera M., Rossowska J., Kulbacki M., Kotulska M. 2016. The Effect of Millisecond Pulsed Electric Fields (msPEF) on Intracellular Drug Transport with Negatively Charged Large Nanocarriers Made of Solid Lipid Nanoparticles (SLN): In Vitro Study, *Journal of Membrane Biology* 249(5): 645–661. DOI: 10.1007/s00232-016-9906-1.

Kurcevskis S., Grainys A., Tolvaisiene S., Ustinavicius T. 2020. High Power Electroporation System in Food Treatment - Review Institute of Electrical and Electronics Engineers (IEEE). DOI: 10.1109/aieee48629.2019.8977026.

Kuthi A., Gabrielsson P., Behrend M. R., Vernier P. T., Gundersen M. A. 2005. Nanosecond Pulse Generator Using Fast Recovery Diodes for Cell Electromanipulation, *IEEE Transactions on Plasma Science* 33(4): 1192–1197. DOI: 10.1109/TPS.2005.852403.

Lamberti P., Romeo S., Sannino A., Zeni L., Zeni O. 2015. The Role of Pulse Repetition Rate in nsPEF-Induced Electroporation: A Biological and Numerical Investigation, *IEEE*

Transactions on Biomedical Engineering 62(9): 2234–2243. DOI: 10.1109/TBME.2015.2419813.

Leguèbe M., Silve A., Mir L. M., Poignard C. 2014. Conducting and permeable states of cell membrane submitted to high voltage pulses: Mathematical and numerical studies validated by the experiments, *Journal of Theoretical Biology* 360: 83–94. DOI: 10.1016/j.jtbi.2014.06.027.

Leveque P., Arnaud-Cormos D. 2012. Generators and applicators for nanosecond pulsed electric field *Proceedings of 6th European Conference on Antennas and Propagation, EuCAP 2012*. DOI: 10.1109/EuCAP.2012.6206693.

Li C., Wang E., Yao C., Mi Y., Tan J., Zhang R. 2017. Compact solid-state Marx-bank sub-nanosecond pulse generator based on gradient transmission line theory, *IEEE Transactions on Dielectrics and Electrical Insulation* 24(4): 2181–2188. DOI: 10.1109/TDEI.2017.006367.

Li C., Wang E., Tan J., Zhang R., Wang S., Yao C., Mi Y. 2018. Design and Development of a Compact All-Solid-State High-Frequency Picosecond-Pulse Generator, *IEEE Transactions on Plasma Science* 46(10): 3249–3256. DOI: 10.1109/TPS.2018.2850153.

Li C., Zhang R., Yao C., Mi Y., Tan J., Dong S., Gong L. 2016. Development and Simulation of a Compact Picosecond Pulse Generator Based on Avalanche Transistorized Marx Circuit and Microstrip Transmission Theory, *IEEE Transactions on Plasma Science* 44(10): 1907–1913. DOI: 10.1109/TPS.2016.2547944.

Li Y., Wu M., Zhao D., Wei Z., Zhong W., Wang X., Liang Z., Li Z. 2015. Electroporation on microchips: the harmful effects of pH changes and scaling down, *Scientific reports* 5: 17817. DOI: 10.1038/srep17817.

Lindblom A. 2006. Inductive Pulse Generation, *Digital Comprehensive Summaries of Uppsala Dissertations from the Faculty of Science and Technology* 159: 93.

Liu Y., Fan R., Zhang X., Tu Z., Zhang J. 2019. Bipolar high voltage pulse generator without H-bridge based on cascade of positive and negative Marx generators, *IEEE Transactions on Dielectrics and Electrical Insulation* 26(2): 476–483. DOI: 10.1109/TDEI.2018.007861.

Lucia O., Sarnago H., Garcia-Sanchez T., Mir L.M., Burdio J. M. 2019. Industrial Electronics for Biomedicine: A New Cancer Treatment Using Electroporation, *IEEE Industrial Electronics Magazine*. DOI: 10.1109/MIE.2019.2942377.

Ma J., Dong S., Liu H., Yu L., Yao C. 2019. A High-gain nanosecond pulse generator based on inductor energy storage and pulse forming line voltage superposition *IEEE International Pulsed Power Conference*. Institute of Electrical and Electronics Engineers Inc. DOI: 10.1109/PPPS34859.2019.9009869.

Manias S. N. 2017. Fully Controlled Semiconductor Devices *Power Electronics and Motor Drive Systems*. Elsevier. DOI: 10.1016/b978-0-12-811798-9.00010-x.

Mao Z., Liu L., Zhang Y., Zhang J., Liu N., Liu Q. H. 2018. Selective electroporation of organelles under an intense picosecond pulsed electric field, *IEEE Journal on Multiscale*

and Multiphysics Computational Techniques 3: 235–245. DOI: 10.1109/JMMCT.2018.2887000.

Mendes J. P. M., Canacsinh H., Redondo L. M., Rossi J. O. 2011. Solid state marx modulator with blumlein stack for bipolar pulse generation, *IEEE Transactions on Dielectrics and Electrical Insulation* 18(4): 1199–1204. DOI: 10.1109/TDEI.2011.5976116.

Merla C., El Amari S., Kenaan M., Liberti M., Apollonio F., Arnaud-Cormos D., Couderc V., Leveque P. 2010. A 10-Ω high-voltage nanosecond pulse generator, *IEEE Transactions on Microwave Theory and Techniques* 58(12 PART 2): 4079–4085. DOI: 10.1109/TMTT.2010.2086470.

Mi Y., Bian C., Li P., Yao C., Li C. 2018. A Modular Generator of Nanosecond Pulses with Adjustable Polarity and High Repetition Rate, *IEEE Transactions on Power Electronics* 33(12): 10654–10662. DOI: 10.1109/TPEL.2018.2805820.

Mi Y., Bian C., Wan J., Xu J., Yao C., Li C. 2017. A modular solid-state nanosecond pulsed generator based on Blumlein-line and transmission line transformer with microstrip line, *IEEE Transactions on Dielectrics and Electrical Insulation* 24(4): 2196–2202. DOI: 10.1109/TDEI.2017.006368.

Mi Y., Wan J., Bian C., Zhang Y., Yao C., Li C. 2016. A Multiparameter Adjustable, Portable High-Voltage Nanosecond Pulse Generator Based on Stacked Blumlein Multilayered PCB Strip Transmission Line, *IEEE Transactions on Plasma Science* 44(10): 2022–2029. DOI: 10.1109/TPS.2016.2576482.

Mi Y., Zhang Y., Wan J., Yao C., Li C. 2016. Nanosecond pulse generator based on an unbalanced blumlein-type multilayered microstrip transmission line and solid-state switches, *IEEE Transactions on Plasma Science* 44(5): 795–802. DOI: 10.1109/TPS.2016.2542521.

Mi Y., Xu J., Tang X., Bian C., Liu H., Yang Q., Tang J. 2018. Scaling Relationship of In Vivo Muscle Contraction Strength of Rabbits Exposed to High-Frequency Nanosecond Pulse Bursts, *Technology in cancer research & treatment*. DOI: 10.1177/1533033818788078.

Microsemi 2003a. APT10035JLL Advanced Power Technology MOSFET, *Technical Datasheet*: 1–5.

Microsemi 2003b. APT10035LLLG Advanced Power Technology MOSFET, *Technical Datasheet*: 1–5.

Miklavčič D., Mali B., Kos B., Heller R., Serša G. 2014. Electrochemotherapy: from the drawing board into medical practice., *Biomedical engineering online* 13(1): 29. DOI: 10.1186/1475-925X-13-29.

Miklavčič D., Reberšek M. 2017. Development of devices and electrodes, *In Proceedings of the Electroporation-Based Technologies and Treatments: International Scientific Workshop and Postgraduate Course*. Ljubljana, Slovenia, November 12-18Electroporation-Based Technol. Treat. 2017, pp 85–93. 85-94.

Miklavcic D., Towhidi L. 2010. Numerical study of the electroporation pulse shape effect on molecular uptake of biological cells., *Radiology and oncology* 44(1): 34–41. DOI: 10.2478/v10019-010-0002-3.

Moisescu M. G., Radu M., Kovacs E., Mir L. M., Savopol T. 2013. Changes of cell electrical parameters induced by electroporation. A dielectrophoresis study, *Biochimica et Biophysica Acta - Biomembranes* 1828(2): 365–372. DOI: 10.1016/j.bbamem.2012.08.030.

Muratori C., Pakhomov A. G., Xiao S., Pakhomova O. N. 2016. Electrosensitization assists cell ablation by nanosecond pulsed electric field in 3D cultures, *Scientific Reports* 6. DOI: 10.1038/srep23225.

Makarov N. S., Ludwig R., Bitar S. J., Ludwig R., Bitar S. J. 2016. Electronic Diode and Diode Circuits *Practical Electrical Engineering*. Springer International Publishing. DOI: 10.1007/978-3-319-21173-2_16.

Neal R. E., Garcia P. A., Robertson J. L., Davalos R. V. 2012. Experimental characterization and numerical modeling of tissue electrical conductivity during pulsed electric fields for irreversible electroporation treatment planning, *IEEE Transactions on Biomedical Engineering* 59(4): 1076–1085. DOI: 10.1109/TBME.2012.2182994.

Nesin O. M., Pakhomova O. N., Xiao S., Pakhomov A. G. 2011. Manipulation of cell volume and membrane pore comparison following single cell permeabilization with 60- and 600-ns electric pulses, *Biochimica et Biophysica Acta* 1808(3): 792–801. DOI: 10.1016/j.bbamem.2010.12.012.

Novickij V., Tabasnikov A., Smith S., Grainys A., Novickij J. 2015. Analysis of planar circular interdigitated electrodes for electroporation, *IETE Technical Review (Institution of Electronics and Telecommunication Engineers, India)* 32(3): 196–203. DOI: 10.1080/02564602.2014.1000982.

Novickij V., Česna R., Perminaite E., Zinkevičiene A., Characiejus D., Novickij J., Šatkauskas S., Ruzgys P., Girkontaite I. 2019. Antitumor response and immunomodulatory effects of sub-microsecond irreversible electroporation and its combination with calcium electroporation, *Cancers* 11(11). DOI: 10.3390/cancers11111763.

Novickij V., Grainys A., Staigvila G., Tolvaisiene S., Ustinavicius T., Novickij J. 2017. Design and optimization of pulsed magnetic field generator for cell magneto-permeabilization, *Elektronika ir Elektrotechnika* 23(2): 21–25. DOI: 10.5755/j01.eie.23.2.17994.

Novickij V. 2015. Development of high power square wave electroporators, Vilnius: Vilniaus Gedimino technikos universiteto leidykla „Technika“.

Novickij V., Zinkevičienė A., Valiulis J., Švedienė J., Paškevičius A., Lastauskienė E., Markovskaja S., Novickij J., Girkontaitė I. 2018. Different permeabilization patterns of splenocytes and thymocytes to combination of pulsed electric and magnetic field treatments, *Bioelectrochemistry* 122: 183–190. DOI: 10.1016/j.bioelechem.2018.04.006.

Novickij V., Rembialkowska N., Staigvila G., Kulbacka J. 2020. Effects of extracellular medium conductivity on cell response in the context of sub-microsecond range calcium electroporation, *Scientific Reports* 10(1): 1–12. DOI: 10.1038/s41598-020-60789-7.

Novickij V., Stanevičienė R., Staigvila G., Gruškienė R., Sereikaitė J., Girkontaitė I., Novickij J., Servienė E. 2020. Effects of pulsed electric fields and mild thermal treatment on antimicrobial efficacy of nisin-loaded pectin nanoparticles for food preservation, *LWT* 120: 108915. DOI: 10.1016/j.lwt.2019.108915.

Novickij V., Tabašnikov A., Smith S., Grainys A., Novickij J., Tolvaišienė S., Markovskaja S. 2017. Feasibility of parylene coating for planar electroporation copper electrodes, *Medziagotyra* 23(2): 93–97. DOI: 10.5755/j01.ms.23.2.14953.

Novickij V., Ruzgys P., Grainys A., Šatkauskas S. 2018. High frequency electroporation efficiency is under control of membrane capacitive charging and voltage potential relaxation, *Bioelectrochemistry* 119: 92–97. DOI: 10.1016/j.bioelechem.2017.09.006.

Novickij V., Švedienė J., Paškevičius A., Novickij J. 2017. In vitro evaluation of nanosecond electroporation against Trichophyton rubrum with or without antifungal drugs and terpenes, *Mycoscience* 58(4): 261–266. DOI: 10.1016/j.myc.2017.03.002.

Novickij V., Zinkevičienė A., Stanevičienė R., et al. 2018. Inactivation of Escherichia coli Using Nanosecond Electric Fields and Nisin Nanoparticles: A Kinetics Study, *Frontiers in Microbiology* 9(DEC): 3006. DOI: 10.3389/fmicb.2018.03006.

Novickij V., Lastauskiene E., Staigvila G., Girkontaite I., Zinkevičiene A., Švediene J., Paškevičius A., Markovskaja S., Novickij J. 2019. Low concentrations of acetic and formic acids enhance the inactivation of Staphylococcus aureus and Pseudomonas aeruginosa with pulsed electric fields, *BMC Microbiology* 19(1): 73. DOI: 10.1186/s12866-019-1447-1.

Novickij V., Girkontaite I., Grainys A., Zinkevičiene A., Lastauskiene E., Švediene J., Paškevičius A., Markovskaja S., Novickij J. 2016. Measurement of Transient Permeability of Sp2/0 Myeloma Cells: Flow Cytometric Study, *Measurement Science Review* 16(6): 300–304. DOI: 10.1515/msr-2016-0038.

Novickij V., Lastauskienė E., et al. 2018. Membrane Permeabilization of Pathogenic Yeast in Alternating Sub-microsecond Electromagnetic Fields in Combination with Conventional Electroporation, *Journal of Membrane Biology* 251(2): 189–195. DOI: 10.1007/s00232-017-9951-4.

Novickij V., Stankevic V., Grainys A., Novickij J., Tolvaisiene S. 2015. Microsecond Electroporator Optimization for Parasitic Load Handling and Damping, *Elektronika ir Elektrotechnika* 21(6). DOI: 10.5755/j01.eee.21.6.13758.

Novickij V., Stankevic V., Zurauskiene N., Balevicius S., Stirke A., Dervinis A., Bleizgys V. 2014. Nanosecond Square-Wave Pulse Generator for Pulsed Electric Field Treatment of Biological Objects, *5th Euro-Asian Pulsed Power Conference* (September): 157–160.

Novickij V., Zinkevičienė A., Perminaitė E., et al. 2018. Non-invasive nanosecond electroporation for biocontrol of surface infections: an in vivo study, *Scientific Reports* 8(1). DOI: 10.1038/s41598-018-32783-7.

Novickij V., Švediene J., Paškevičius A., Markovskaja S., Girkontaite I., Zinkevičiene A., Lastauskiene E., Novickij J. 2018. Pulsed electric field-assisted sensitization of multidrug-resistant Candida albicans to antifungal drugs, *Future Microbiology* 13(5): 535–546. DOI: 10.2217/fmb-2017-0245.

ON Semiconductor 2013a. 2SK3747 N-Channel Power MOSFET, *Technical Datasheet* (PS No.7767): 1–7.

ON Semiconductor 2013b. NDFP03N150C N-Channel Power MOSFET, *Technical Datasheet* (PS No.A2232): 1–5.

ON Semiconductor 2013c. WPH4003 N-Channel Power MOSFET, *Technical Datasheet* (PS No. A1967): 1–7. DOI: 10.5Ω.

Pakhomov A. G., et al. 2019. Excitation and electroporation by MHz bursts of nanosecond stimuli, *Biochemical and Biophysical Research Communications* 518(4): 759–764. DOI: 10.1016/j.bbrc.2019.08.133.

Pavliha D., Reberšek M., Miklavčič D. 2011. Design and Quality Assessment of the Graphical User Interface Software of a High-voltage Signal Generator, *Elektrotehniški vestnik* 78(5): 281–286.

Ping W., Jiali B., Hong W., Huiping W. 2003. Multi-Pulse Generator for Electroporation *Annual International Conference of the IEEE Engineering in Medicine and Biology - Proceedings*. DOI: 10.1109/iembs.2003.1280542.

Pirc E., Miklavčič D., Reberšek M. 2019. Nanosecond Pulse Electroporator With Silicon Carbide MOSFETs: Development and Evaluation, *IEEE Transactions on Biomedical Engineering* 66(12). DOI: 10.1109/TBME.2019.2907165.

Pirc E., Reberšek M., Miklavčič D. 2017. Dosimetry in Electroporation-Based Technologies and Treatments M. Markov, sud. *Dosimetry in bioelectromagnetics*. Ed. 6000 Broken Sound Parkway NW, Suite 300, Boca Raton, FL 33487–2742: CRC Press.

Pliquett U., Nuccitelli R. 2014. Measurement and simulation of Joule heating during treatment of B-16 melanoma tumors in mice with nanosecond pulsed electric fields, *Bioelectrochemistry* 100: 62–68. DOI: 10.1016/j.bioelechem.2014.03.001.

Pollock R. 2019. Voltage Clamping Circuits for Large Voltage Step-Down Coupled Inductor Converters, *Renewable Energy and Sustainable Development* 5(1): 23. DOI: 10.21622/resd.2019.05.1.023.

Puc M., Čorović S., Flisar K., Petkovšek M., Nastran J., Miklavčič D. 2004. Techniques of signal generation required for electropermeabilization. Survey of electropermeabilization devices, *Bioelectrochemistry* 64(2): 113–124. DOI: 10.1016/j.bioelechem.2004.04.001.

Pucihar G., Krmelj J., Reberšek M., Napotnik T. B., Miklavčič D. 2011. Equivalent pulse parameters for electroporation, *IEEE Transactions on Biomedical Engineering* 58(11): 3279–3288. DOI: 10.1109/TBME.2011.2167232.

Rebersek M., Kranjc M., Pavliha D., Batista-Napotnik T., Vrtanik D., Amon S., Miklavi D. 2009. Blumlein configuration for high-repetition-rate pulse generation of variable duration and polarity using synchronized switch control, *IEEE Transactions on Biomedical Engineering* 56(11): 2642–2648. DOI: 10.1109/TBME.2009.2027422.

Reberšek M., Miklavčič D., Bertacchini C., Sack M. 2014. Cell membrane electroporation-Part 3: The equipment, *IEEE Electrical Insulation Magazine* 30(3): 8–18. DOI: 10.1109/MEI.2014.6804737.

Rebersek M., Miklavcic D. 2011. Advantages and Disadvantages of Different Concepts of Electroporation Pulse Generation, *ATKAFF* 52(1): 11–19.

Reberšek M., Miklavcic D. 2010. Concepts of Electroporation Pulse Generation and Overview of Electric Pulse Generators for Cell and Tissue Electroporation, *Advanced Electroporation Techniques in Biology and Medicine*: 323–339. DOI: 10.1201/ebk1439819067.

Redondo L. M., Kandratsyeu A., Barnes M. J., Calatroni S., Wuensch W. 2017. Solid-state Marx generator for the compact linear collider breakdown studies *2016 IEEE International Power Modulator and High Voltage Conference, IPMHVC 2016*. Institute of Electrical and Electronics Engineers Inc. DOI: 10.1109/IPMHVC.2016.8012824.

Redondo L. M., Zahyka M., Kandratsyeu A. 2019. Solid-State Generation of High-Frequency Burst of Bipolar Pulses for Medical Applications, *IEEE Transactions on Plasma Science* 47(8): 4091–4095. DOI: 10.1109/TPS.2019.2923570.

Redondo L. M. S. 2017. Basic concepts of high-voltage pulse generation *Handbook of Electroporation*. Springer International Publishing. DOI: 10.1007/978-3-319-32886-7_209.

Rems L., Miklavčič D. 2016. Tutorial: Electroporation of cells in complex materials and tissue, *Journal of Applied Physics* 119(20). DOI: 10.1063/1.4949264.

Rodaite-Riseviciene R., Saule R., Snitka V., Saulis G. 2014. Release of iron ions from the stainless steel anode occurring during high-voltage pulses and its consequences for cell electroporation technology, *IEEE Transactions on Plasma Science* 42(1): 249–254. DOI: 10.1109/TPS.2013.2287499.

Romeo S., D'Avino C., Zeni O., Zeni L. 2013. A blumlein-type, nanosecond pulse generator with interchangeable transmission lines for bioelectrical applications, *IEEE Transactions on Dielectrics and Electrical Insulation* 20(4): 1224–1230. DOI: 10.1109/TDEI.2013.6571438.

Rubin A. E., Levkov K., Usta O.B., Yarmush M., Golberg A. 2019. IGBT-Based Pulsed Electric Fields Generator for Disinfection: Design and In Vitro Studies on Pseudomonas aeruginosa, *Annals of Biomedical Engineering*. DOI: 10.1007/s10439-019-02225-0.

Ruzgys P., Novickij V., Novickij J., Šatkauskas S. 2019. Influence of the electrode material on ROS generation and electroporation efficiency in low and high frequency nanosecond pulse range, *Bioelectrochemistry* 127: 87–93. DOI: 10.1016/j.bioelechem.2019.02.002.

Ruzgys P., Novickij V., Novickij J., Šatkauskas S. 2018. Nanosecond range electric pulse application as a non-viral gene delivery method: proof of concept, *Scientific Reports* 8(1): 1–8. DOI: 10.1038/s41598-018-33912-y.

Sack M., Ruf J., Hochberg M., Herzog D., Mueller G. 2017. A device for combined thermal and pulsed electric field treatment of food *Proceedings - 2017 International Conference on Optimization of Electrical and Electronic Equipment, OPTIM 2017 and 2017 Intl Aegean Conference on Electrical Machines and Power Electronics, ACEMP 2017*. Institute of Electrical and Electronics Engineers Inc. DOI: 10.1109/OPTIM.2017.7974943.

Sack M. 2017. Marx-Generator Design and Development for Biomass Electroporation, *Handbook of Electroporation*: 793–812. DOI: 10.1007/978-3-319-26779-1_203-1.

Sack M., et al. 2010. Research on industrial-scale electroporation devices fostering the extraction of substances from biological tissue, *Food Engineering Reviews* 2(2): 147–156. DOI: 10.1007/s12393-010-9017-1.

Sack M., Hochberg M., Mueller G. 2016. Synchronized Switching and Active Clamping of IGBT Switches in a Simple Marx Generator - VDE Conference Publication *PCIM Europe 2016; International Exhibition and Conference for Power Electronics, Intelligent Motion, Renewable Energy and Energy Management*. , Nuremberg: VDE VERLAG.

Sack M., Mueller G. 2017. Design considerations for electroporation reactors, *IEEE Transactions on Dielectrics and Electrical Insulation* 24(4): 1992–2000. DOI: 10.1109/TDEI.2016.006219.

Sakamoto T., Akiyama H. 2013. Solid-state dual marx generator with a short pulsewidth, *IEEE Transactions on Plasma Science* 41(10): 2649–2653. DOI: 10.1109/TPS.2013.2272946.

Sanders J. M., Kuthi A., Wu Y. H., Vernier P. T., Gundersen M. A. 2009. A linear, single-stage, nanosecond pulse generator for delivering intense electric fields to biological loads, *IEEE Transactions on Dielectrics and Electrical Insulation* 16(4): 1048–1054. DOI: 10.1109/TDEI.2009.5211853.

Sano M. B., et al. 2015. Bursts of Bipolar Microsecond Pulses Inhibit Tumor Growth, *Scientific Reports* 5(1): 1–13. DOI: 10.1038/srep14999.

Sano M. B., Arena C. B., DeWitt M. R., Saur D., Davalos R. V. 2014. In-vitro bipolar nano- and microsecond electro-pulse bursts for irreversible electroporation therapies, *Bioelectrochemistry* 100: 69–79. DOI: 10.1016/j.bioelechem.2014.07.010.

Schmitt M. A., Friedrich O., Gilbert D. F. 2019. Portoporator © : A portable low-cost electroporation device for gene transfer to cultured cells in biotechnology, biomedical research and education, *Biosensors and Bioelectronics*. DOI: 10.1016/j.bios.2019.02.024.

Schoenbach K. H., Pakhomov A. G., Semenov I., Xiao S., Pakhomova O. N., Ibey B .L. 2015. Ion transport into cells exposed to monopolar and bipolar nanosecond pulses, *Bioelectrochemistry* 103: 44–51. DOI: 10.1016/j.bioelechem.2014.08.015.

Schoenbach K. H., Abou-Ghazala a., Vithoulkas T., Alden R. W., Turner R., Beebe S. 1997. The effect of pulsed electrical fields on biological cells, *Digest of Technical Papers. 11th IEEE International Pulsed Power Conference (Cat. No.97CH36127)* 1: 73–78. DOI: 10.1109/PPC.1997.679279.

Schoenbach K. H., Joshi R. P. 2010. Bioelectric Effects of Intense Ultrashort Pulses, *Critical Reviews™ in Biomedical Engineering* 38(3): 255–304. DOI: 10.1615/CritRevBiomedEng.v38.i3.20.

Scuderi M., Rebersek M., Miklavcic D., Dermol-Cerne J. 2019. The use of high-frequency short bipolar pulses in cisplatin electrochemotherapy in vitro, *Radiology and Oncology* 53(2): 194–205. DOI: 10.2478/raon-2019-0025.

Semenov I., Xiao S., Kang D., Schoenbach K. H., Pakhomov A.G. 2015. Cell stimulation and calcium mobilization by picosecond electric pulses, *Bioelectrochemistry* 105: 65–71. DOI: 10.1016/j.bioelechem.2015.05.013.

Semenov I., Xiao S., Pakhomov A. G. 2016. Electroporation by subnanosecond pulses, *Biochemistry and Biophysics Reports* 6: 253–259. DOI: 10.1016/j.bbrep.2016.05.002.

Sersa G., Kranjc S., Scancar J., Krzan M., Cemazar M. 2010. Electrochemotherapy of mouse sarcoma tumors using electric pulse trains with repetition frequencies of 1 Hz and 5 kHz, *Journal of Membrane Biology* 236(1): 155–162. DOI: 10.1007/s00232-010-9268-z.

Shi G., Edelblute C., Arpag S., Lundberg C., Heller R. 2018. IL-12 gene electrotransfer triggers a change in immune response within mouse tumors, *Cancers*. 10(12), 498. DOI: 10.3390/cancers10120498.

Silve A., Guimerà Brunet A., Al-Sakere B., Ivorra A., Mir L. M. 2014. Comparison of the effects of the repetition rate between microsecond and nanosecond pulses: Electropermeabilization-induced electro-desensitization?, *Biochimica et Biophysica Acta - General Subjects* 1840(7): 2139–2151. DOI: 10.1016/j.bbagen.2014.02.011.

Sitzmann W., Vorobiev E., Lebovka N. 2016. Applications of electricity and specifically pulsed electric fields in food processing: Historical backgrounds, *Innovative Food Science and Emerging Technologies* 37: 302–311. DOI: 10.1016/j.ifset.2016.09.021.

Son R. S., Gowrishankar T. R., Smith K. C., Weaver J. C. 2016. Modeling a Conventional Electroporation Pulse Train: Decreased Pore Number, Cumulative Calcium Transport and an Example of Electrosensitization, *IEEE Transactions on Biomedical Engineering* 63(3): 571–580. DOI: 10.1109/TBME.2015.2466234.

Stankevic V., Simonis P., Zurauskiene N., Stirke A., Dervinis A., Bleizgys V., Kersulis S., Balevicius S. 2020. Compact Square-Wave Pulse Electroporator with Controlled Electroporation Efficiency and Cell Viability, *Symmetry* 12(3): 412. DOI: 10.3390/sym12030412.

Steelman Z. A., Tolstykh G. P., Beier H. T., Ibey B. L. 2016. Cellular response to high pulse repetition rate nanosecond pulses varies with fluorescent marker identity, *Biochemical and Biophysical Research Communications* 478(3): 1261–1267. DOI: 10.1016/j.bbrc.2016.08.107.

STMicroelectronics 2015. STFW3N170 N-channel Power MOSFET, *Technical Datasheet* (DocID023985 Rev 3): 1–12.

STMicroelectronics 2018. STH2N120K5-2AG Automotive-grade N-channel Power MOSFET, (DS12486-Rev 4): 1–15.

Subramani K., Veeraraghavalu R. 2018. Diode clamped gate driver-based high voltage pulse generator for electroporation, *Turkish Journal of Electrical Engineering and Computer Sciences* 26(5): 2374–2384. DOI: 10.3906/elk-1710-133.

Sundararajan R. 2009. Nanosecond electroporation: Another look, *Molecular Biotechnology* 41(1): 69–82. DOI: 10.1007/s12033-008-9107-y.

Sunkam R. K., Selmic R. R., Haynie D. T., Hill J.S. 2004. Solid-state nanopulse generator: Application in ultra-wideband bioeffects research *Conference Proceedings - IEEE SOUTHEASTCON*. DOI: 10.1109/secon.2004.1287931.

Sweeney D. C., Reberšek M., Dermol J., Rems L., Miklavčič D., Davalos R. V. 2016. Quantification of cell membrane permeability induced by monopolar and high-frequency bipolar bursts of electrical pulses, *Biochimica et Biophysica Acta - Biomembranes* 1858(11): 2689–2698. DOI: 10.1016/j.bbamem.2016.06.024.

Tang J., et al. 2020. Interpretation of the molecular mechanism of the electroporation induced by symmetrical bipolar picosecond pulse trains, *Biochimica et Biophysica Acta - Biomembranes* 1862(5): 183213. DOI: 10.1016/j.bbamem.2020.183213.

Tang T., Wang F., Kuthi A., Gundersen M. 2007. Nanosecond pulse generator using diode opening switch for cell electroperturbation studies *Digest of Technical Papers-IEEE International Pulsed Power Conference*. DOI: 10.1109/PPC.2005.300584.

Tinschmann A., Okumura T., Taniwaki M. 2008. A Novel Crowbar Impulse Current Circuit for Testing the Switch-Type SPD, *Plasma Science and Technology* 10(2).

Tsong T. Y. 1991. Electroporation of cell membranes, *Biophysical Journal* 60(2): 297–306. DOI: 10.1016/S0006-3495(91)82054-9.

Venslauskas M. S., Šatkauskas S. 2015. Mechanisms of transfer of bioactive molecules through the cell membrane by electroporation, *European Biophysics Journal* 44(5): 277–289. DOI: 10.1007/s00249-015-1025-x.

Vishay Siliconix 2016. Power MOSFET IRFBG20, *Technical Datasheet* (91000): 1–9.

Vishay Siliconix 2014. Power MOSFET IRFPG50, *Technical Datasheet* (91000): 1–9.

Wagstaff P. G. K., Buijs M., van den Bos W., de Bruin D. M., Zondervan P. J., de la Rosette J. J. M. C. H., Laguna Pes M. P. 2016. Irreversible electroporation: State of the art, *OncoTargets and Therapy* 9: 2437–2446. DOI: 10.2147/OTT.S88086.

Wandel A., Ben-David E., Ulusoy B. S., Neal R., Faruja M., Nissenbaum I., Gourovich S., Goldberg S. N. 2016. Optimizing Irreversible Electroporation Ablation with a Bipolar Electrode, *Journal of Vascular and Interventional Radiology* 27(9): 1441-1450.e2. DOI: 10.1016/j.jvir.2016.06.001.

Warindi, Hadi S. P., Berahim H., Suharyanto 2017. Impedance Measurement System of a Biological Material Undergoing Pulsed Electric Field Exposed *Procedia Engineering*. Elsevier Ltd. DOI: 10.1016/j.proeng.2017.03.066.

Xiao S., Zhou C., Yang E., Rajulapati S. R. 2018. Nanosecond bipolar pulse generators for bioelectrics, *Bioelectrochemistry* 123: 77–87. DOI: 10.1016/j.bioelechem.2018.04.017.

Yao C., Dong S., Zhao Y., Mi Y., Li C. 2016. A Novel Configuration of Modular Bipolar Pulse Generator Topology Based on Marx Generator with Double Power Charging, *IEEE Transactions on Plasma Science* 44(10): 1872–1878. DOI: 10.1109/TPS.2016.2542103.

Yao C., Sun C., Mi Y., Xiong L., Wang S. 2004. Experimental studies on killing and inhibiting effects of steep pulsed electric field (SPEF) to target cancer cell and solid tumor, *IEEE Transactions on Plasma Science* 32(4 II): 1626–1633. DOI: 10.1109/TPS.2004.832621.

Yao C., Zhang X., Guo F., Dong S., Mi Y., Sun C. 2012. FPGA-controlled all-solid-state nanosecond pulse generator for biological applications, *IEEE Transactions on Plasma Science* 40(10 PART 1): 2366–2372. DOI: 10.1109/TPS.2012.2188908.

Yao C., Dong S., Zhao Y., Zhou Y., Mi Y., Li C. 2016. High-frequency composite pulse generator based on full-bridge inverter and soft switching for biological applications, *IEEE Transactions on Dielectrics and Electrical Insulation* 23(5): 2730–2737. DOI: 10.1109/TDEI.2016.7736832.

Yao C., Zhao Z., Dong S., Zuo Z. 2015. High-voltage subnanosecond pulsed power source with repetitive frequency based on Marx structure, *IEEE Transactions on Dielectrics and Electrical Insulation* 22(4): 1896–1901. DOI: 10.1109/TDEI.2015.004966.

Yarmush M.L., Golberg A., Serša G., Kotnik T., Miklavčič D. 2014. Electroporation-Based Technologies for Medicine: Principles, Applications, and Challenges, *Annual Review of Biomedical Engineering* 16(1): 295–320. DOI: 10.1146/annurev-bioeng-071813-104622.

Zajc A., Miklavcic D., Rebersek. Matej 2019. Expanding the power pulse duration range for electroporation *28th International Electrotechnical and Computer Science Conference*. , Portorož: Društvo Slovenska sekcija IEEE.

Zeng W., Yu L., Dong S., Ma J., Wang Y., He Y., Wang X., Yao C. 2020. A Novel High Frequency Bipolar Pulsed Power Generator for Biological Applications, *IEEE Transactions on Power Electronics*: 1–1. DOI: 10.1109/tpel.2020.2994333.

Zeng W., Yao C., Dong S., Wang Y., Ma J., He Y., Yu L. 2020. Self-triggering High-frequency Nanosecond Pulse Generator, *IEEE Transactions on Power Electronics*: 1–1. DOI: 10.1109/tpel.2020.2967183.

Zhong Z., Chen Y., Zhang P., Kang Y. 2014. A Cost-effective Circuit for Three-Level Flying- Capacitor Buck Converter Combining the Soft-start , Flying Capacitor Pre-charging and Snubber Functions, *Energy Conversion Congress and Exposition (ECCE) 2014 IEEE* (20120142120026): 3658–3663.

Zou Y., Wang C., Peng R., Wang L., Hu X. 2015. Theoretical Analyses of Cellular Transmembrane Voltage in Suspensions Induced by High-frequency Fields, *Bioelectrochemistry* 102: 64–72. DOI: 10.1016/j.bioelechem.2014.12.002.

List of Scientific Publications by the Author on the Topic of the Dissertation

Papers in the Reviewed Scientific Journals

Novickij V., Grainys A., Butkus P., Tolvaišienė S., Švedienė J., Paškevičius A., Novickij J. 2016. High-frequency submicrosecond electroporator. *Biotechnology & Biotechnological Equipment* 30(3): 607–613. DOI: 10.1080/13102818.2016.1150792 (Clarivate Analytics Web of Science).

Butkus P. 2018. Development of planar electrodes for real-time electroporation. *Mokslas – Lietuvos ateitis / Science – Future of Lithuania*. 1–4. DOI: 10.3846/mla.2018.3084.

Butkus P., Tolvaišienė S., Kurčevskis S. 2019. Validation of a SPICE Model for High Frequency Electroporation Systems, *Electronics* 8(6): 2–10. DOI: 10.3390/electronics8060710 (Clarivate Analytics Web of Science).

Butkus P., Murauskas A., Tolvaišienė S., Novickij V. 2020. Concepts and Capabilities of In-House Built Nanosecond Pulsed Electric Field (nsPEF) Generators for Electroporation: State of Art, *Appl. Sci*., 10(12): 1–20. DOI: 10.3390/app10124244 (Clarivate Analytics Web of Science).

Papers in Other Editions

Butkus P., Kurcevskis S., Tolvaisiene S., Grainys A. 2017. Computer model of the high frequency up to 30 kV/cm electric field generator. Proceeding of *5th IEEE Workshop on Advances in Information, Electronic and Electrical Engineering (AIEEE)*. Riga, Latvia. pp. 1–3. doi: 10.1109/AIEEE.2017.8270542 (Clarivate Analytics Proceedings).

Butkus P., Tolvaišienė S. 2019. The comparison of technical capabilities of six pulse generators for biological applications, Proceeding of *7th IEEE Workshop on Advances in Information, Electronic and Electrical Engineering (AIEEE)*. Liepaja, Latvia. pp. 1–4. doi: 10.1109/AIEEE48629.2019.8976927 (Clarivate Analytics Proceedings).

Summary in Lithuanian

Įvadas

Problemos formulavimas

Susidomėjimas biologinių ląstelių membranos pralaidumo reguliavimu taikant impulsinį elektrinį lauką, dar vadinamu elektroporacija, įvairiuose taikymo srityse sparčiai auga. Dėl šio fenomeno tarpdisciplininio pobūdžio, specifinis elektroporacijos poveikis ir jo efektyvumas skirtingose taikymo srityse priklauso nuo elektrinio impulso parametrų: amplitudė, trukmė, elektrinio lauko stiprumas, pasikartojimo dažnis, impulso forma ir pakartojimų skaičius. Visi šie parametrai turi būti kruopščiai parenkami siekiant optimalaus taikymo efektyvumo.

Dauguma elektroporacijos protokolų yra sukurti mikrosekundžių diapazono prietaisams, tačiau pastaruoju metu susiformavo ypatingas mokslinis susidomėjimas didelės galios ir aukšto dažnio submikrosekundžių ir nanosekundžių (nsPEF) impulsų tyrimais dėl pirmiausia neterminio poveikio ir galimybės tiesiogiai paveikti ląstelių vidinius organoidus. Be to, galimybė keisti impulso pakartojimo dažnį plačiame diapazone leidžia ištirti elektroporacijos efektyvumo priklausomybę nuo impulsų dažnio ir sukurti naujus taikymo protokolus. Aukštos įtampos ir aukšto dažnio elektroporatorių trūkumas yra viena iš pagrindinių priežasčių, kodėl aukšto dažnio submikrosekundžių impulsų elektroporacijos taikymo sritis yra vis dar nepakankamai išnagrinėta.

Pastarųjų kelių metų silicio karbido (SiC) MOSFET technologijos progresas išplėtė šių jungiklių taikymo galimybes aukštos įtampos ir aukšto dažnio impulsų diapazone, kuris atitinka submikrosekundžių ir nanosekundžių elektroporacijos tyrimų reikalavimus. Šis progresas netrukus lėmė naujos konfigūracijos pažangių ir MOSFET jungiklių

valdymu pagrįstų submikrosekundžių elektroporatorių su reguliuojamais impulsų parametrais vystymo bangą. Nepaisant SiC MOSFET technologijos pažangos, aukštos įtampos impulsų generavimas nanosekundžių impulsų diapazone vis dar yra sudėtinga užduotis, dėl pereinamųjų vyksmų įtakos impulsų formai ir parametrams. Atitinkamai, apie trečdalis naujai sukurtų prietaisų pasižymi prasta impulso formos kokybe, be to dauguma atvejų impulso galinio fronto kritimo trukmė priklauso nuo tyrime naudojamos apkrovos varžos.

Darbo aktualumas

Įvairiais elektroporacijos taikymo atvejais elektros impulsai gali būti skirtingos formos. Individualaus impulso trukmė gali kisti nuo kelių šimtų pikosekundžių iki sekundžių, o įtampos amplitudė gali kisti nuo kelių mV iki kelių kV. Taikomi skirtingi impulsų pasikartojimo dažniai – nuo Hz iki kelių GHz. Pasiekti tokį platų impulsų parametrų kitimo spektrą naudojant vieną elektroporacijos sistemą netikslinga, tad skirtingi prietaisai naudojami skirtingiems atvejams.

Tuo tarpu, „Google Scholar“ pateikia daugiau nei 1500 nuorodų, susijusių su aukštos įtampos ir aukšto dažnio elektroporacijos tyrimais 2019 metais. Tyrimų skaičius nuo 1990 m. nuolat auga ir atspindi didėjantį mokslininkų susidomėjimą aukštos įtampos ir aukšto dažnio elektroporacija. Dėl to aukštos įtampos ir aukšto dažnio elektroporacijos sistemos su plataus impulso parametrų pasirinkimo diapazonu suteikia galimybę išplėsti taikomųjų tyrimų sritį ir tirti naujus elektroporacijos sukeliamus procesus bei jų praktinį taikymą. Tad nauja aukšto dažnio elektroporacijos sistema prisidės prie šių tyrimų plėtros. Tokiu būdu bus sudaromos galimybės geriau suvokti pavienių porų formavimo procesą, leidžiantį sklandžiau kontroliuoti ir optimizuoti elektroporacijos protokolus bei tobulinti jau egzistuojančius biotechnologinius ir biomedicininius metodus.

Atitinkamai, disertacijoje pateikti rezultatai prisideda prie elektroporacijos taikomųjų tyrimų plėtros ir koordinacijos. Naujai išvystyta aukšto dažnio elektroporacijos sistema, bus naudojama elektroporacijos tyrimuose biomedicinos srityje.

Tyrimo objektas

Disertacijos tyrimo objektas yra aukšto dažnio stačiakampių impulsų elektroporacijos sistema.

Darbo tikslas

Darbo tikslas – sukurti aukšto dažnio stačiakampių impulsų elektroporacijos sistemą ištyrus elektrinių impulsų pereinamuosius vyksmus ir jų kompensavimo grandines.

Darbo uždaviniai

Norint išspręsti iškeltą problemą ir įgyvendinti darbo tikslus, suformuluoti šie uždaviniai:

1. Pasinaudojus geriausia impulsų formavimo ir pereinamųjų vyksmų kompensavimo grandinių praktika, sukurti aukšto dažnio stačiakampių impulsų

elektroporacijos sistemos modelį bei ištirti pereinamųjų vyksmų ir grandinės parazitinių elementų įtaką generuojamai impulsų formai.
2. Pasiūlyti planarių elektroporacijos elektrodų topologiją pavienių ląstelių realaus laiko manipuliacijoms ir pateikti elektrinio lauko pasiskirstymo ir homogeniškumo tyrimo modelį.
3. Sukurti aukšto dažnio submikrosekundžių impulsų elektroporacijos sistemos prototipą *in vitro* elektroporacijos tyrimui ir taikymui.
4. Atlikti impulsų formavimo grandinės imitacinio modelio ir sukurto prototipo eksperimentinių rezultatų palyginimą bei pateikti neapibrėžties vertinimą.

Tyrimų metodika

Sistemos vystymo ir taikymo metu buvo naudojami skaitiniai ir eksperimentiniai metodai. Impulsų formavimo grandinės pereinamųjų vyksmų įtaka impulsų formai buvo tiriama panaudojant SPICE modelį ir LTspice programinį paketą. Planarių elektroporacijos elektrodų elektrinio lauko pasiskirstymo tyrimai buvo atliekami taikant baigtinių elementų metodu grįstą COMSOL Multiphysics programinį paketą.

Mokslinis naujumas

Atliekant darbe aprašytus tyrimus buvo gauti šie elektros ir elektronikos inžinerijos mokslui nauji rezultatai:

1. Sukurtas aukšto dažnio submikrosekundžių impulsų elektroporacijos sistemos modelis, tinkamas impulso formavimo pereinamųjų vyksmų bei grandinės parazitinių elementų tyrimams atlikti.
2. Pasiūlyta planarių elektrodų topologija realaus laiko elektroporacijos taikymui ir sukurtas elektrinio lauko pasiskirstymo ir homogeniškumo tyrimo modelis.
3. Pasiūta valdoma kirtiklio pakopa užtikrina nuo apkrovos nepriklausomą galinio fronto kritimo trukmę.
4. Sukurtas elektroporacijos sistemos prototipas, generuojantis impulsus, kurių amplitudė, dažnis ir impulso trukmė gali būti valdoma atitinkamai nuo 0 kV iki 3 kV, nuo 1 Hz iki 3,5 MHz ir nuo 100 ns iki 1 ms diapazonuose.

Darbo rezultatų praktinė reikšmė

Sukurta nauja aukšto dažnio submikrosekundžių impulsų elektroporacijos sistema, galinti generuoti aukštos įtampos (iki 3 kV), pasirenkamos trukmės (nuo 100 ns iki 1 ms) ir dažnio (nuo 1 Hz iki 3,5 MHz) stačiakampius impulsus (nuo 1 iki 100), o pasiūlyta valdoma kirtiklio pakopa užtikrina nuo apkrovos varžos nepriklausomą impulso galinio fronto kritimo trukmę. Ši savybė itin svarbi atliekant elektroporacijos tyrimus ir užtikrinant perduodamos energijos kontrolę.

Sukurta aukšto dažnio stačiakampių impulsų elektroporacijos sistema buvo sėkmingai išbandyta ir kartu su Gamtos tyrimų centro mokslininkais pritaikyta nagrinėjant

elektrinio lauko poveikį biologiniams objektams. Taikomųjų tyrimų metu pademonstruota, kad nauja sistema suderinama ir gali būti naudojama su standartinėmis komercinėmis eletroporacijos kiuvetėmis.

Sukurta nauja aukšto dažnio submikrosekundžių stačiakampių impulsų elektroporacijos sistema įgalina tolimesnius elektroporacijos reiškinio tyrimus šiuo metu mažiausiai išnagrinėtame elektros impulsų dažnio ir stiprio diapazone.

Ginamieji teiginiai

1. Pasiūlytas impulsų formavimo grandinės imitacinis modelis yra tinkamas pereinamųjų procesų analizei ir pateikia generuotų elektrinių impulsų parametrų rezultatus su ±21 % (95,4 % pasikliovimo lygis) neapibrėžtimi submikrosekundžių impulsų diapazone.
2. Sukurta aukšto dažnio elektroporacijos sistema gali užtikrinti 18 ns impulso galinio fronto kritimo trukmę, kuri yra nepriklausomos nuo apkrovos varžos.
3. Sukurta impulsų formavimo grandinė gali generuoti aukštos įtampos (iki 3 kV), pasirenkamos trukmės (nuo 100 ns iki 1 ms) ir dažnio (nuo 1 Hz iki 3,5 MHz) stačiakampius impulsus.
4. Pasiūlyta planarių elektrodų topologija užtikrina daugiau nei 1 kV/cm elektrinio lauko stiprį ir homogeniškumą realaus laiko pavienių ląstelių elektroporacijos tyrimams.

Disertacijos aprobavimas

Disertacijos tema paskelbti 6 moksliniai straipsniai: trys – recenzuojamuose mokslo žurnaluose, įtrauktuose į *Clarivate Analytics Web of Science* duomenų bazę (Novickij et al. 2016; Butkus et al. 2019; Butkus, Murauskas, et al. 2020), du tarptautinių konferencijų medžiagose, įtrauktose į *Clarivate Analytics Web of Science* „*Conference Proceedings*“ duomenų bazę (Butkus et al. 2017; Butkus, Tolvaisiene 2020), vienas – mokslo žurnale, referuojamame kitose tarptautinėse duomenų bazėse (Butkus 2018).

Disertacijoje atliktų tyrimų rezultatai buvo paskelbti dešimtyje mokslinių konferencijų Lietuvoje ir užsienyje:

- 20-ojoje Jaunųjų mokslininkų konferencijoje „*Mokslas – Lietuvos ateitis. Elektronika ir elektrotechnika“*. 2017. Vilnius, Lietuva.
- 60-oje tarptautinėje fizika ir gamtos mokslų studentų ir jaunųjų mokslininkų konferencijoje “*Open Readings 2017*”. 2017. Vilnius, Lietuva.
- VGTU Elektronikos fakulteto seminarų cikle. 2017. Vilnius, Lietuva;
- Tarptautinėje konferencijoje IEEE 5th Workshop on “*Advances in Information, Electronic and Electrical Engineering (AIEE)”*. 2017. Riga, Latvija.
- KTU nacionalinėje „*PhD week*” konferencijoje “*What do PhD students do*?”. 2018. Kaunas, Lietuva.

- Antrojoje tarptautinėje elektros, elektronikos ir informatikos mokslų konferencijoje *"eStream 2018* ". 2018. Vilnius, Lietuva.
- 21-ojoje Jaunųjų mokslininkų konferencijoje „*Mokslas – Lietuvos ateitis. Elektronika ir elektrotechnika"*. 2018. Vilnius, Lietuva.
- 62-oje tarptautinėje fizika ir gamtos mokslų studentų ir jaunųjų mokslininkų konferencijoje "*Open Readings 2019*". 2019. Vilnius, Lietuva.
- Trečiojoje tarptautinėje elektros, elektronikos ir informatikos mokslų konferencijoje *"eStream 2019"*. 2019. Vilnius, Lietuva.
- Tarptautinėje konferencijoje IEEE 7th Workshop on "*Advances in Information, Electronic and Electrical Engineering (AIEE)"*. 2019. Liepoja, Latvija.

Disertacijos struktūra

Disertaciją sudaro: įvadas, trys pagrindiniai skyriai, bendrosios išvados, literatūros sąrašas, autoriaus publikacijų disertacijos tema sąrašas ir santrauka lietuvių kalba.

Disertacijos apimtis – 125 puslapių, kuriuose pateikiamos 40 paveikslai, 1 formulė ir 8 lentelės. Disertacijoje panaudoti 209 literatūros šaltiniai.

Padėka

Šis darbas buvo atliktas naudojantis Vilniaus Gedimino technikos universiteto Stiprių magnetinių laukų instituto (Vilnius, Lietuva) ir Gamtos tyrimų centro Biodestruktorių tyrimo laboratorijos (Vilnius, Lietuva) infrastruktūra.

Noriu padėkoti savo vadovei doc. dr. Sonatai Tolvaišienei už didžiulę paramą žengiant į priekį. Ypatingos padėkos nusipelno dr. Vitalij Novickij ir dr. Audrius Grainys už išskirtinę pagalbą ir suteiktus patarimus disertacijos rengimo metu. Taip pat norėčiau padėkoti visiems savo kolegoms iš Elektros inžinerijos katedros ir Valstybinio mokslinių tyrimų instituto Fizinių ir technologijos mokslų centro už skirtą brangų laiką vertingoms diskusijoms disertacijos temomis. Doktorantūros studijų metu mano sukauptos mokslo, profesinės ir specifinės kompetencijos yra jūsų visų indėlio rezultatas.

Esu itin dėkingas savo šeimai už suteiktą palaikymą visus šiuos metus.

1. Impulsinių elektrinių laukų generavimo ir taikymo apžvalga

Susidomėjimas biologinių ląstelių membranos pralaidumo reguliavimu įvairiuose taikymo srityse sparčiai auga. Elektroporacijos metu elektros impulsai sukelia lipidų perorientavimą ir porų susidarymą ląstelės membranoje, dėl kurio padidėja membranos pralaidumas ir įvairių subjektų įterpimo į ląstelę galimybės. Priklausomai nuo impulsų įtampos ir trukmės gaunamas skirtingas elektroporacijos poveikis ir praktinis taikymas.

Norint optimizuoti elektroporacijos efektyvumą, turi būti kruopščiai parinkta ne tik impulsų amplitudė ir trukmė, bet ir impulsų pasikartojimo dažnis, impulso forma ir naudojamų impulsų skaičius. Įvairiais elektroporacijos taikymo atvejais visi šie parametrai skiriasi. Naudojamos skirtingos impulso formos, o individualaus impulso

trukmė gali varijuoti nuo kelių šimtų pikosekundžių iki sekundžių, įtampos amplitudė gali kisti nuo kelių mV iki kelių kV. Taip pat naudojami skirtingi impulsų pasikartojimo dažniai – nuo Hz iki kelių GHz. Pasiekti tokį platų impulsų parametrų kitimo spektrą naudojant vieną elektroporacijos sistemą netikslinga, tad skirtingi prietaisai naudojami skirtingiems atvejams.

Atlikus šiuolaikinių impulso parametrų poreikio analizę elektroporacijos tyrimų srityje nustatyta, kad šiuo metu yra didžiausias poreikis elektroporacijos sistemos, sugebančios generuoti plataus spektro ir kontroliuojamų parametrų stačiakampius impulsus, kurių amplitudė gali siekti iki kelių kilovoltų, o pasikartojimo dažnis iki MHz eilės. Impulsų trukmė turėtų varijuoti nuo šimtų nanosekundžių iki milisekundžių. Elektroporacijos tyrimų metu taip pat svarbu užtikrinti ne tik šių parametrų kontrolę, bet ir pastovią stačiakampio impulso formą, kuri lemia perduodamos energijos kiekį. Kadangi eksperimento metu gali kisti skirtingų mėginių varžos, svarbu, kad naudojamo impulso galinio fronto kritimo trukmė (t. y. perduodamos energijos kiekis) nepriklausytų nuo apkrovos dydžio. Tokio tipo sistema suteikia galimybes atlikti plataus diapazono tyrimus padengiant tiek dažnai taikomas, tiek ir mažiausiai ištirtas elektroporacijos sritis.

Siekiant parinkti tinkamiausią impulsų formavimo grandinės koncepciją, atlikta šių koncepcijų apžvalga. Remiantis energijos kaupimo būdais, impulsų generatorius galima suskirstyti į tris grupes: tiesioginės kondensatoriaus iškrovos grandinės, perdavimo linijos iškrovos grandinės ir indukcinio klaupimo iškrovos grandinės. Kiekvienas iš jų turi privalumų ir trūkumų, tačiau bendru atveju visos gali būti panaudotos aukšto dažnio submikrosekundžių impulsų generavimui.

Kita vertus, tiesioginės kondensatoriaus iškrovos grandinės pasižymi kokybiškesne impulso forma, o IGBT arba MOSFET jungikliai suteikia galimybę lengvai keisti impulsų trukmę ir pasikartojimo dažnį. Maža to, pastarųjų kelių metų silicio karbido (SiC) MOSFET technologijos progresas išplėtė šių jungiklių taikymo sritį, kuri dabar taip pat apima aukštos įtampos ir aukšto dažnio impulsų diapazoną, t. y. atitinka submikrosekundžių ir nanosekundžių elektroporacijos tyrimų reikalavimus.

Šis progresas netrukus lėmė naujos konfigūracijos pažangių ir MOSFET jungiklių valdymu pagrįstų submikrosekundžių elektroporatorių, su reguliuojamais impulsų parametrais, vystymo bangą. Tačiau, nepaisant SiC MOSFET technologijos pažangos, aukštos įtampos impulsų generavimas submikrosekundžių impulsų diapazone vis dar yra sudėtinga užduotis, dėl pereinamųjų vyksmų ir jungiklių sinchronizacijos įtakos, kuri neigiamai veikia impulsų formą ir parametrus. Atitinkamai, apie trečdalis naujai sukurtų prietaisų pasižymi prasta impulso formos kokybe bei dauguma atvejų impulso galinio fronto kritimo trukmė priklauso nuo tyrime naudojamos apkrovos varžos.

Kiekvienu impulsų formavimo grandinės atveju individualios pereinamųjų vyksmų kompensavimo grandinės turi būti kruopščiai parinktos, siekiant užtikrinti aukštą impulsų formos kokybę, o integruota valdoma kirtiklio pakopa gali padėti užtikrinti impulsų galinio fronto kritimo trukmės nepriklausomybę nuo apkrovos varžos.

Apibendrinant, pirmajame disertacijos skyriuje pateikiama mokslinės literatūros šaltinių apžvalga, kurioje pristatomi elektroporacijos reiškiniai ir submikrosekundžių impulsų elektrinių laukų poveikis. Taip pat, apžvelgiami submikrosekundžių ir nanosekundžių elektrinių impulsų generatoriai, jų koncepcijos, ir aukšto dažnio grandinių pereinamasis procesas bei jų kompensacijos grandinės. Išnagrinėti skirtingi

elektroporacijos sistemų privalumai ir trūkumai. Skyriaus pabaigoje suformuluotas pagrindinis tyrimo tikslas ir uždaviniai.

2. Elektroporacijos sistemos imitacinis modelis

Antrajame darbo skyriuje nustatyti tikslūs impulsų formavimo grandinės reikalavimai ir parinkta grandinės tipologija. Remiantis šiais kriterijais sudarytas detalus grandinės SPICE (angl. *Simulation Program with Integrated Circuit Emphasis*) modelis ir panaudojant LTspice programinį paketą atlikta parazitinių grandinės elementų bei pereinamųjų vyksmų įtakos impulsų formai analizė. Remiantis gautais rezultatais parinktos optimalios kompensacinės grandinės vertės.

Norint sudaryti optimalią impulsų formavimo grandinės schemą ir jos elementus, reikia aiškiai apibrėžti reikalavimus impulsams. Remiantis praėjusio skyriaus rezultatais buvo nuspręsta, kad pageidaujama elektroporacijos sistema turi būti kompaktiška, pasižymėti aukšta stačiakampio impulso formos kokybe bei užtikrinti priekinio fronto kilimo ir galinio fronto kritimo trukmių nepriklausomybę nuo naudojamos apkrovos. Sistema taip pat turi užtikrinti plataus diapazono impulso parametrų pasirinkimą, suteikiant galimybę keisti impulso trukmę nuo 100 ns iki 1 ms, impulsų pasikartojimo dažnis – nuo 1 Hz iki 1 MHz, įtampos amplitudė nuo 0 kV iki 3 kV. Įrenginys turi pasižymėti didelės galios impulsais ir atlaikyti iki 60 A impulso srovę. Remiantis nustatytais parametrais sudarytos impulsų formavimo grandinės SPICE modelis pavaizduotas S2.1 paveiksle.

Grandinę sudaro nuolatinės įtampos šaltinis V, šeši aukšto dažnio ir aukštos įtampos C2M0080120D SiC MOSFET tranzistoriniai raktai SW1–SW6, apkrovos varža R_{LOAD} ir pereinamųjų vyksmų kompensavimo grandinės, susidedančios iš viršsrovių ir viršįtampių ribojančios RC grandinės (R_{S1}–R_{S6}, C_{S1}–C_{S6}), bei atgalinę srovę kompensuojančios trumpiklių grandinės D1–D6. Visų šešių raktų valdymas atliekamas mikrovaldiklio pagalba su MOSFET tranzistoriniais raktais sujungtais per atitinkamai šešis DR1–DR6 transformatorius imituojančius valdiklius užtikrinančius raktų galvanišką atskyrimą ir šešias įtampą ribojančias varžas R_{DR1}–R_{DR6}. Parazitinių elementų įtaka aproksimuota kaip L_P ir C_P.

Varijuojant apkrovos, parazitinių elementų ir kompensavimo grandinių komponentų vertes buvo parinkti optimalūs kompensavimo grandinių komponentai ir jų parametrai užtikrinantys stačiakampio impulso formos kokybę ir nepriklausomumą nuo skirtingos apkrovos. Stačiakampio impulso formos palyginimas prieš ir po kompensuojančių grandinių panaudojimą pavaizduotas S2.2 paveiksle.

Siekiant užtikrinti impulso galinio fronto kritimo trukmės nepriklausomybę nuo apkrovos, į impulsų formavimo grandinę buvo integruota valdoma kirtiklio pakopa (raktai SW5–SW6). Šios pakopos įtaka impulso galinio fronto kritimo trukmei pavaizduota S2.3 paveiksle. Matoma, kad tokia konfigūracija užtikrina impulso formos nepriklausomybę nuo naudojamos apkrovos ir ženkliai sutrumpina impulso galinio fronto kritimo trukmę esant didelėms apkrovoms.

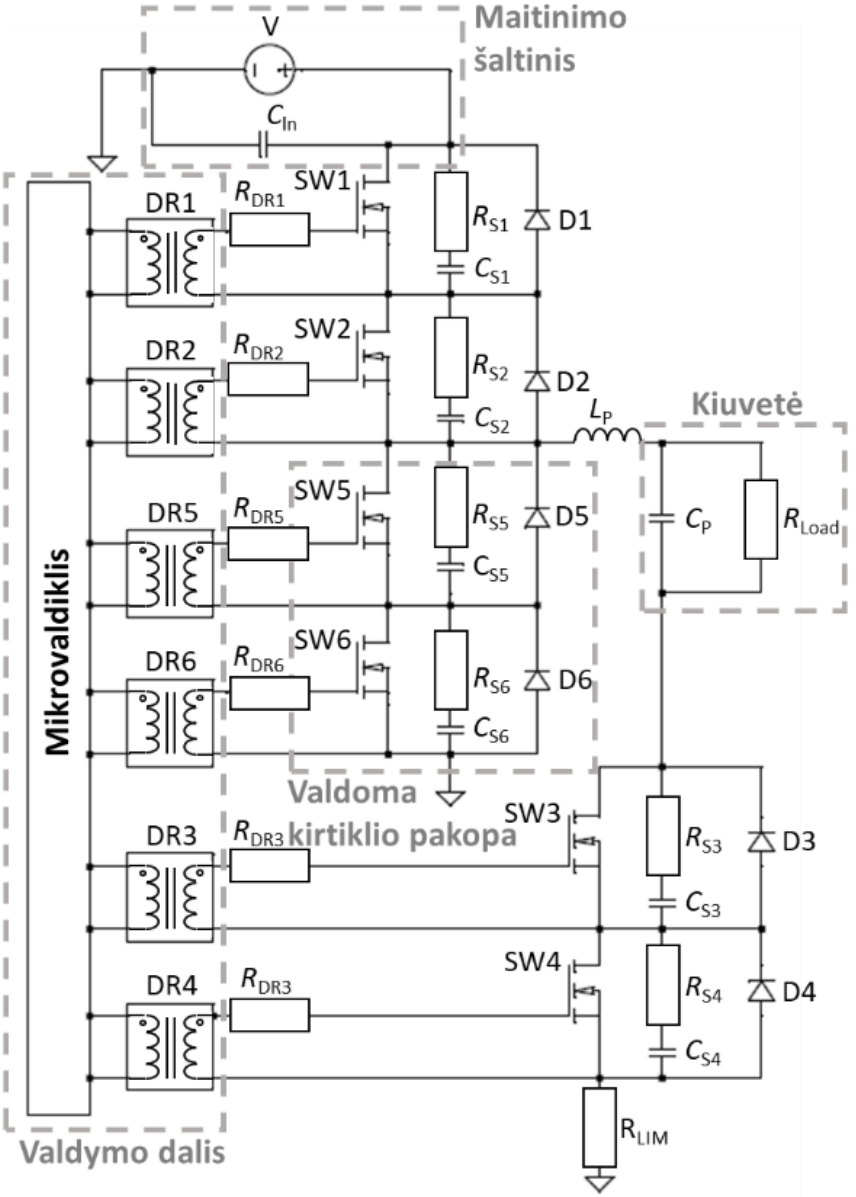

S2.1 pav. Aukšto dažnio stačiakampių impulsų elektroporacijos sistemos impulsų formavimo grandinės schema

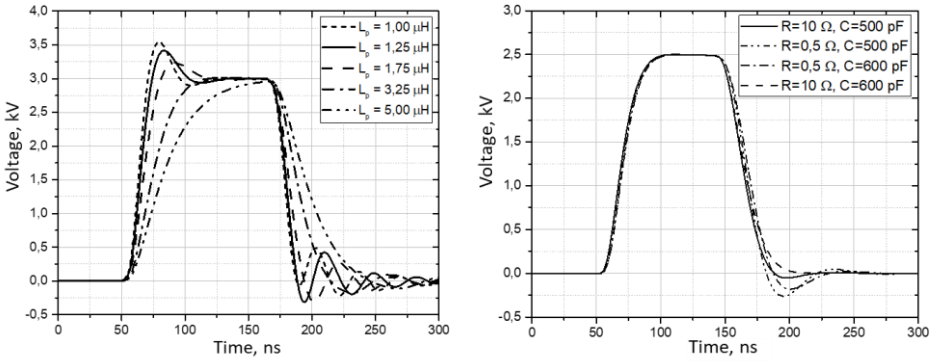

a) b)

S2.2 pav. Parazitinių grandinės elementų įtaka stačiakampio impulso formai: a) prieš kompensacinių grandinių panaudojimą; b) po kompensacinių grandinių panaudojimo

Apibendrinus tyrimo rezultatus, nustatyta, kad siekiant užtikrinti trumpiausias priekinio fronto kilimo ir galinio fronto kritimo trukmes, pereinamųjų vyksmų kompensavimo grandinės varžos optimali vertė turi būti 10 Ω, o kondensatoriaus talpa – 500 pF. Valdoma kirtiklio pakopa minimizuoja impulso nepriklausomybę nuo apkrovos, o pasiūlyta impulsų formavimo grandinė pasižymi pastoviomis 25 ns priekinio fronto kilimo ir ne didesne nei 18 ns galinio fronto kritimo trukmėmis. Remiantis MOSFET rakto charakteristikomis, trumpiausio impulso trukmė turėtų siekti apie 75 ns, o maksimali impulso srovė – 60 A.

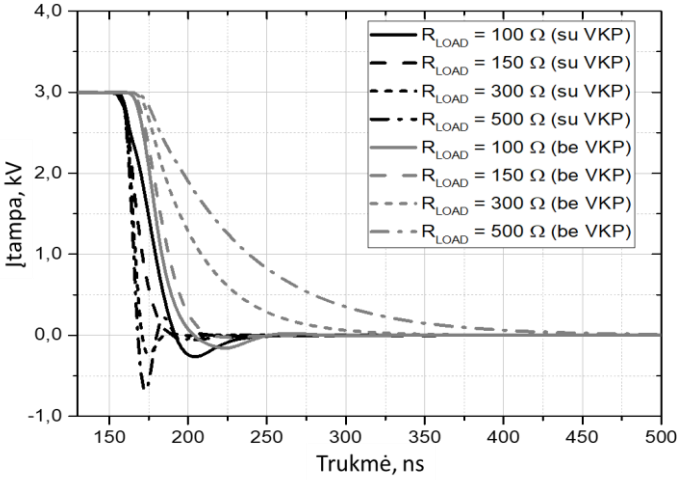

S2.3 pav. Valdomos kirtiklio pakopos įtaka impulso galinio fronto kritimo trukmei esant skirtingoms apkrovos varžoms

Skyriuje taip pat diskutuojama planarių elektroporacijos elektrodų panaudojimo perspektyvos ir poreikis. Pasiūloma planarių elektroporacijos elektrodų topologiją realaus laiko *in vitro* elektroporacijos taikymui. Panaudojant COMSOL Multiphysics programinį paketą sudaromas elektroporacijos elektrodų imitacinis modelis ir atliekamas elektrinio lauko pasiskirstymo tyrimas taikant baigtinių elementų metodą.

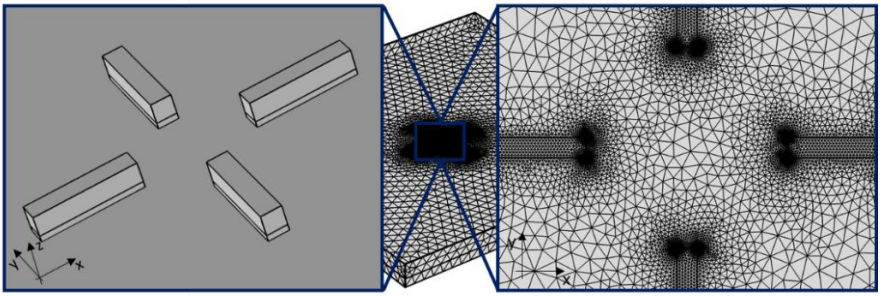

S2.4 pav. Supaprastintas 3D planarių realaus laiko elektroporacijos elektrodų (kairėje) ir laisvojo tetraedrinio tinklelio elektrinio lauko tyrimams baigtinių elementų metodu (dešinėje) topologijos

Pasiūlyta planarių elektrodų topologiją realaus laiko elektroporacijos taikymams pavaizduota S2.4 paveiksle. Vertinamos skirtingos elektrodų išmatavimų ir atstumų vertės. Remiantis gautais rezultatais pasiūloma optimali elektrodų topologiją, sudaranti galimybes pavienių ląstelių manipuliacijoms ir tuo pat metu užtikrinanti elektrinio lauko homogeniškumą ląstelių poveikio zonoje.

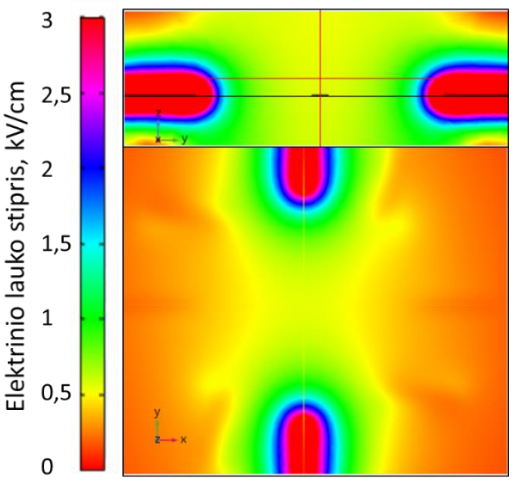

S2.5 pav. Elektrinio lauko pasiskirstymo rezultatų pavyzdys tarp dviejų 350 µm atstumu nutolusių planarių elektrodų porų YZ (viršuje) ir XY (apačioje) plokštumose

Elektrinio lauko pasiskirstymo modeliavimo rezultatų pavyzdys tarp dviejų planarių elektrodų porų YZ ir XY plokštumose pateiktas S2.5 paveiksle. Kadangi elektrodai reprezentuoja identiškas poras, pateikiama tik vienos poros elektrinio lauko pasiskirstymo rezultatai, tačiau šie rezultatai yra analogiški ir antrajai elektrodų porai.

Atstumas tarp S2.5 paveiksle vaizduojamų elektrodų yra 350 µm, o naudojama įtampa – 30 V. Keičiant atstumą tarp elektrodų buvo tiriamas elektrinio lauko pasiskirstymas. Buvo nustatyta, kad optimalios elektrodų topologijos atveju tarpas tarp atskirų elektrodų tūri būti 250–350 µm ruože. Tokiu atveju užtikrinamas elektrinio lauko homogeniškumas bei pasiekiamas kompromisas tarp naudojamos įtampos (mažesnės nei 100 V) ir gaunamo elektrinio lauko stiprio (daugiau kaip 1 kV/cm), būtino elektroporacijos procesui biologiniuose mėginiuose inicijuoti.

3. Elektroporacijos sistemos sukūrimas ir tyrimas

Trečiajame skyriuje pateikiamas aukšto dažnio stačiakampių impulsų elektroporacijos sistemos prototipo sukūrimas ir atliekamas įrangos testavimas. Eksperimentu nustatomos tikrosios impulso parametrų vertės, kurios sulyginamos su analogiškų prietaisų parametrais.

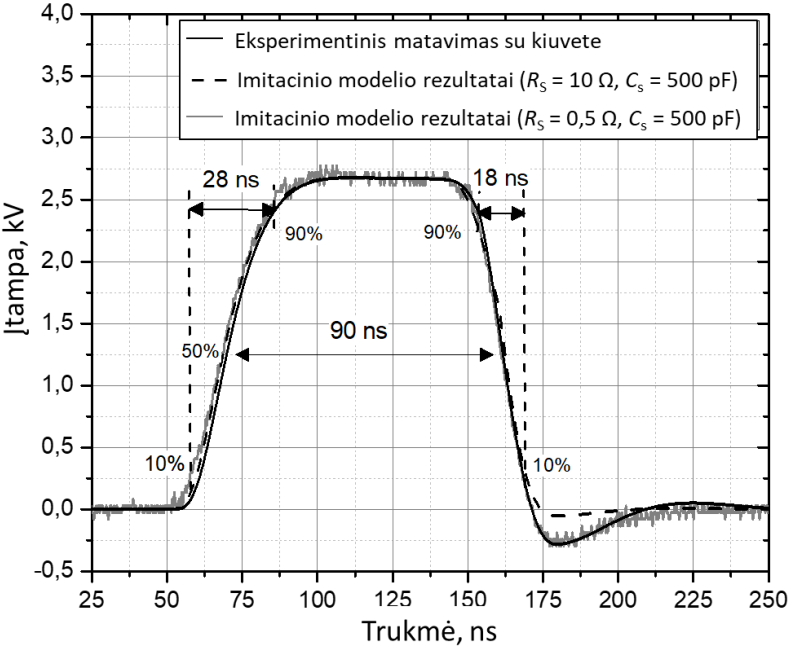

S3.1 pav. Aukšto dažnio elektroporacijos sistemos prototipo trumpiausio išmatuoto impulso bangos forma ir jos verčių sulyginimas su modeliavimo rezultatais (Butkus et al. 2019)

Šiame skyriuje taip pat atliekamas antrame skyriuje pristatymo impulsų formavimo grandinės imitacinio modelio rezultatų palyginimas su eksperimentiniais ir atliekamas neapibrėžties vertinimas. Atliekami taikomieji elektroporacijos tyrimai, kurių metu pademonstruojama naujos sistemos tinkamumas elektroporacijos tyrimams ir suderinamumas su standartinėmis komercinėmis eletroporacijos kiuvetėmis.

Sukurtas elektroporacijos sistemos prototipas pasižymi kompaktiškais matmenimis (18×29×22 cm) bei pasižymi mažu bendros impulsų formavimo grandinės parazitiniu induktyvumu. Eksperimentinių tyrimų metu nustatytos sistemos generuojamų stačiakampių impulsų parametrų ribinės vertės, kurios buvo matuojamos naudojant DPO 4034 skaitmeninį osciloskopą su 100:1 aukštos įtampos ir dažnio zondu. Galutinės eksperimentu nustatytos impulso parametrų vertės pateikiamos kaip penkių matavimų vidurkis. Tokiu būdu išmatuoto trumpiausio impulso forma pavaizduotas S3.1 paveiksle.

Kaip matyti S3.1 paveiksle, trumpiausia impulso trukmė (matuojama 50 % U_{max}) yra 90 ns (±10 %). Minimalią impulsų trukmę riboja MOSFET rakto perjungimo charakteristikos ir grandinės parazitiniai parametrai. Pasiūlyta valdoma kirtiklio pakopa užtikrino mažas impulso priekinio fronto kilimo ir galinio fronto kritimo trukmes, kurios (matuojamos tarp 10–90 % U_{max}) atitinkamai siekia 28 ns ir 18 ns.

Siekiant nustatyti imitacinio modelio paklaidą buvo atliktas palyginimas tarp imitacinio modelio rezultatų ir eksperimentiškai išmatuotų trumpiausio impulso verčių (S3.1 pav.). Nustatyta, kad pasiūlytas impulsų formavimo grandinės imitacinis modelis yra adekvatus sukurtos elektroporacijos sistemos prototipo eksperimentiškai nustatytiems rezultatams ir leidžia modeliuoti generuojamų elektrinių impulsų parametrus su neapibrėžtimi neviršijančia ±21 % (95,4 % pasikliovimo lygis).

Pasiūlytos valdomos kirtiklio pakopos įtakos impulso galinio fronto kritimo trukmei eksperimentiniai rezultatai pavaizduoti S3.2 paveiksle. Kaip matyti paveiksle, neaktyvavus valdomą kirtiklio pakopą, impulso galinio fronto kritimo trukmė priklauso nuo apkrovos varžos. Tuo tarpu, aktyvavus valdomą kirtiklio pakopą, impulso galinio fronto kritimo trukmė tampa nepriklausoma nuo apkrovos varžos ir ženkliai sumažėja. Tokiu būdų elektroporacijos tyrimų metu leidžiama užtikrinti vienodą elektrinio lauko intensyvumą nepriklausomai nuo apkrovos.

Bendru atveju, atlikus visų aukšto dažnio elektroporacijos sistemos parametrų matavimus, nustatyta, kad sistema gali generuoti aukštos įtampos (iki 3 kV), pasirenkamos trukmės (nuo 100 ns iki 1 ms) ir dažnio (nuo 1 Hz iki 3,5 MHz) stačiakampius impulsus (nuo 1 iki 100), o maksimali grandinės impulso srovė gali siekti iki 60 A.

Siekiant pademonstruoti naujos sistemos tinkamumą elektroporacijos tyrimams, buvo atlikti elektroporacijos taikomieji *in vitro* tyrimai su *Candida albicans* grybų ląstelėmis naudojant standartinę 1 mm elektroporacijos kiuvetę. Taikomųjų tyrimų metu pademonstruota, kad paveikus Candida albicans grybų ląsteles dešimtimi (10 Hz) 100 µs trukmės ir 30 kV/cm elektrinio lauko stiprio (3 kV amplitudės) impulsais, bendras kolonijos gyvybingumas sumažėjo iki 20 %. Taigi buvo patvirtinta, kad sukurta aukšto dažnio elektroporatocijos sistema suderinama su standartinėmis komercinėmis eletroporacijos kiuvetėmis ir yra tinkama *in vitro* elektroporacijos tyrimams.

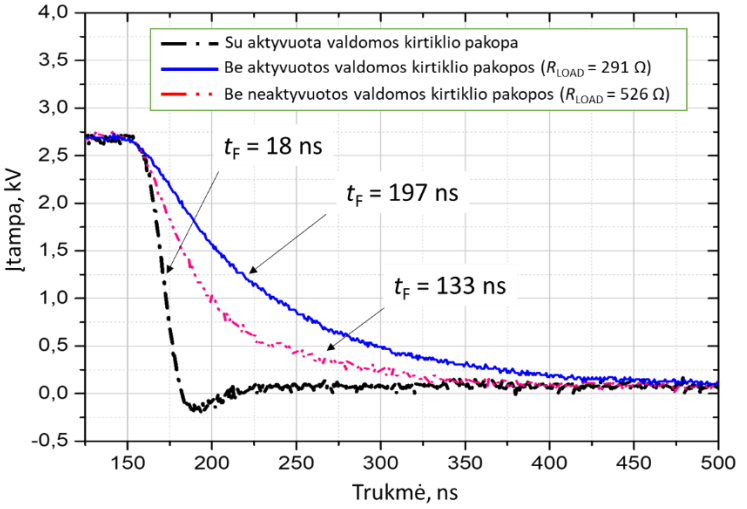

S3.2 pav. Valdomos kirtiklio pakopos įtakos impulso galinio fronto kritimo trukmei eksperimentiniai rezultatai (Novickij et al. 2016)

Plataus spektro impulso parametrų pasirinkimas leidžia naudoti sistemą plačiame elektroporacijos tyrimų diapazone išplečiant taikomųjų tyrimų sritį. Remiantis turimomis žiniomis, darbe pateikta elektroporacijos sistema yra pirmoji, kuri pasižymi nuo apkrovos nepriklausomų stačiakampių, aukšto dažnio (iki MHz eilės), aukštos įtampos (iki 3 kV), plataus diapazono trukmių (nuo 100 ns iki 1 ms) impulsų generavimu. Atitinkamai, elektroporacijos sistema suteikia galimybę tirti elektroporacijos reiškinį tiek mažiausiai ištirtuose elektrinio lauko stiprio ir dažnio diapazonuose, tiek įprastame elektroporacijos taikymų diapazone.

Bendrosios išvados

1. Sukurta nauja aukšto dažnio stačiakampių impulsų elektroporacijos sistema, kuri gali generuoti aukštos įtampos (iki 3 kV), pasirenkamos trukmės (nuo 100 ns iki 1 ms) ir dažnio (nuo 1 Hz iki 3,5 MHz) stačiakampius impulsus.
2. Pasiūlyta sinchronizuotai valdoma kirtiklio pakopa yra efektyvi ir užtikrina stačiakampio impulso galinio fronto kritimo 18 ns trukmę, kuri yra nepriklausomą nuo naudojamos apkrovos varžos.
3. Nustatyta, kad pasiūlyto aukšto dažnio stačiakampių impulsų formavimo grandinės imitacinio modelio rezultatai atitinka eksperimentiškai nustatytus rezultatus su neapibrėžtimi neviršijančia ±21 % (95,4 % pasikliovimo lygis). Pasiūlytas imitacinis modelis yra tinkamas vertinti pereinamųjų vyksmų ir grandinės parazitinių elementų įtaką submikrosekundžių impulsų formai.
4. Remiantis planarių elektrodų modelio, sudaryto COMSOL Multiphysics programine įranga, rezultatais nustatyta, kad pasiūlyta planarių elektrodų

topologija yra tinkama realaus laiko elektroporacijos tyrimams, o 250–350 μm tarpas tarp elektrodų užtikrina daugiau nei 1 kV/cm stiprio ir homogenišką elektrinio lauko pasiskirstymą.

Annexes[1]

Annex A. Declaration of Academic Integrity
Annex B. Coauthors' Agreements to Present Publications in the Dissertation
Annex C. Copies of Scientific Publications by the Author on the Topic of the Dissertation

[1]The annexes are supplied in the enclosed compact disc.

Paulius BUTKUS

RESEARCH AND DEVELOPMENT OF
THE HIGH-FREQUENCY SQUARE-WAVE
PULSE ELECTROPORATION SYSTEM

Doctoral Dissertation

Technological Sciences,
Electrical and Electronic Engineering (T 001)

AUKŠTO DAŽNIO STAČIAKAMPIŲ IMPULSŲ
ELEKTROPORACIJOS SISTEMOS KŪRIMAS
IR TYRIMAS

Daktaro disertacija

Technologijos mokslai,
elektros ir elektronikos inžinerija (T 001)

2020 11 17. 11 sp. l. Tiražas 20 egz.
Leidinio el. versija https://doi.org/10.20334/2020-040-M
Vilniaus Gedimino technikos universitetas,
Saulėtekio al. 11, 10223 Vilnius,
Spausdino BĮ UAB „Baltijos kopija“
Kareivių g. 13B, 09109 Vilnius